Diogo Luzia Brázio

Bio-electronic transducers to interact with cancer cells

2020

Diogo Luzia Brázio

Bio-electronic transducers to interact with cancer cells

Mestrado Integrado em
Engenharia Eletrónica e Telecomunicações

Trabalho efetuado sob a orientação de:
Professor Dr. Henrique Leonel Gomes

O presente trabalho foi parcialmente financiado pelas seguintes instituições:
Instituto de Telecomunicações (IT), UID/EEA/50008/2020
Fundação para a Ciência e Tecnologia (FCT) no âmbito do projeto: IMPLANTABLE ORGANIC DEVICES FOR ADVANCED THERAPIES (INNOVATE) ref: PTDC/EEI-AUT/5442/2014

2020

Declaração de autoria do trabalho

Declaro ser o autor deste trabalho, que é original e inédito. Autores e trabalhos consultados estão devidamente citados no texto e constam da listagem de referências incluída.

(Diogo Luzia Brázio)

Copyright © Diogo Luzia Brázio, 2020

"A Universidade do Algarve tem o direito, perpétuo e sem limites geográficos, de arquivar e publicitar este trabalho através de exemplares impressos reproduzidos em papel ou de forma digital, ou por qualquer outro meio conhecido ou que venha a ser inventado, de o divulgar através de repositórios científicos e de admitir a sua cópia e distribuição com objetivos educacionais ou de investigação, não comerciais, desde que seja dado crédito ao autor e editor."

Acknowledgments

I would like to acknowledge to Drª Patricia Madureira, and to Rita Monteiro from Centre for Biomedical Research, Universidade do Algarve, for providing the U87 cell cultures and the High-Grade Glioma (HGG), named here HOPE cells cultures. The HOPE cells were only possible thanks to efforts of the Drª Clara Romero and to Dr. Artur Lourenço, both from the Hospital de Faro and Algarve Biomedical Centre (ABC). Drª Clara Romero and to Dr. Artur Lourenço extracted and purified HOPE cell cultures.

A man is found in the unknown dark skies of the wind that's coming from every and nowhere, to nowhere, everywhere, elsewhere, whose path is not besides himself, but rather, a tale of the inner sinner for almost try to exist some time, somewhere, somehow, in a running subtle breezy breeze. Therefore, however it tackles down the core left to shake up, there is just an option left: to know himself, acknowledge the other, so one day to unveil the world without fear of how simply it is.

The following investigation work comes to live thanks to Universidade do Algarve (UAlg), Instituto de Telecomunicações (IT) and Fundação para a Ciência e Tecnologia (FCT), who have partially sponsored it on the project "Implantable devices for advanced therapies".

To the honer of our beloved Professor Henrique Gomes, a spiritual leader who always acts as scientific and moral compass pointing north through the complexity of reality. As his student, I could testify a calm and gentle man whose sharp eyes and courageous behavior towards the hardships of everyday have inspired me to keep on fighting. Always emphatic, helpful and resourceful with his students, Professor help was a crucial ace for proceeding on the right steps during the entire thesis, and for all of that I cannot express how grateful I am for having the chance to work with him. Putting all in an idea, I would describe Professor as somebody whose remarkable fear is to never get wrong, so he and we all around him can be marveled once again with the world we have to learn about.

To the honer of Ana Mestre and Pedro Inácio, Professor's skillful assistants who were responsible for managing and distributing every kind of material which I have dealt with, raw data, graphical information as concept diagrams and plots, reference papers. Such shadows followed me as shadows do, to where there is light. It would not be fair to forget any other member of the

laboratory, even the ones who I have barely met or I have never had the chance to, because we all have found each other in a common place that have contributed for something bigger. My sincere thank you very much for all your effort towards my thesis.

Should we all listen a simple story of a simple man? Isn't it much of value as a story of a knight? All in all, both have the urge to focus on the need of accomplish the reality, by breaking its sword of the finite. Then, the universal essence gives them the legitimacy to do so, unleashing the keen quintessence in himself, not just because, also because, there's not other away around to round the squares of truth told long ago, even a single simple living being is saved.

Abstract

This thesis is focused on the study of electrophysiological signals in populations of cancer cells measured using extracellular electrodes. The cells under study are derived from cells known as glia cells. Glia cells are part of the brain but are significantly different from neurons. An important function of glia cells is to regulate communication between neurons. Glia cells can mutate and turn into cancer cells. When this happens, they give rise to very aggressive tumors (gliomas). The study of electrophysiological signals in cells of this type is relevant because in principle it can give information about how this type of cells is organized and communicates to perform simple tasks, such as migrating or proliferating.

In contrast to neurons, or cardiomyocytes, glia cells do not generate action potentials and therefore, are included in the class of non-electrogenic cells. However, glia cells have developed an information transmission mechanism that is based on the generation of a local ionic oscillation. This oscillation can travel to neighboring cells like a wave. To generate the oscillation, the cells generate a flow of ions, for example of calcium or sodium ions, the associated electrical oscillations are known as calcium or sodium waves, respectively. Ionic oscillations can travel long distances (millimeters). For the oscillation to travel through the cell population, cells must be connected to form a compact biological tissue.

The formation of the wave also requires that the cells have the ability to synchronize their activity. Unlike an action potential, that is an oscillation generated by an individual cell, the oscillations generated by glia cells are a property of a set of cells that synchronize to generate electrical fluctuation. Note that both the action potential and the wave generated by the glia cells are both electrical signals that travel like waves. However, there are important differences in the characteristics of the two signals. An action potential is a fast signal (meters / s) and short duration (milliseconds). A calcium wave is an oscillation that can last for several seconds and propagates through the population of cells at speeds of a few tens of micrometers per second. A calcium wave is typically a thousand times slower than an action potential.

The measurement and interpretation of action potentials using extracellular electrodes is well documented in the literature. As for the electrical waves generated by the synchronized activity of cells, the knowledge is very poor. Until now, this type of bio-electrical signaling mechanism has been studied using optical markers and fluorescence techniques.

Although, optical techniques can visualize the wave, they suffer from a set of limitations, both from experimental as well as from a biological point of view. For example, optical markers have a relatively short lifetime (hours), and can be toxic to cells. Additionally, light can disturb the measurements. Optical florescence has in its favor the fact that it is a selective technique and allows to know exactly the ionic species that is involved in the process. Electrical techniques cannot differentiate which ion is involved, but they can observe oscillations in real time in a totally non-invasive way and for extended periods (weeks or months).

The existing literature on the signal analysis and processing of signals that are result from synchronized cell activity is practically non-existent. This scientific area is still in its infancy. This thesis aims to contribute to increase our knowledge about this type of bio-electric signaling.

The objective of the work presented in this thesis was to study how the design of extracellular electrodes determines the shape of the measured electrical signal. Since the signal is an electric wave that travels through the cell population, it is obvious that the shape of the signal is essentially determined by a number of factors, namely the; (i) number of cells that are able to synchronize, (ii) electrode design, (iii) electrode active area, and even (iv) spatial arrangement of the electrodes in relation to the wave propagation direction.

This study processed a large number of signals collected using electrodes with different areas and geometries. The signals were first cataloged and classified according to the shape of the measured signal. Then, relationships were established between the power of the measured signal and the active area of the measured electrode, the periodicity of the signal and the spacing of the sensor electrodes. The components of the signal that vary exponentially have been quantified to determine the physical origin of the exponential behavior, or in other words if it originates in a biological process or if it is determined by the time constant (physics) of the electrode. Finally, several signal patterns were characterized and classified. Among the most interesting patterns, a

pattern in which the frequency increases following an exponential law (called a blueshift) and a pattern where the frequency decays exponentially (redshift) were observed.

The results of the signal analysis and their relationship with the geometry of the electrodes allowed us to quantify the role of the electrode in defining the shape and the duration of the signal. Guidelines for the optimization of the electrodes was also an important outcome of this thesis.

Finally, it is important to note that from the biological point of view it is expected that the optimization of the electrodes will allow to decode signaling patterns that correspond to specific biological instructions. For example, assuming that cell migration is a process instructed by an electrical oscillation with a certain pattern, decoding this pattern will eventually enable us to inhibit cell migration, thus paving the way for new technologies for cancer therapy. The limitations of using radiotherapy and chemotherapy in the brain make electrical techniques particularly appealing to treat brain tumors.

Keywords: Glia cells signals, Bio-electricity, Bio-electronics, Extracellular electrodes, Non-electrogenic cells, Cancer cells.

Sumário

Esta tese incidiu sobre o estudo de sinais eletrofisiológicos em populações de células cancerosas, medidos usando elétrodos extra-celulares. As células em estudo derivam de células conhecidas por células da glia. As células da glia fazem parte do cérebro, mas são significativamente diferentes dos neurónios. Uma função importante das células da glia é regular a comunicação entre neurónios. As células da glia podem sofrer mutações e transformar-se em células cancerosas. Quando isso acontece dão origem a tumores muito agressivos (gliomas). O estudo de sinais eletrofisiológicos em células deste tipo é relevante porque em princípio podem dar informação sobre como este tipo de células se organizam e comunicam para realizar tarefas simples, como migrar ou proliferar.

Em contraste com os neurónios, ou com os cardiomiócitos, as células da glia não geram potenciais de ação e por isso são incluídas na classe das células não electrogénicas. No entanto, as células da glia desenvolveram um mecanismo de transmissão de informação que se baseia na geração de uma oscilação local de iões. Esta oscilação pode-se propagar às células vizinhas como uma onda. Para gerar a oscilação as células geram um fluxo de iões, por exemplo iões de cálcio ou de sódio, as oscilações elétricas associadas são conhecidas por ondas de cálcio ou de sódio respetivamente. As oscilações iónicas conseguem viajar a longas distâncias (milímetros). Para que a oscilação viaje pela população de células é preciso que as células estejam ligadas umas as outras formando um tecido biológico compacto.

A formação da onda requer também que as células tenham a capacidade de sincronizar sua atividade. Ao contrário de um potencial de ação que é uma oscilação gerada por uma célula individual, as oscilações geradas pelas células da glia são uma propriedade de um conjunto de células que se sincronizam para gerar a flutuação elétrica. Note-se que, quer o potencial de ação, quer a onda gerada pelas células da glia são ambas sinais elétricos que viajam como ondas. No entanto, existem diferenças importantes nas características dos dois sinais. Um potencial de ação é um sinal rápido (metros /s) e de curta duração (milissegundos). Uma onda de cálcio é uma oscilação que pode durar vários segundos e propaga-se pela população das células a velocidades de algumas de dezenas de micrómetros por segundo. Uma onda de cálcio é tipicamente mil vez mais lenta que um potencial de ação.

A medição e a interpretação dos potenciais de ação usando elétrodos extra-celulares está bem documentada na literatura. Já no que diz respeito às ondas elétricas geradas pela atividade sincronizada de células, o conhecimento é praticamente inexistente. Até agora, este tipo de sinalização elétrica tem sido estudado usando marcadores óticos e técnicas de fluorescência que permitem visualizar a oscilação a viajar pela população das células.

Apesar das técnicas óticas conseguirem visualizar a onda, sofrem de um conjunto de limitações quer experimentais quer biológicas. Por exemplo, os marcadores óticos tem um tempo de vida relativamente curto (horas), e podem ser tóxicos para as células. Adicionalmente, a iluminação pode perturbar as células e as medidas. A florescência, tem a seu favor o facto de ser uma técnica seletiva e permitir determinar a espécie iónica que está envolvida no processo. As técnicas elétricas não conseguem diferenciar qual o ião envolvido, mas podem observar as oscilações em tempo real de uma forma totalmente não invasiva por períodos extensos (semanas ou meses).

A literatura existente sobre a análise e o processamento dos sinais elétricos que são recolhidos por elétrodos extra-celulares e que resultam de uma atividade sincronizadas das células, é praticamente inexistente. Esta área científica ainda está na sua infância. Esta tese pretende contribuir para aumentar os nossos conhecimentos sobre este tipo de sinalização bioelétrica.

O objetivo concreto do trabalho apresentado nesta tese foi estudar como o desenho dos elétrodos extra-celulares determinam a forma do sinal elétrico medido. Sendo o sinal uma onda elétrica que viaja pela população das células, é óbvio que a forma do sinal é essencialmente determinada por um conjunto de fatores, nomeadamente pelo; (i) número de células que é capaz de sincronizar, (ii) desenho do elétrodo, (iii) área ativa do elétrodo, e até pela (iv) disposição espacial dos elétrodos em relação à direção de propagação da onda.

Este estudo processou um número elevado de sinais recolhido usando elétrodos com áreas e geometrias diferentes. Os sinais foram primeiro catalogados e classificados de acordo com a forma do sinal medido. De seguida foram estabelecidas relações entre a potência do sinal medido e a área ativa do elétrodo medido, a periodicidade do sinal e o espaçamento dos elétrodos sensores. As componentes do sinal que variam exponencialmente foram quantificadas para determinar a origem física do comportamento exponencial, ou por outras palavras se tem origem num processo biológico ou se é determinada pela constante de tempo (física) do elétrodo. Por último, vários padrões de sinais foram caracterizados e classificados. Entre os padrões mais interessantes foi observado um

padrão de sinais em que a frequência do sinal cresce seguindo uma lei exponencial (designado de desvio para o azul) e um padrão onde a frequência do sinal decai também exponencialmente (desvio para o vermelho).

Os resultados da análise dos sinais e da sua relação com a geometria dos elétrodos permitiu quantificar o papel do elétrodo na definição da forma e duração do sinal. Um outro resultado importante deste trabalho foi a fornecer diretrizes para a otimização do desenho dos elétrodos.

Por último, é importante referir que do ponto de vista biológico espera-se que a otimização dos elétrodos permita num futuro próximo descodificar os padrões de sinalização que correspondem a instruções biológicas especificas. Por exemplo, assumindo que a migração celular é um processo instruído por uma oscilação elétrica com um determinado padrão, a descodificação deste padrão permitirá eventualmente instruir as células a inibir a migração, abrindo desta forma o caminho para novas formas de terapia do cancro. As limitações do uso da radioterapia e da quimioterapia no cérebro tornam as técnicas elétricas particularmente apelativas para combater tumores no cérebro.

Palavras-chave: Sinais de células da glia, Bioeletricidade, Bioelectrónica, Elétrodos extra-celulares, Células não-electrogénicas, Células cancerosas.

Table of contents

Index of Figures

Chapter 6

Index of Tables

Chapter 1

Introduction

This chapter provides a view on the state-of-art about bio-electrical measurements in cancer cell populations. It outlines the relevance of bio-electrical measurements in cancer cells, our current understanding and the research needs. It also describes how the thesis is organized.

1.1 Introduction

The bio-electrical activity of cells and tissues is often associated with neurons, cardiac cells, and muscle cells. These types of cells they generate bio-electrical signals know as action potentials and they are recorded using micro-electrode arrays[1, 2, 3, 4]. An action potential can be viewed as a traveling ionic oscillation (wave).

Nervous cells are classified as electrogenic cells. The other types of cells that do not fire action potentials are classified as non-electrogenic cells. For instance a cell from the skin or from the liver is classified as a non-electrogenic type of cell. Non-electrogenic cells also communicate using ionic traveling waves that resemble to an action potential. The information is still carried from cell to cell using a traveling wave.

Waves are a very convenient way to transmit information at long distances and it is natural that both types of cells (electrogenic and non-electrogenic) use waves to transmit information. However, there are some important differences between the two types of cells. In a neuron, the traveling wave is a property of an individual cell, while in a non-electrogenic cell the wave is generated by cooperative cell phenomena. This means an ensemble of cells gets synchronized to produce an ionic oscillation that moves along the cell population. Examples of a traveling wave are calcium waves[5, 6, 7, 8, 9].

Another important difference between electrogenic and non-electrogenic cells is related with the traveling speed of the wave. While an action potential moves at meters per second, the typical velocity of a calcium wave is 20-30 micrometer per second. This means that calcium wave is one million times slower than an action potential. Finally, the signal generated by a traveling wave in a population of non-electrogenic cells is in a scale of a few micro-volts, which is significant weaker than a signal generated by a neuron that can reach milli-volts.

Cancer cells are classified as non-electrogenic cells, but this does not mean they are electrically silent. Our research team has shown that cancer cells are extremely active and they produce long lasting bio-electrical signals that are a result of a cooperative activity[10,11]. Measurements of bioelectrical signals in cancer cells is a relatively new field. The reason for that is related with the fact that the scientific community has focused their efforts on studying electrogenic cells. Indeed, the neuron-neuron communication is a very interesting and appealing field, therefore, researchers have been focused on developing devices to record action potentials. But these devices to measure neurons are totally blind to the bio-electrical signals generated by non-electrogenic cells.

The reason is because the signals are located in very different frequency windows. To record an action potential we need a bandwidth of a few kilohertz while to record a bio-electrical signal generated by a non-electrogenic cell population we need to measure signals with frequency of millihertz. Furthermore, when we record non-electrogenic cells, we need to measure a cell population and not a single cell as in the case of a neuron. For this reason the electronic technology to measure the long-range communication in non-electrogenic (or non-nervous) types of cells is still in its infancy.

Our group has pioneered this research on bio-electrical signaling on non-electrogenic cells, and our first papers in this area were published in 2016 and in 2017[12, 13, 14, 15]. Our methods and approaches are currently attracting the attention of the scientific community and several groups inspired in our work are using our approach to explore a variety of cell-cell communication mechanisms, particularly in the area of cancer research[16] and astrocytes[17]. Our major achievement was to show that signals generated by non-electrogenic cells could be recorded using extracellular bio-electronic devices. Previously, it was an accepted view that these signals were too weak to be detected by extracellular devices and could only be observed by fluorescence methods. We demonstrated the electronic detection of signals generated by non-electrogenic cells and, recently, we also demonstrated the potential of this method by recording in real time the establishment of communication patterns in cancer cells as they migrate and invade a cell free region[18].

Currently, there is very little information about the signals generated by populations of non-electrogenic cells. For example it is not know what is the biological mechanism (ionic channels) involved in these signals. In addition it is not know how the electrode geometry controls the signal shape. Often the signals are modulated in frequency and in amplitude, but the purpose of this signal modulation is still a mystery.

The correlation between the signals and the biological process causing them is not a trivial one, and it is outside the objectives of this thesis. Before this correlation with biological mechanisms is attempted, the signals have to be characterized in detail. The first important step is to characterize discrete individual signals, classified the signals according to their shape, amplitude and duration. Inspect, how the signal depends on the geometry of the electrode used to record it.

This correlation is needed because the current hypothesis assumes that the signals generated by non-electrogenic cells are traveling waves. If this is true, then the geometry of the electrode defines the duration and amplitude of the signal recorded. The next stage in this signal-processing task is to look for correlations in burst of signals, characterize the modulation in frequency and in

amplitude. Explore the differences and similarities between signals produce by different cell populations. The detailed electrical characterization of all the signals recorded in cancer cell populations is the goal of this work.

This thesis is organized into seven chapters, after this introduction, Chapter 2 describes the instrumentation used to record the cell signals. The ensemble of signals recorded is analyzed in detail on Chapter 3. Each signal is classified and named according to their characteristics (duration, amplitude and shape). Chapter 4 looks at the individual details of each signal. Here the time constants associated with rising and decaying components of each individual signal are presented and analyzed. On Chapter 5 it is studied how the sensing electrode geometry affects the signal shape and power. The analysis of long and complex time traces showing frequency and amplitude modulation is presented and discussed on Chapter 6. Finally, Chapter 7 summarizes the major achievements and presents some suggestions for further work.

References

1. M.E.J. Obien, K. Deligkaris, T. Bullmann, D.J. Bakkum, U. Frey, Revealing neuronal function through microelectrode array recordings, Front. Neurosci. 8 (2015) 423. doi:10.3389/fnins.2014.00423.

2. K. Mathieson, S. Kachiguine, C. Adams, W. Cunningham, D. Gunning, V. O'Shea, K.M. Smith, E.J. Chichilnisky, A.M. Litke, A. Sher, M. Rahman, Large-area microelectrode arrays for recording of neural signals, IEEE Trans. Nucl. Sci. 51 (2004) 2027–2031. doi:10.1109/TNS.2004.835873.

3. B. Eversmann, M. Jenkner, F. Hofmann, C. Paulus, R. Brederlow, B. Holzapfl, P. Fromherz, M. Merz, M. Brenner, M. Schreiter, R. Gabl, K. Plehnert, M. Steinhauser, G. Eckstein, D. Schmitt-Landsiedel, R. Thewes, A 128 x 128 CMOS Biosensor Array for Extracellular\rRecording of Neural Activity, Ieee J. Solid-State Circuits,. 38 (2003) 2306–2317.

4. A. Hierlemann, U. Frey, S. Hafizovic, F. Heer, Growing Cells Atop Microelectronic Chips: Interfacing Electrogenic Cells In Vitro With CMOS-Based Microelectrode Arrays, Proc. IEEE. 99 (2011) 252–284. doi:10.1109/JPROC.2010.2066532.
5. T. Sasaki, N. Takahashi, N. Matsuki, Y. Ikegaya, Calcium Fluctuations, J Neurophysiol. (2008) 1668–1676. doi:10.1152/jn.00084.2008.

6. B.S. Khakh, K.D. McCarthy, Astrocyte calcium signaling: From observations to functions and the challenges therein, Cold Spring Harb. Perspect. Biol. 7 (2015) 1–18. doi:10.1101/cshperspect.a020404.

7. T. Höfer, L. Venance, C. Giaume, Control and plasticity of intercellular calcium waves in astrocytes: a modeling approach., J. Neurosci. 22 (2002) 4850–9. doi:20026493.

8. L. Gelens, G.A. Anderson, J.E. Ferrell, Spatial trigger waves: positive feedback gets you a long way, Mol. Biol. Cell. 25 (2014) 3486–3493. doi:10.1091/mbc.E14-08-1306.

9. C.G. Schipke, C. Boucsein, C. Ohlemeyer, F. Kirchhoff, H. Kettenmann, Astrocyte calcium waves trigger responses in microglial cells in brain slices, FASEB J. 16 (2002) 255–257.

10. A.L.G. Mestre, P.M.C. Inácio, Y. Elamine, S. Asgarifar, A.S. Lourenço, M.L.S. Cristiano, P. Aguiar, M.C.R. Medeiros, I.M. Araújo, J. Ventura, H.L. Gomes, Extracellular Electrophysiological Measurements of Cooperative Signals in Astrocytes Populations, Front. Neural Circuits. 11 (2017) 1–9. doi:10.3389/fncir.2017.00080.

11. P.R.F. Rocha, M.C.R. Medeiros, U. Kintzel, J. Vogt, I.M. Araújo, A.L.G. Mestre, V. Mailänder, P. Schlett, M. Dröge, L. Schneider, F. Biscarini, D.M. de Leeuw, H.L. Gomes, Extracellular electrical recording of pH-triggered bursts in C6 glioma cell populations, Sci. Adv. 2 (2016) e1600516. doi:10.1126/sciadv.1600516.

12. M.C.R. Medeiros, A. Mestre, P. Inácio, S. Asgarif, I.M. Araújo, P.C. Hubbard, Z. Velez, M.L. Cancela, P.R.F. Rocha, D.M. de Leeuw, F. Biscarini, H.L. Gomes, An electrical method to measure low-frequency collective and synchronized cell activity using extracellular electrodes, Sens. Bio-Sensing Res. 10 (2016) 1–8. doi:10.1016/j.sbsr.2016.06.002.

13. M.C.R. Medeiros, A.L.G. Mestre, P.M.C. Inácio, J.M.L. Santos, I.M. Araujo, J. Bragancą, F. Biscarini, H.L. Gomes, Performance assessment of polymer based electrodes for in vitro electrophysiological sensing: The role of the electrode impedance, in: Proc. SPIE - Int. Soc. Opt. Eng., 2016. doi:10.1117/12.2237659.

14. P.R.F. Rocha, P. Schlett, U. Kintzel, V. Mailänder, L.K.J. Vandamme, G. Zeck, H.L. Gomes, F. Biscarini, D.M. de Leeuw, Electrochemical noise and impedance of Au electrode/electrolyte interfaces enabling extracellular detection of glioma cell populations, Sci. Rep. 6 (2016) 34843. doi:10.1038/srep34843.

15. A.L.G. Mestre, M. Cerquido, P.M.C. Inácio, S. Asgarifar, A.S. Lourenço, M.L.S. Cristiano, P. Aguiar, M.C.R. Medeiros, I.M. Araújo, J. Ventura, H.L. Gomes, Ultrasensitive gold micro-structured electrodes enabling the detection of extra-cellular long-lasting potentials in astrocytes populations, Sci. Rep. 7 (2017) 14284. doi:10.1038/s41598-017-14697-y.

16. M. Cabello, H. Ge, C. Aracil, D. Moschou, P. Estrela, J.M. Quero, S.I. Pascu, P.R.F. Rocha, Extracellular electrophysiology in the prostate cancer cell model PC-3, Sensors (Switzerland). 19 (2019) 1–11. doi:10.3390/s19010139.

17. A.I. Borrachero-Conejo, E. Saracino, M. Natali, F. Prescimone, S. Karges, S. Bonetti, G.P. Nicchia, F. Formaggio, M. Caprini, R. Zamboni, F. Mercuri, S. Toffanin, M. Muccini, V. Benfenati, Electrical Stimulation by an Organic Transistor Architecture Induces Calcium Signaling in Nonexcitable Brain Cells, Adv. Healthc. Mater. 8 (2019) 1–12. doi:10.1002/adhm.201801139.

18. S. Asgarifar, A.L.G. Mestre, R.C. Félix, P.M.C. Inácio, M.L.S. Cristiano, M.C.R. Medeiros, I.M. Araújo, D.M. Power, H.L. Gomes, Extracellular electrophysiological based sensor to monitor cancer cells cooperative migration and cell-cell connections, Biosens. Bioelectron. 145 (2019) 111708. doi:10.1016/j.bios.2019.111708.

Chapter 2

Experimental set-up, procedures and biological cells

This chapter describes the instrumentation and the procedures followed to record electrophysiological signals from non-electrogenic cell populations. The basic features of the instruments used are outlined. The software to analyze and process the data is briefly explained. The biological cells used in the experiments are also presented.

2.1 Introduction

The experimental procedures and the instrumentation used to record electrophysiological signals from cell populations *in vitro* are described in detail in this chapter. The instrumentation is comprised of several different modules; (i) electrical techniques to characterize the sensing electrodes, (ii) electrical methods to record bio-electrical signals, (iii) incubator to keep the cells under proper environmental conditions (5% CO_2 and 37ºC), (iv) guarding shields to minimize the external sources of noise, and (v) programs for data processing and analysis.

Before electrophysiological measurements are carried out, the sensing electrodes are electrically characterized in detail. This electrical characterization procedure begins with the assembly of the electrodes on a chip holder, a full detailed characterization of the bare sensing system (without cells) and an elimination of all sources of interference. The schematic diagram in Figure 2.1 outlines the basic procedures carried out in a typical electrophysiological experiment.

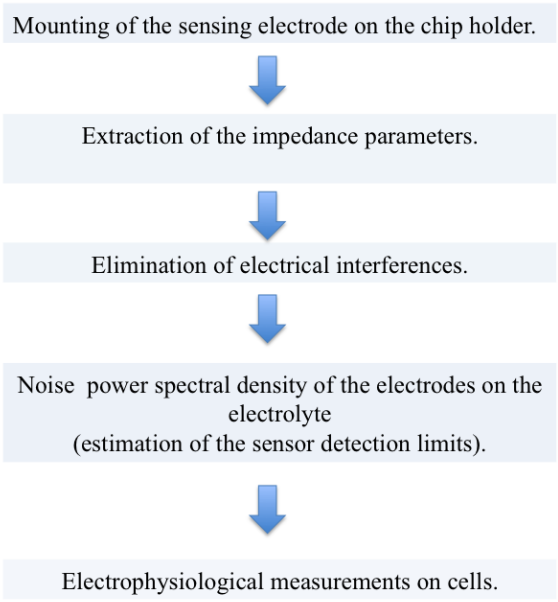

Figure 2.1: Schematic diagram showing the procedures followed in experiments.

This chapter begins by presenting an overall view of the measuring set-up. This global vision of the measuring system is then followed by a detail description of each measuring block and their purpose. The procedures to perform measurements, including procedures for the cell handling are also described in detail. Finally, the post processing of the data is outlined.

2.2 Instrumentation

Figure 2.2 shows a schematic diagram of the experimental arrangement used to measure cell populations. The chip holder and the low–noise pre-amplifier are located inside a cell incubator. The cell incubator is placed inside of a large Faraday cage. In the vicinity of the Faraday cage there are two additional electrical systems that can be coupled to the chip holder when required. These two systems are an impedance analyzer, and an electro-optical stimulation system.

The impedance analyzer is used to characterize the sensing electrodes but also as an "Electrical imaging technique" to follow in real time the cell population. Indeed, the impedance of the electrode/electrolyte interface is extremely sensitive to the properties of cells adherent to the electrode. If the cells change morphology or detach from the electrode, they cause immediately changes in the impedance. Therefore, impedance provides a convenient way to visualize the state of the cell population under study.

The electro-optical stimulation system is used to stimulate the cells with electrical, with optical pulses or even with thermal pulses. A CO_2 bottle connected to the incubator is also represented in the diagram of Figure 2.2 The CO_2 is used to keep the atmosphere inside the incubator at 5% of CO_2. Figure 2.3 shows a photograph of pre-amplifier inside the incubator. The aluminum box that holds the chip holder appears on the photograph.

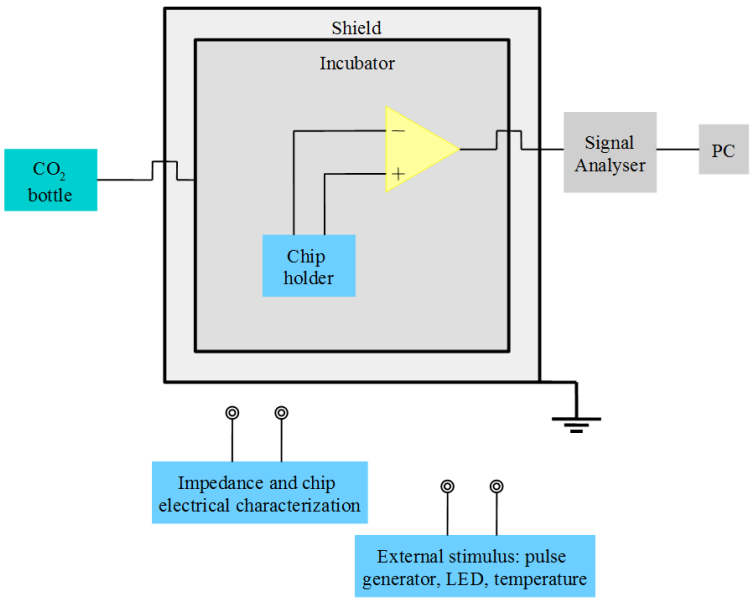

Figure 2.2: Schematic diagram of the measuring instrumentation.

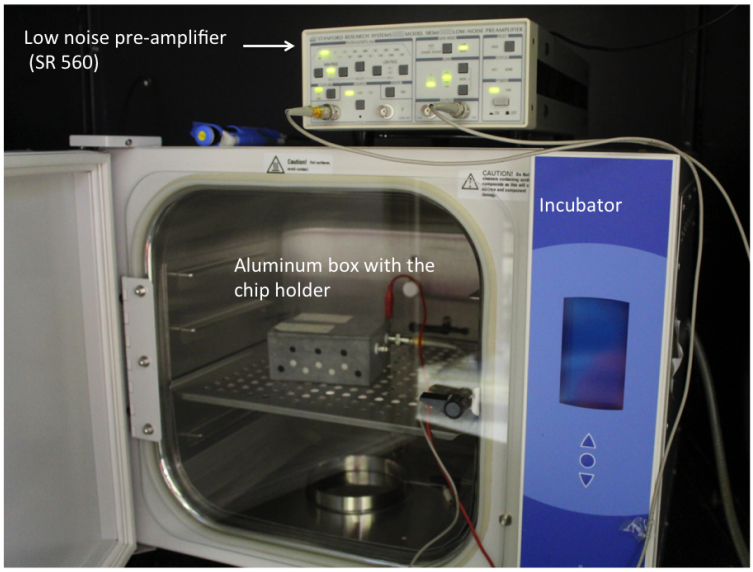

Figure 2.3: Photograph of the pre-amplifier and the incubator.
The all system is inside the Faraday cage.

The basic instrumentation used in the experiments is comprised of the following instruments:

(i) **Sensing electrodes:** The recording electrodes were made of thin films of gold deposited on plastic, silicon and on glass substrates. One of the electrodes is used as sensing electrode and the other as reference or counter electrode. The counter or reference electrode is connected to the ground terminal of the pre-amplifier. The area and geometry of the electrodes used were variable. In this thesis, interdigitated, square and round geometries were used. A silver wire immersed in the cell culture medium can also be used as a reference electrode;

(ii) **Chip holder:** The chip holder is a structure designed to establish electrical connections to the sensing electrodes and to hold the cell culture medium. Often the chip holders used conventional petri-dish in their structure to keep the electrolyte medium;

(iii) **Shielding and grounding:** Interference signals are captured by a Faraday cage, which is grounded to an external and dedicated ground (independent of power electrical network);

(iv) **Signal amplification and recording:** The first stage of amplification is carried out by a low noise pre-amplifier from Stanford Instruments, the SR 560. This instrument is battery operated and therefore isolated from the building electric network. A dynamic signal analyzer, the Agilent 35670 A, carries out the second stage of amplification and processing. This instrument collects the signals from the pre-amplifier. To minimize

drift, the current amplifier is calibrated and the set-up is stabilized for at least 30 minutes hours before measuring;

(v) **Impedance analyzer:** A Fluke 6406 is used to measure both the resistance and the capacitance as function of the frequency from 60Hz up to 1MHz;

(vi) **Pico-ammeter voltage source:** This instrument is used to perform quasi-static current voltage loops. These loops are dominated by the displacement current across the electrical double-layer capacitor and therefore they can be used to determine the quasi-static capacitance;

(vii) **External electric-optical stimulus module:** This module is comprised of a programmable waveform generator, an LED and a Peltier element. The signal source can apply voltages wave forms to The LED can expose the sample to light pulses and the Peltier can heat or cool the cell medium;

2.3 Sensing electrodes

Several types of sensing devise have been used in this work. Each device is made of different materials and designs. The flat substrate where the electrodes are made is then incorporated in a structure to hold the device, to provide the electrical connections, and to support the cell culture medium (chip holder). Figure 2.4 shows a typical chip holder. The sensing substrate is placed under the petri-dish, which is perforated so the cell culture medium is in direct contact with the sensing surface.

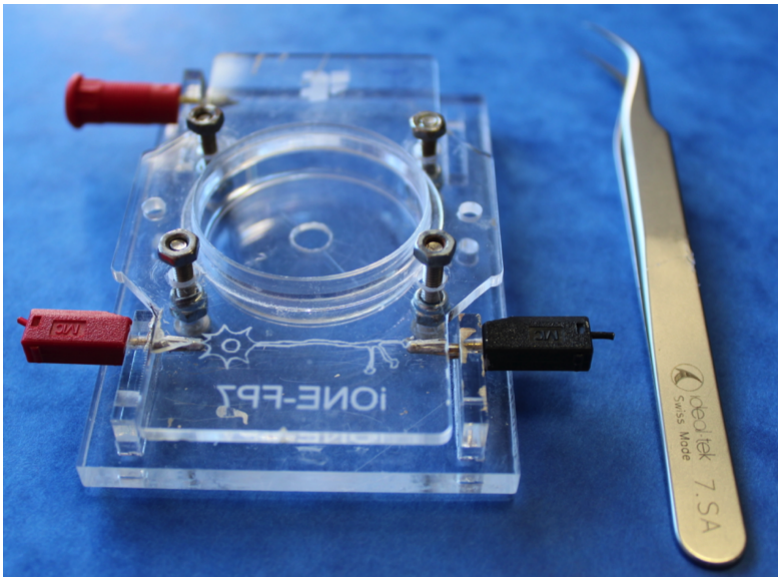

Figure 2.4: A typical chip holder structure making use of a standard petri-dish to hold the cell culture medium.

In this thesis, 3 types of sensing devices were used. These devices were named “Mushroom”, “PHILIPS” and “IBIDI”. The name “Mushroom” originates from its nano-structured surface, which is comprised of an array of micro features with a mushroom shape. The named “PHILIPS” and “IBIDI originated from the company fabricating them. Below, we outline the major and relevant features of each type of device.

(i) Mushroom device:

The Mushroom device was fabricated by Mónica Cerquido, Instituto de Nanociências e Nanotecnologia, Universidade do Porto (Departamento de Física) in the laboratories of Prof. João Ventura. The fabrication details of the mushroom like structures can be found in the work by Mónica Cerquido [1]. The gold surface is micro structured with an array of mushroom like shapes also made of gold. These structures were made in purpose to enhance the surface-active area in contact with the cells. Figure 2.5 shows a scanning electron microscopy photograph of an array of

mushrooms on top of a gold surface. The micro-structure density is 4753 mushrooms per mm^2.

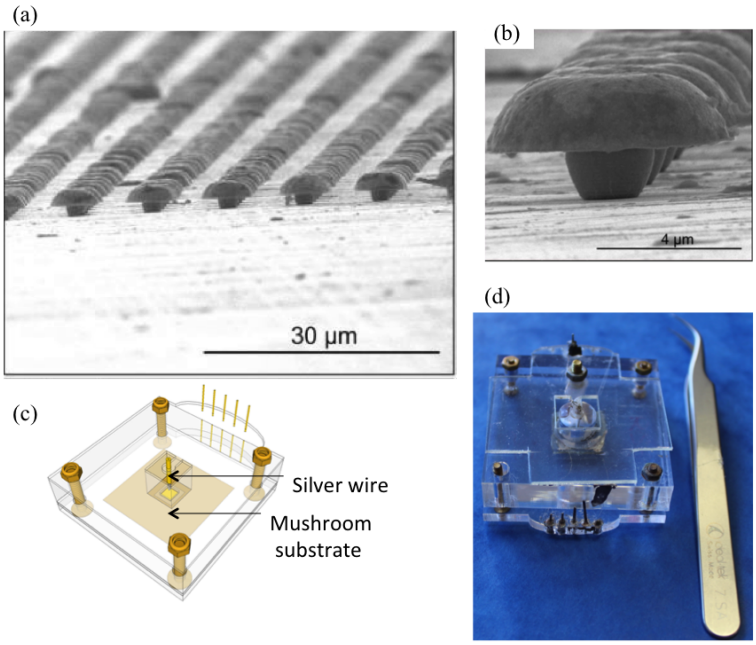

Figure 2.5: Mushroom device. (a) Scanning electron Microscopy photograph of an array of micro-mushrooms. (b) Photograph of an individual mushroom. (b) Schematic diagram of the substrate holder. (d) Photograph of the real assembled device. The SEM photo were reproduced from Mónica Cerquido thesis, see reference [1].

(ii) PHILIPS device:

PHILIPS devices were made at PHILIPS Research Laboratories in Eindhoven, Netherlands, in collaboration with the group of Dago de Leeuw. These devices have an interdigitated structure as represented in Figure 2.6. They are two co-planar, parallel gold fingers deposited by thermal evaporation on top of a thermal oxidized silicon wafer. The relevant electrode dimensions are the electrode width (W), the inter-electrode distance (g), and the electrode length (l). The device used in this thesis had the following dimensions; W = 5µm, l = 1000µm and g = 10µm. Each device has 10 interdigitated fingers. The vessel to hold the cell culture medium is fabricated using a PMMA compartment attached to the silicon surface by bio-compatible glue. To avoid cell culture medium evaporation, the vessel is loosely covered with a lid. This procedure makes sure there is enough cell culture medium to keep the cells alive over more than 24 hours without change of medium.

Due to the small dimensions this chip holder has a set of electrical contacts using springs that connect to the gold pads on the chip as seen in Figure 2.6 (e).

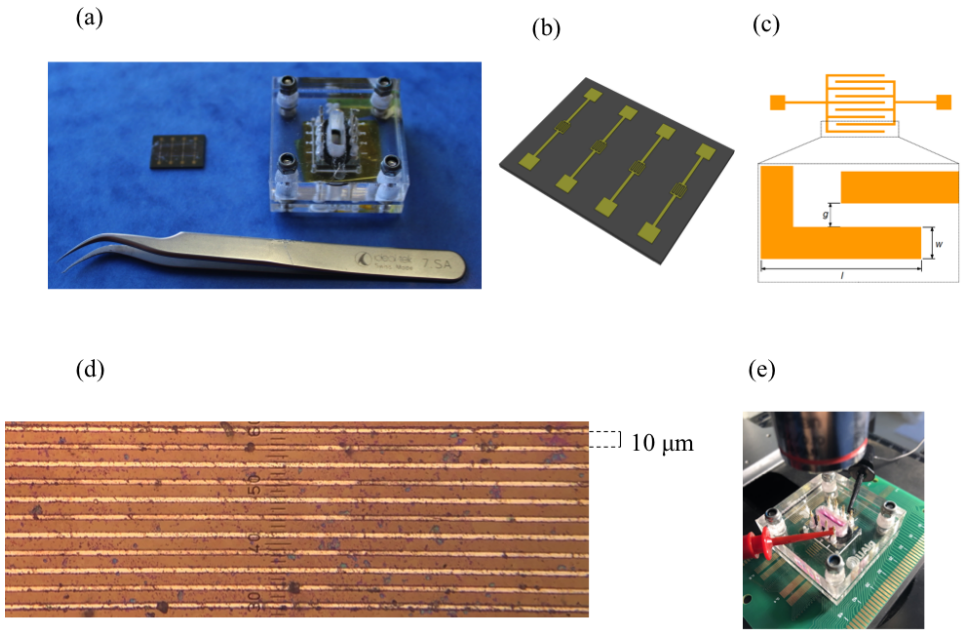

Figure 2.6: PHILIPS device. (a) On the left is photo of a silicon substrate with 4 sensing devices and on the right a photo of the device assembled on a chip holder. (b) Schematic drawing of silicon substrate with 4 interdigitated devices. (c) Dimensions of the interdigitated electrode array W = 5µm, l = 1000µm and g = 10µm. (d) photograph of the gold sensing tracks on a single device. (e) Device assembled and mounted under an optical microscope.

(iii) IBIDI device:

The IBIDI device is commercialized by Applied Biophysics (in USA) and by IBIDI (Germany) in Europe. Two type of electrode designs were used an interdigitated array and circular electrode geometry. In a similar way as the PHILIPS based device, the electrode structure is also interdigitated electrode array geometry. Both designs are show in Figure 2.7. The dimensions of the interdigitated electrode array are significant larger than the PHILIPS based device. The dimensions of the interdigitated IBIDI device are the following ones W = 100µm, l = 3254µm and g = 325µm.

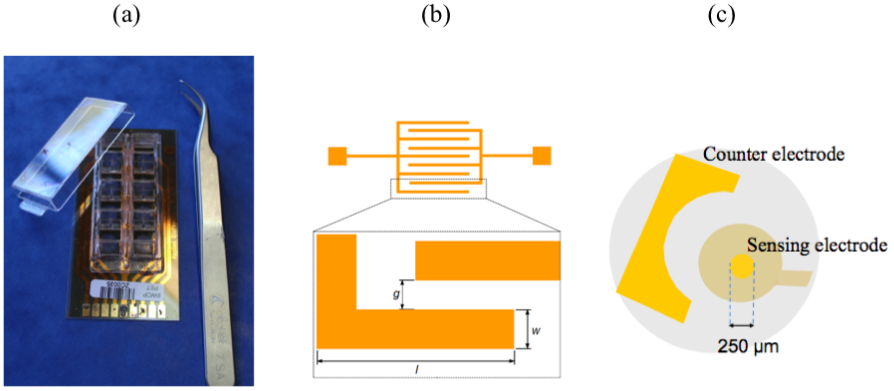

Figure 2.7: IBIDI sensing device structure. (a) Photograph of an IBIDI sensing devices, (b) schematic diagram showing the interdigitated electrode geometry used. l = 3254µm, w = 100µm g = 325µm. (c) Design structure and dimensions of a circular IBIDI device geometry.

2.4 Small signal impedance measurements

Once the electrodes are mounted on the chip holder, the sensing electrodes are electrical characterized. The characterization of the impedance as function of the frequency is a crucial aspect of the measurements. The impedance of the sensing electrodes in contact with the cell culture medium is measured using an impedance analyzer (Fluke PM 6306) in the frequency range from 60 Hz to 1 MHz. The first objective of an impedance characterization is to assure that electrical connections are not faulty, the second objective is to inspect for the low frequency capacitance and resistance. A relatively high capacitance is desirable, because it provides a low impedance path for the bio-electrical signals.

The electrodes immersed into an electrolyte solution (cell culture medium) behave as a parallel RC circuit as shown in Figure 2.8. The impedance analyzer assumes that the sample (electrode) is indeed a parallel RC circuit. The impedance analyzer measures the parallel capacitance (C_P) and the parallel resistance (R_P). These two impedance parameters are related with internal structure of the sensing device.

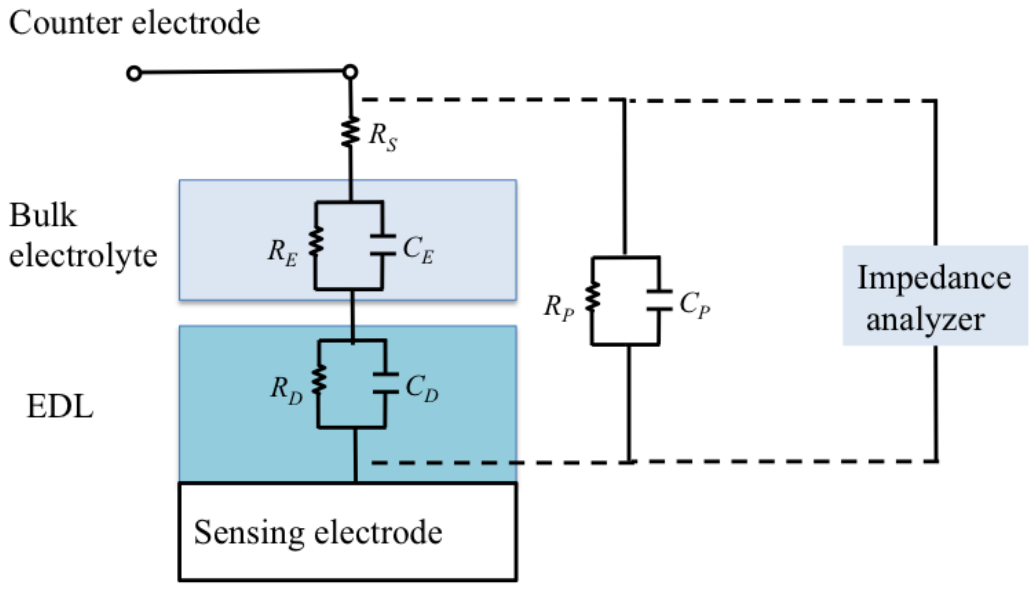

Figure 2.8: The equivalent electrical network used to model the electrodes immersed into the cell culture medium. C_P and R_P are the parameters measured by the impedance analyzer. C_D and R_D are the parameters of the electrical double-layer and C_E and R_E the impedance parameters of the bulk electrolyte.

The entire system is in fact comprised of two distinct regions, the electrical double-layer (EDL) near the sensing electrode and the rest of the volume of the solution which we designed here as a bulk electrolyte. The bulk layer is in series with the electrical double-layer (interfacial layer). A parallel equivalent network can be used to describe each layer.

The EDL is due to the polarization of the interface; therefore it has a very high capacitance and resistance. When compared with the EDL, the bulk electrolyte region and has a relatively low resistance (determined by the electrolyte) and also a relatively low capacitance (determined by the distance and between the electrodes as well as by the area). Figure 2.8 outlines the basic relations between the impedance parameters measured and the device physical structure.

2.5 Noise and interference

The first relevant aspect about the measuring system is related with the specifications required to measure ultra-weak signals. The detection limit of our electrical systems must only be limited by intrinsic noise sources. Since noise plays an important role, it is important to review some of concepts about electrical noise in electrophysiological recording systems.

Basically, there are two types of noises; (i) the extrinsic noise, and the (ii) intrinsic noise. The extrinsic noise is generated outside of our measuring apparatus and is somehow coupled into our measuring system. An example of an extrinsic noise sources is the 50Hz signal from the main electrical power: Other sources of extrinsic noise are signals generated by nearby operating equipment (for instance fans, and switches), triboelectric effects caused by the presence of persons moving in the proximity, mechanical vibrations in the building and mechanical vibrations or pressure exerted in the cables.

The extrinsic noise sources must be careful eliminated by using shields and ground techniques. For this reason we use a large Faraday case with a dedicated and independent (from the power electrical network) ground. Inside the Faraday cage is placed the sensitive part of the instrumentation, the chip holder, and the low noise pre-amplifier. The chip holder must be kept under an atmosphere of 5% of CO_2 and at the temperature of 37 ºC, provided by a cell incubator. The entire system, chip holder, pre-amplifier and cell incubator must be kept inside the Faraday cage.

The electrical noise is also evaluated. Firstly, the magnitude of the 50 Hz interference is assessed. If 50 Hz interference is too high, the wiring of the chip to the low noise amplifier must be inspected. Secondly, rearranging the electrical connections also eliminates all spurious signals. A common spurious source of signals in the frequency between 14 Hz and 22 Hz. We believed this interference is caused by nearby operating instrumentation. After the elimination of the electrical interference, the power spectrum of the noise is measured. From the noise we can determine the detection limit of the sensing electrodes and evaluate if the electrodes are suitable to perform the planed electrophysiological measurements.

Having describing the methods used to minimize the external noise sources, we proceed with the analysis of the intrinsic noise sources. The intrinsic noise is essential of two types; (i)

thermal noise generated by passive elements (resistances) and (ii) the 1/*f*, also named pink noise.

The first strategy to minimize the intrinsic noise is to use a low-noise pre-amplifier. We will show that in our recording system the noise of the SR 560 is lower than the noise generated by the sensing electrode. Therefore, our fundamental level of detection is limited by the noise generated by the electrode. The noise of the amplifier depends on the bandwidth used. Figure 2.9 shows the noise of the SR 560 as function of the frequency. The amplifier's input voltage noise approximates that of a 1000 Ω resistor (about 4 nV/√Hz). Notice that the voltage noise rises at lower frequencies (1/*f* noise).

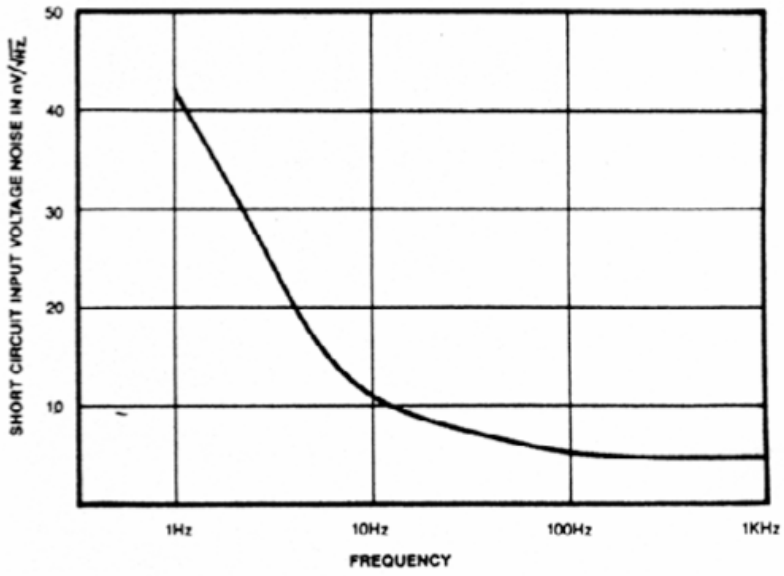

Figure 2.9: Frequency dependence of the SR 560 input voltage noise. Figure reproduced from the user manual of the SR 560 (Stanford Research Systems) [2].

The thermal and pink noise generated by the electrodes immersed into the electrolyte solution (cell culture medium) is significant higher than the noise generated by the amplifier. Therefore, the efforts to minimize the intrinsic noise should be focused on the design of the sensing electrodes.

In summary, to eliminate extrinsic noise sources we used shields. To minimize the intrinsic noise we pay attention to the design of the electrodes. The 1/*f* type of noise (also know as pink noise) appears at very low frequencies (f<10Hz). This type noise is caused by electrochemical reactions continuously occurring at the electrode/electrolyte interface. Chemical species are continuously exchanging electrons with the electrodes. If the ionic exchanges are controlled by a

diffusion process, the noise has frequency dependence of the type $1/f$, if the ionic exchange is controlled by an electrical field, the noise has a frequency dependence of the type $1/f^2$.

The 50 Hz interference also known as power line interference is very difficult to remove. It may be removed using filters. The easiest is to create a notch filter, which basically involves taking the FFT of the signal, zeroing out the Fourier coefficients around 50 Hz. However, it is only convenient to do this in the processing stages of the data. In a real experiment the 50 Hz interference must be minimized. The best way to minimize the 50 Hz interference is to use all the instruments decoupled from the building electric power supply. This can be done if the instruments have the facility to operate with a battery, or using special transforms to decouple the 50 Hz of the electrical network. In our set-up only the pre-amplifiers are battery operated.

Vibrations from the building are caused by people walking, road traffic in the vicinity, falling objects, and small cracks. Vibration in buildings are typically below 10 Hz therefore, they fall in the frequency band were typical signals from non-electrogenic cells are recorded. Particular care should be taken to eliminate them. The best strategy is to mechanically decouple the entire measuring system from the building.

2.6 Data acquisition

To visualize and to process the data recorded from the signal analyzer, a home made program implemented in Matlab was used. This program named “RC software”, was implemented by Pedro Inácio (unpublished work). Basically, this application allows us to visualize on real time, the data, both on the time domain as well as on the frequency domain. Figure 2.10 shows a screen shot of the front-end menu of software developed. The user may set all the measurement parameters, such as frequency bandwidth, the resolution and the gain of the amplifier. The RC software also allows the user to see all the history of the measurements.

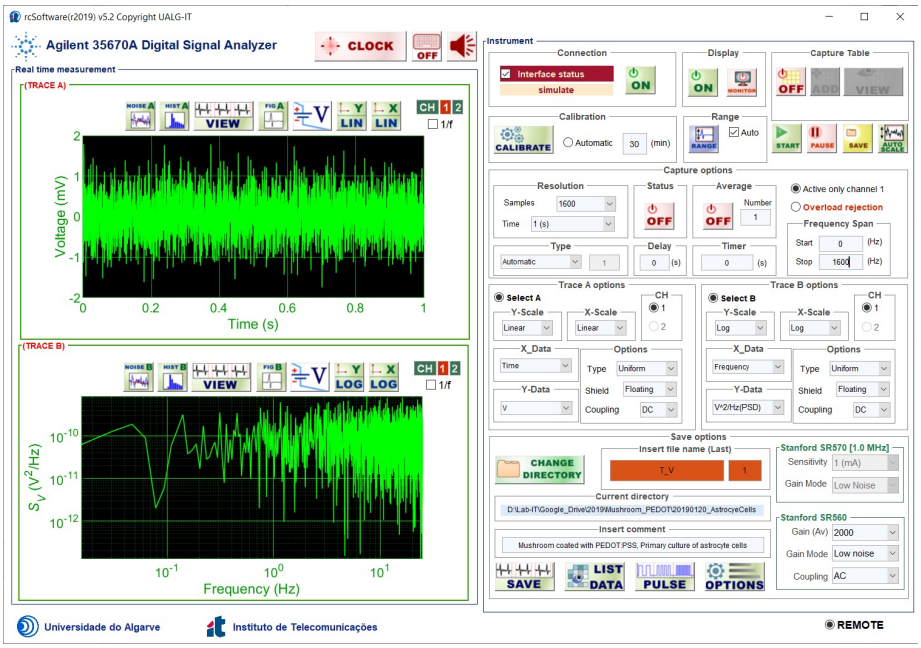

Figure 2.10: RC software application developed by Pedro Inácio (unpublished) for processing and visualizing data in real time.

2.7 Biological cells

In research, scientists routinely use cell lines as a model for healthy or diseased tissue. Two types of cells were selected (i) immortalized cell lines and (ii) primary cell cultures. An immortalized cell line is a population of cells from a multi-cellular organism, which would normally not proliferate indefinitely but due to mutation, can keep undergoing division and can, thus, be cultured over several generations. The mutations required for immortality can occur naturally or be intentionally induced for experimental purposes. There are many advantages to using immortalized cell lines. Because these are standard lines used by many different labs, immortalized cells are well characterized. They are, at least theoretically, homogeneous, genetically identical populations, which aid in providing consistent and reproducible results. Primary cells are isolated directly from tissues and retain the morphological and functional characteristics of their tissue of origin. For example, original tumor tissue from a glioblastoma preserves several tumor markers and known microRNAs. In comparison, immortalized cell lines display differences in their expression. In this thesis we use commercial available cell lines named C6 and U87. The C6 are cells derived from Rat brain tumour (glioma) and provided from American Type Culture Collection (ATCC). The U87 cell lines they derive from a human brain tumor (Glioblastoma astrocytoma). Both C6 cells and U87 cells are available from Sigma-Aldrich. This thesis also reports data obtained in primary cell lines. These cells were extracted by human biopsy-derived High-Grade Glioma (HGG) at the Faro hospital. In this thesis these cells are named HOPE cells.

Below we describe the basic aspects related with the culture of these cells:

- C6, cells line: glioma cells with high mobility cancerous cells, useful for cells migration research. These cells are cultivated in F-12 K nutrient mixture supplemented with 15% fetal horse serum, 2.5% fetal bovine serum, and 1% penicillin and streptomycin. The cells were harvested from the culture plates and diluted in culture medium to yield cell suspensions with a known cell density and transferred to the sensing devices.

- U87, primary cells: human glioma cell line cultured in EMEM supplemented with 10% of fetal bovine serum (FBS) and 1% penicillin and streptomycin. The cells were cultured from the culture plates and diluted in culture medium to obtain cell suspensions with a known cell density and transferred to the sensing devices.

- **HOPE, primary cells:** Primary culture extracted by human biopsy-derived High-Grade Glioma (HGG) were cultured. Cells were cultured in DMEM medium with 10% FBS and 1% Penicillin-streptomycin. The passage of this cell lines is done approximately once per week, when cells achieve 80% confluence.

2.8 Experimental procedures

2.8.1 Electrical procedures

Figure 2.11 shows how the voltage pre-amplifier is connected to the sensing electrodes. One of the electrodes is connect to the ground terminal of the amplifier. This electrode is referred as counter or reference electrode. The other electrode is connected to the amplifier and it is named sensing electrode.

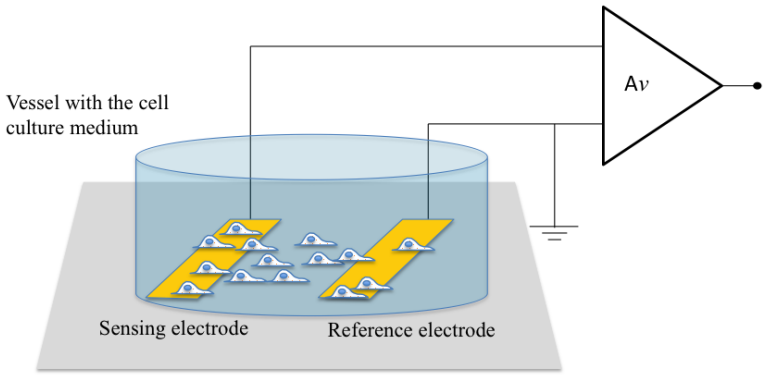

Figure 2.11: Schematic diagram showing how the low noise voltage amplifier is connected to the electrodes.

When small voltages signals are measured in electrolyte systems, we have to keep in mind that the electrode is polarized by an electrical-double-layer (EDL). The EDL behaves as a leaky capacitor and stores charges. The stored charge generates and internal field (voltage) that varies with time and is picked up by the amplifier as a DC offset. The DC offset may be large and if not removed, it may saturate the amplifier or impose severe limitations to the amplifying capability of the pre-amplifier.

The DC offset was removed by adjusting a tuning capacitance using the front-end offset potentiometer of the SR 560 amplifier. Also the amplifier must be set to ac coupling.

When measuring cells we have a roughly feeling for the type of signals we would expect to measure. This initial guess will allow us to define the bandwidth to be selected to start the experiment. Basically, we have access to 16 time windows, as show in Table I. For each time span we can also fix the number of data points that will be taken. This is basically the resolution of our measurements and can be fixed from 400 data points up to 1600 data points per frequency window selected. For instance, if we select our time window in 32 seconds with a resolution of 1600 data points we fix the range of frequency between 25.25 mHz up to 50 Hz (see Table I). For non-electrogenic cells

measure in this thesis, we use temporal windows of 64s 126s and 256s. Therefore, we only record signals below 25 Hz.

There are situations were we use the entire frequency bandwidth of the amplifier (1 MHz). For instance when we characterize the intrinsic noise of the sensing electrode. To access the full bandwidth with a proper resolution we have to divide the entire frequency spectrum into smaller intervals. We measure each interval with a maximum resolution (1600 data points) and also using average. After averaging in all the frequency spans, all the spectrum recorded are glued to reconstruct the full power spectrum density of noise over the entire bandwidth.

Table I: Range of frequency bandwidths and resolutions that can be set in the signal analyzer, Agilent 35670. Extracted from the Master thesis by Inácio, Pedro Miguel Cavaco Carrilho dos Santos, "Electrical characterization of electronic interfaces to communicate with electrogenic cells in vitro" http://hdl.handle.net/10400.1/6051 [2,3]

Time window	**Frequency range**				
	Number of samples	**200**	**400**	**800**	**1600**
	f_{start}	f_{stop}	f_{stop}	f_{stop}	f_{stop}
1024 *s*	0.977 mHz	195 mHz	390.6 mHz	781.25 mHz	1.5625 Hz
512 *s*	1.95 mHz	390.6 mHz	781.25 mHz	1.5625 Hz	3.125 Hz
256 *s*	3.906 mHz	781.25 mHz	1.5625 Hz	3.125 Hz	6.25 Hz
128 *s*	7.8125 mHz	1.5625 Hz	3.125 Hz	6.25 Hz	12.5 Hz
64 *s*	15.625 mHz	3.125 Hz	6.25 Hz	12.5 Hz	25 Hz
32 *s*	31.25 mHz	6.25 Hz	12.5 Hz	25 Hz	50 Hz
16 *s*	62.5 mHz	12.5 Hz	25 Hz	50 Hz	100 Hz
8 *s*	125 mHz	25 Hz	50 Hz	100 Hz	200 Hz
4 *s*	250 mHz	50 Hz	100 Hz	200 Hz	400 Hz
2 *s*	500 mHz	100 Hz	200 Hz	400 Hz	800 Hz
1 *s*	1 Hz	200 Hz	400 Hz	800 Hz	1.6 kHz
500 *ms*	2 Hz	400 Hz	800 Hz	1.6 kHz	3.2 kHz
250 *ms*	4 Hz	800 Hz	1.6 kHz	3.2 kHz	6.4 kHz
125 *ms*	8 Hz	1.6 kHz	3.2 kHz	6.4 kHz	12.8 kHz
62.5 *ms*	16 Hz	3.2 kHz	6.4 kHz	12.8 kHz	25.6 kHz
31.25 *ms*	32 Hz	6.4 kHz	12.8 kHz	25.6 kHz	51.2 kHz
15.625 *ms*	64 Hz	12.8 kHz	25.6 kHz	51.2 kHz	102.4 kHz
7.8125 *ms*	128 Hz	25.6 kHz	51.2 kHz	102.4 kHz	
3.90625 *ms*	256 Hz	51.2 kHz	102.4 kHz		

Figure 2.12: Frequency range table of data acquisition time window.

2.8.2 Cell handling and seeding on the sensing device

All the sensing electrodes were coated with a thin polymer layer know as Poly-L-lysine. Poly-L-lysine is a polymer used to promote cell adhesion to solid substrates. The entire system including the chip holder was sterilized under UV for approximately 15 minutes. The cells were harvested and typically 50,000 cells were transferred to the sensing device in 400 µL of medium. The cell suspension generated a confluent mono-layer of cells that covered the entire device surface.

References

1. M. Cerquido, Fabrication of biocompatible gold mushrooms-shaped microelectrodes for the recording of neuronal signals, (2016). https://sigarra.up.pt/fcup/pt/teses.tese?P_ALUNO_ID=105069&p_processo=23810.

2. L. Preamplifier, MODEL SR560 preamplifier, Stanford Res. Syst. 0 (2013). https://www.thinksrs.com/downloads/pdfs/manuals/SR560m.pdf.

3. P. Miguel, C. Carrilho, Electrical characterization of electronic interfaces to communicate with electrogenic cells in vitro, (2013).

Chapter 3

Library of discrete signals

A well-defined set of discrete signals were recorded and identified in cell populations. Signals were classified and named according to their characteristic shape. For each signal shape, it is analyzed the amplitude, the duration, and the area under the signal.

3.1 Introduction

Cell activity is often characterized by burst of signals comprised of individual and well-defined signals. Figure 3.1 shows a typical time trace with signals recorded in a HOPE cell population using an IBIDI Circular device. This chapter classifies the individual signals accordingly on their shape and properties. For example, a biphasic signal with a fast upward component followed by a slow downward component is named “Biphasic Fast Upward” with the acronym BFUp.

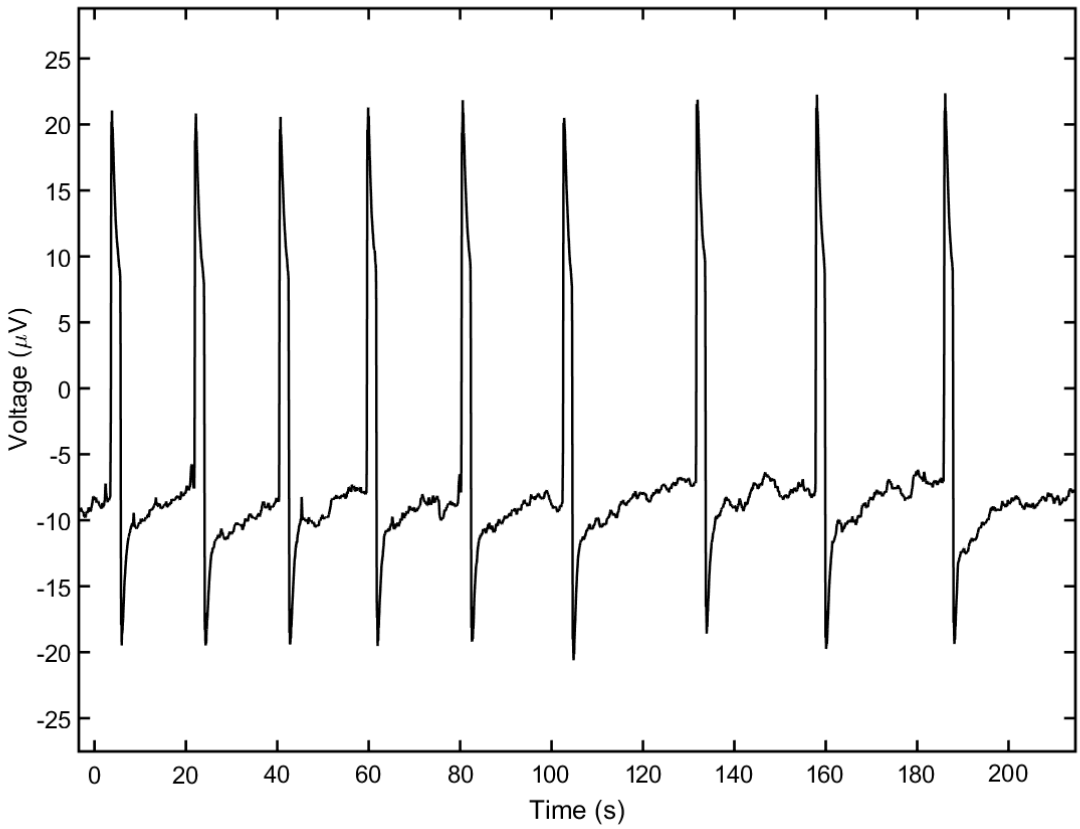

Figure 3.1: Time trace of signals named Square-Like (SL). Square-Like signals were recorded in HOPE type of cells using an IBIDI Circular device.

To the best of our knowledge, there are no reports in the literature about electrophysiological signals generated by populations of non-excitable cells and recorded using extracellular electrodes. The few observations of this type of signaling mechanism reported in the literature rely on optical fluorescence methods. Optical signals differ from electrical ones, because they only have an upward component. This means all the optical signals are monophasic while electrical signals as the ones presented here can be biphasic. Therefore, a direct comparison between electrical and optical signals is not easy.

This chapter starts by proposing a classification for the several signals shapes observed. Each signal is named according to its shape. Then, for each signal shape, we quantify the basic shapes features, namely, the relation between duration and signal amplitude. For biphasic signals, the relation between the upward and the downward component is also studied. A detailed analysis of all the data is presented in the Annex I. This chapter only shows a few representative graphs of the behavior observed. Finally, in the Discussion section we tentatively established a relation between the recorded signals and some known biological process.

3.2 Results

3.2.1 Classification of signals

Each individual signal is characterized by a number of parameters, namely, amplitude, duration, area under the signal. As it will be explained later, the signal area is expected to be proportional to ionic flow across the cell membrane. Signals were recorded in a variety of cell populations (C6, HOPE, U87 and N2A).

Figure 3.2 shows all the signals shapes recorded. The signals were named according to their shapes. The signal shapes were characterized by a number of parameters. These parameters are; downward peak voltage (V_D), downward component duration (t_D), downward peak area (A_D), upward peak voltage (V_U), upward component duration (t_U) and upward peak beneath area (A_U).

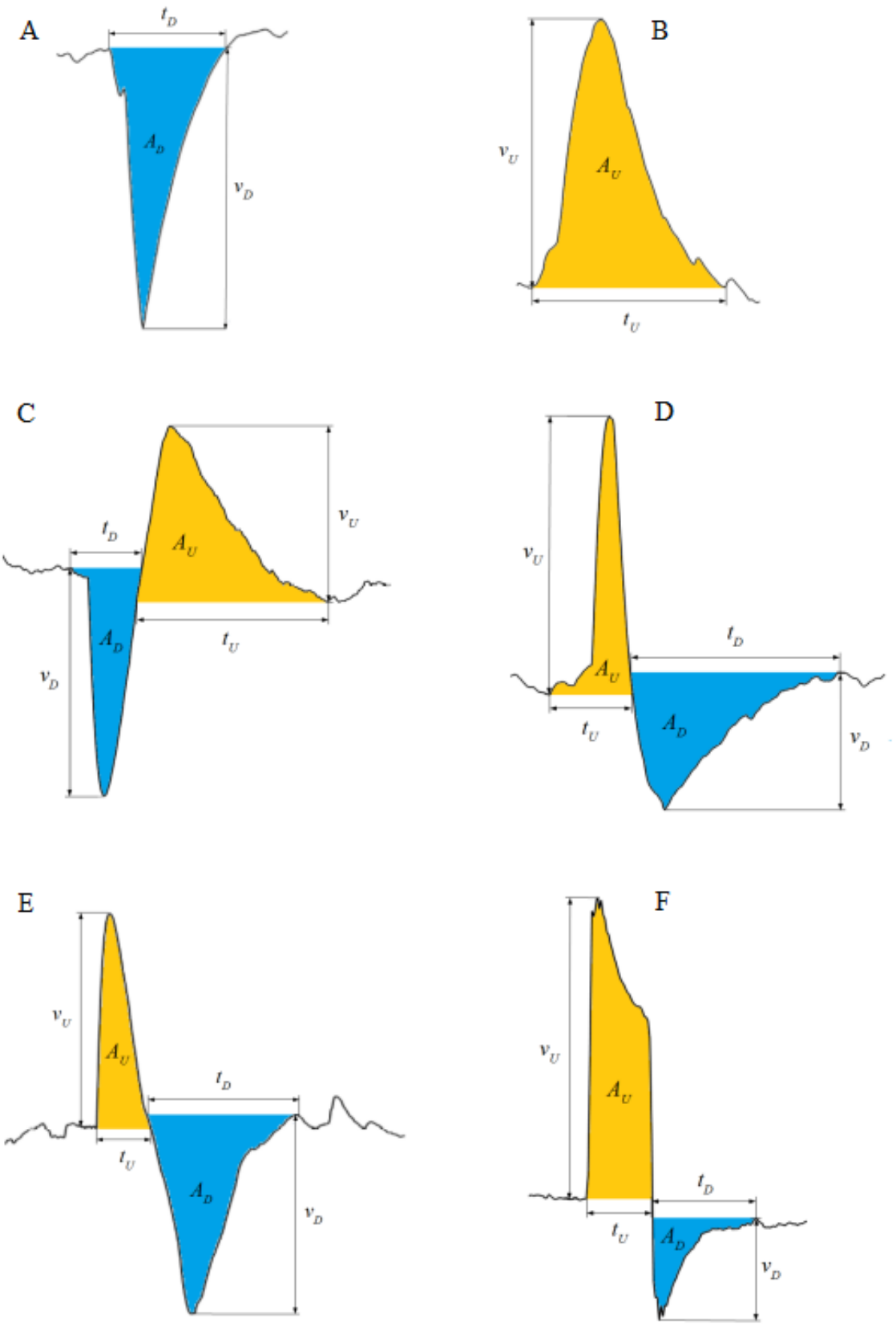

Figure 3.2: Discrete signals observed over successive timelines while recording different cell lines, C6, HOPE, U87, and N2A, in several sensing devices.

Table I provides a list of all the signals shapes, including, their designation, their acronym and in the cell type where it was recorded.

Table I: Signal shapes recorded in different cell types studied and its metrics/parameters/ratios. According to the data presented on Table I, HOPE cells exhibit all the different types of signal shapes. However, N2A only shows the BFUp type of signal. The U87 cell line only generates biphasic signals.

Figure 3.1 signal display			**Signal metrics**					**Cells**			
Signal	**Designation**	**Acronym**	V_U/V_D	t_U/t_D	A_U/A_D	V_D/t_D	V_U/t_U	**C6**	**HOPE**	**U87**	**Neurons (N2A)**
A	Monophasic Fast Downward	MDown				X		X	X		
B	Monophasic Fast Upward	MUp					X	X	X		
C	Biphasic Fast Downward	BFDown	X	X	X			X	X	X	
D	Biphasic Fast Upward	BFUp	X	X	X			X	X	X	X
E	Biphasic Symmetric	BS	X	X	X			X	X		
F	Square-Like	SL	X	X	X				X		

3.2.2 Characterization of signal shapes

Assuming that signals are a result of a synchronized cell activity, two important predictions can be made. These predictions are outlined below:

- The first prediction can be formulated as follows; the signal power should be proportional to the electrode sensing area. This relationship is expected because large sensing areas probe a higher number of cells. Another way to formulate this prediction, is to say that the longer the signal, the higher the amplitude.
- The second prediction is related with the signal shape. A particular signal should always have similar ratio between upward and downward component. This ratio should be independent of the signal amplitude. In other words, we may have a distribution of signal amplitudes, from very weak to strong signals, but the signals should exhibit an identical ratio between the upward and downward signal components.

In order to inspect if the two predictions outline above, are experimentally observed, we plot several relationships between signal properties. Figure 3.3 shows the amplitude of the upward component versus and the downward signal amplitude. The signal under analysis is a BFUp signal measured in a Mushroom type of device. The straight line fitting the data points has a slope of 1.8. Basically, this plot shows that for the BFUp signals the upward component scales up with the downward component.

The experimental data points were fitted with a linear regression according to equation (1):

$$Parameter\ y = m\ (Parameter\ x) + b\ (\pm e) \qquad (1)$$

where m is the slope of the straight line, b the intercept at the origin, and e the error.

Figure 3.3 plots the duration of each signal component. The duration of the upward component scales up with the duration of the downward component. Figure 3.4 plots the areas of the signal components. The area of the signal is in volts per second. Later we will show that can be related with the charge. Again, the higher the area of the upward component, the higher is the area of the downward component. In Figure 3.4 the constant of proportionality is 1. Figure 3.5 plots the area of the upward component *versus* the area do the downward component for a BFUp signal, recorded on N2A type of cells. In this case, the two components are related with a constant of proportionality of 0.5.

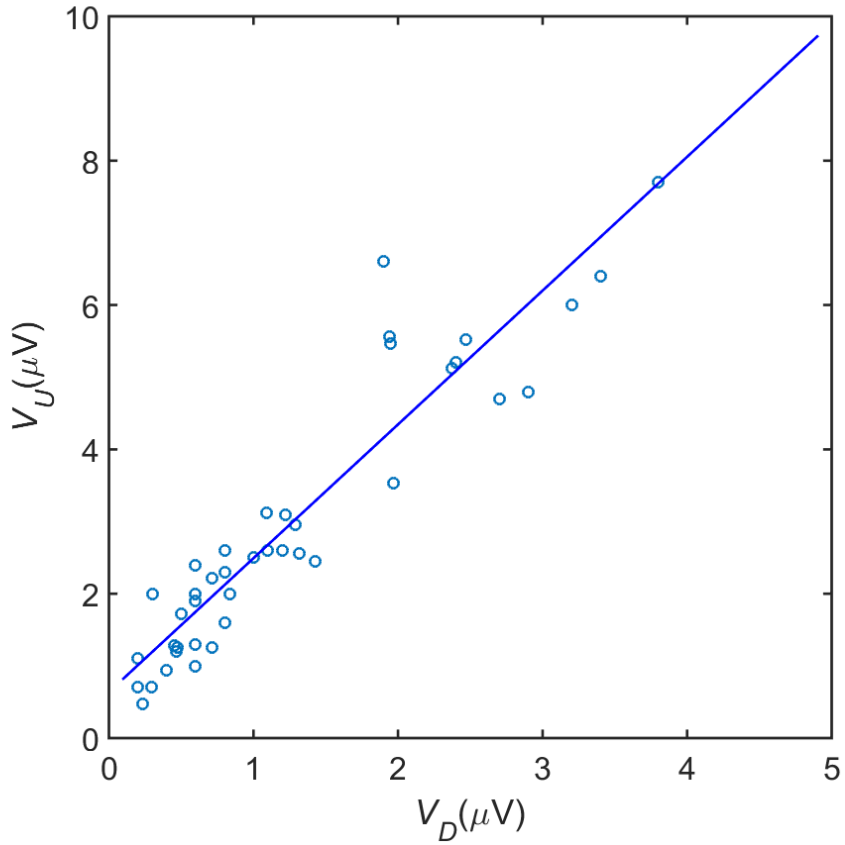

Figure 3.3: Relationship between the amplitude of the downward spike V_D and the amplitude of the upward spike V_U in a BFUp type of signal. The data is for C6 BFUp signals and it was measured using a Mushroom sensing device. The straight line passing trough the experimental data points is a minimum squares fit, it has a slope close of 2, and the full equation is $V_U \sim 1.85V_D + 0.64$ (±0.23).

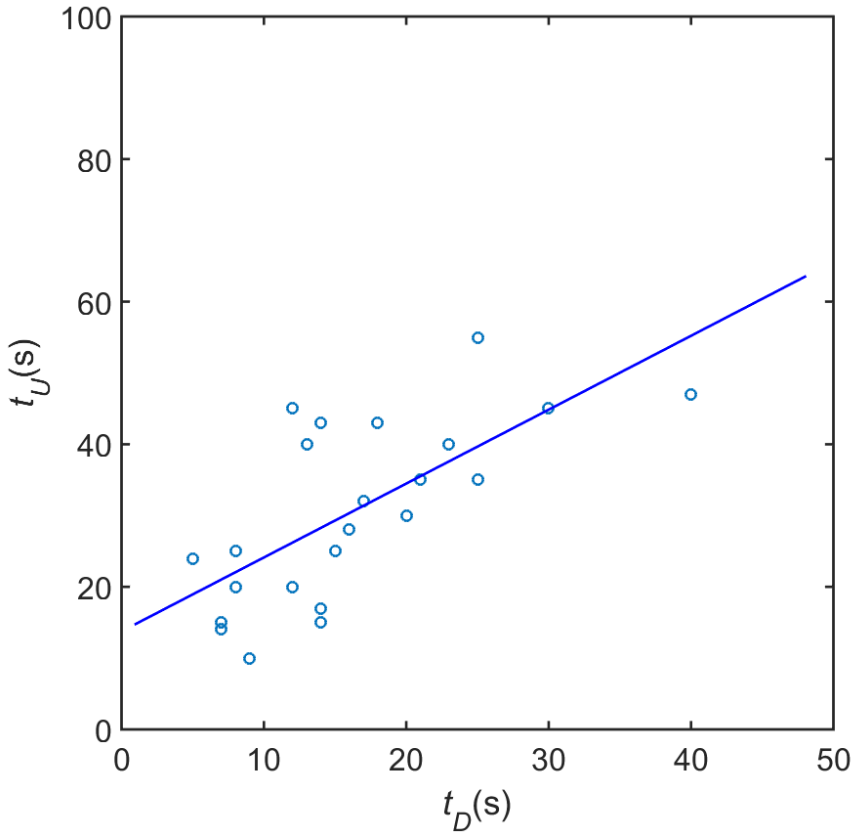

Figure 3.4: Relationship between the time duration of the downward spike t_D and the amplitude of the upward spike t_U in BFDown signals. The data was measured in HOPE cells using a Mushroom device. The straight line passing trough the experimental data points is a minimum squares fit, its slope is close of 1 but with large offset. Its equation: $t_U \sim 1.04t_D + 13.76$ (±0.5).

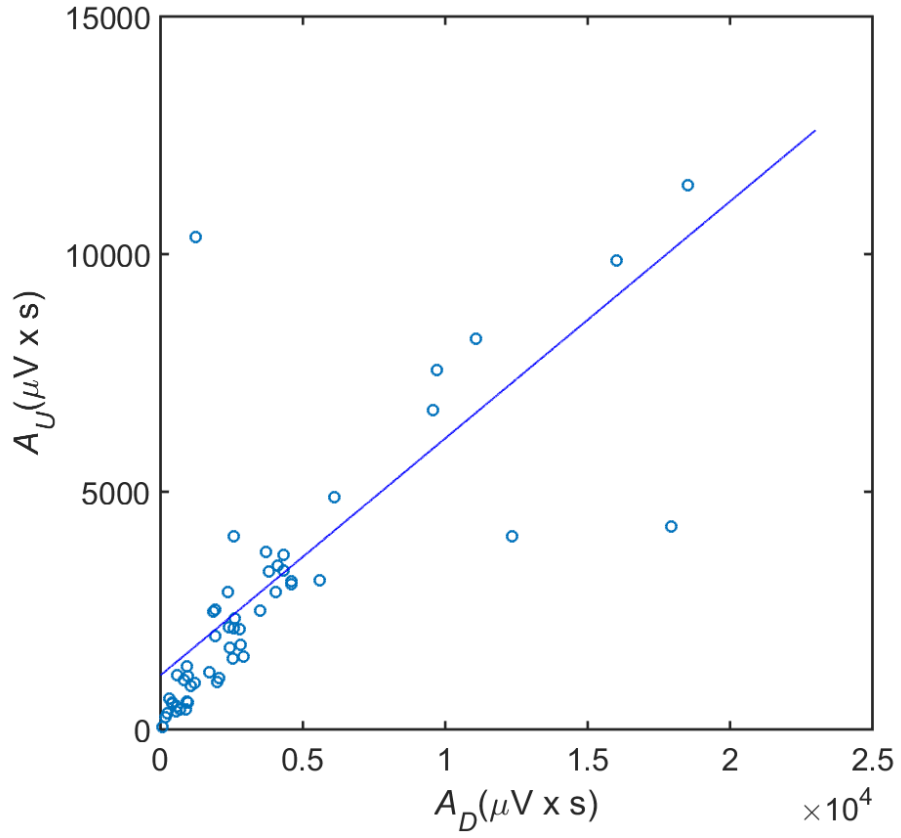

Figure 3.5: Relationship between the area of the downward spike A_D and the area of the upward spike A_U in BFUp signals shapes, when measuring neurons in Mushroom sensing device. The straight line passing trough the experimental data points is a minimum squares fit and it has a slope close of 0.5 but with a very large offset. Its full equation is $A_U \sim 0.5A_D + 1.14 \times 10^3$ (±0.08).

We can observe very weak signals, or strong and long lasting signals, but their aspect ratio is kept constant. The plots also show the typical ranges of signals for a particular device. C6 signals can reach a maximum of 10 μV of amplitude in a mushroom device. A HOPE cell population can generate in a mushroom device signals as long as 80 seconds.

The purpose of the plots like the ones from Figure 3.3 to Figure 3.5 is to show the device capability to record signals in a particular cell population. For instance, a Mushroom device with C6 cells can provide signals with maximum amplitude of 8 μV approximately. The distribution of data points also shows the properties of the most frequency signals. For example, Figure 3.3 shows that most frequent signals have amplitudes of approximately 2 μV. Table II summarizes all the relationships obtained and their corresponding fitting parameters.

Table II: Summary of all relations between the signal parameters obtained using different cell types and different devices.

Cell type	Signal type	Spikes amplitude ratio	Spikes duration ratio	Spikes area ratio	Amplitude-Duration ratio	Sensing device
C6	MDown	----------	----------	----------	$v_D \sim 0.13t_D$+0.35	Mush
	MUp	----------	----------	----------	v_U ~0.01t_U +1.5	Mush
	BFDown	$v_U \sim 0.19v_D$ *+1.01*	$t_U \sim 1.4t_D$ *+11.74*	$A_U \sim 0.61A_D$ *+10.97*	----------	Mush
	BFUp	$v_U \sim 1.85v_D$+0.64	$t_U \sim 0.25t_D$ *+ 4.76*	$A_U \sim 1.09A_D$ *+ 1.71*	----------	Mush
	BS	$v_U \sim 1.16v_D$ *-0.05*	$t_U \sim 0.31t_D$ *-6.08*	$A_U \sim 0.44A_D$ *+ 5.44*	----------	Mush
Hope	MDown	----------	----------	----------	$v_D \sim 2.4t_D$ *– 80.2*	Mush
	MUp	----------	----------	----------	$v_U \sim 0.7t_U$ *+22*	Mush
	BFDown	$v_U \sim 0.29v_D$ *+5.18*	t_U ~1.04t_D*+13.76*	$A_U \sim 0.51A_D$ *+150.95*	----------	Mush
	BFDown	$v_U \sim 0.21v_D$ *+5.25*	t_U ~1.48t_D*+31.81*	$A_U \sim 0.54A_D$ *+202.8*	----------	IBIDI I
	BFUp	$v_U \sim 1.67v_D$*+87.51*	$t_U \sim 0.14t_D$*+8.6*	$A_U \sim 0.72A_D$*+430.94*	----------	Mush
	BFUp	$v_U \sim 2.36v_D$*+2.78*	$t_U \sim 0.42t_D$*+0.39*	$A_U \sim 1.59A_D$*+0.11*	----------	IBIDI C
	BFUp	$v_U \sim 1.67v_D$*+1.72*	$t_U \sim 0.3t_D$ *-0.67*	$A_U \sim 0.53A_D$ *-2.82*		IBIDI I
	BFUp	V_U *~1.75*V_D*+11.91*	$t_U \sim 0.25t_D$*+0.03*	$A_U \sim 0.7A_D$*+0.44*	----------	PH
	SL	$v_U \sim 0.07v_D$*+28.79*	$t_U \sim 0.36t_D$*+1.7*	$A_U \sim 1.28A_D$*+44.81*	----------	IBIDI C
U87	BFDown	$v_U \sim 0.44v_D$*-34.65*	$t_U \sim 0.06t_D$*+26.76*	A_U~1.34A_D*-843.14*	----------	Mush
	BFUp	$v_U \sim 1.5v_D$*+167.1*	$t_U \sim 0.17t_D$*+15.16*	$A_U \sim 0.28A_D$*+1.25e3*	----------	Mush
Neurons	BFUp	$v_U \sim 1.6v_D$*+115.74*	$t_U \sim 0.14t_D$*+12.17*	$A_U \sim 0.5A_D$*+1.14e3*	----------	Mush

Note that in Table II "Mush" is short name for the sensing device named Mushroom, "PH" stands for PHILIPS sensing device, "IBIDI C" is the term for IBIDI Circular sensing device, and "IBIDI I" stands for IBIDI Interdigitated. The following analysis is focused on biphasic type of signals because these signals are observed in all cell populations.

From the data presented on Table II we can draw, for each individual signal a number of conclusions outlined below:

(i) BFUp signal

The BFUp signal is observed in all types of device structures as well in all cell types. The BFUp signal is strongly asymmetric. The upward amplitude is approximately twice (v_U/v_D=1.77) the downward amplitude, but the upward component is very short. The downward component is approximately 4 times longer than the upward component. The ratio between the areas of each

signal component is approximately 0.7. These relations are relatively independent of the device geometry and cell type, suggesting that is signal common to all cancer cells.

(ii) BFDown signal

The BFDown signal was observed in mushroom and on IBID interdigitated device. These devices are characterized for being relatively large area devices. The downward component is typical 3.5 higher in amplitude than the upward component.

(iii) MDown and MUp signals

Monophasic signals, such as the MDown and the MUp were only analyzed on the mushroom device. Therefore, it was not possible to extract conclusions about the role of the electrode geometry on the signal aspect ratio.

Table II also shows the relation between the signal area. It is important to note here that the area under the signal is expressed in volts per second. We expect this area is proportional to the charge. The assumption is based on the following relationships:

$$I = \frac{Q}{t} = \frac{V}{R} \qquad (2)$$

here I is the current, Q the charge, V the voltage and R resistance.

Then we can re-write equation. (2) as:

$$V \times t = Q \times R \qquad (3)$$

$V \times t$ is the area under voltage signal, and assuming that R is a constant, then from equation (3) we can consider that the area under a voltage signal is proportional to the total amount of charge involved in the signal.

Knowing the amount of charge involved in a particular signal is helpful. The amount of charge may provide insight about the ion channels involved. Ion channels are specialized pores that transport charges across the cell membrane. When a channel is active some charge flows in and others flow out. A well-known example is the action potential. At the onset of the action potential the sodium channel opens and Na^+ moves into the cell. Because, sodium has a positive charge, so the neuron becomes more positive and becomes depolarized. Next, the potassium channels open. When they do open, potassium rushes out of the cell, reversing the depolarization. Also at about this time, sodium channels start to close. In summary, the action potential is generated by an inflow of Na^+ and an outflow of K^+ [1, 2, 3].

For the signals presented and discussed in this thesis, we do not have information about the ionic species involved and their dynamics across the cell membrane. However, we can analyze the net flow of charge and the charge ratio between the upward and downward components of the signal. This analysis is providing in the 4th column of Table II (Spikes area ratio).

The analysis starts with the BFUp type of signal. With a few exceptions, the BFUp signal has a charge ratio between upward and downward component in the range of 0.5-0.7. This is true for C6, HOPE and Neurons (N2A). The downward component has approximately twice the amount of charge of the upward signal component. The BFDown signal follows a similar trend. Here the U87 type of cells were one exception, because the ratio between upward and downward component is very high and approximately 1.3.

3.3 Discussion and conclusions

Cancer cell populations generate discrete bio-electrical signals. The signals have well-defined shapes that have been quantitatively characterized and named according to their basic shapes, namely the relation between upward and downward signal components.

A long-term recording experiment generates a large number of signals. For each type of signal a broad distribution of signal amplitudes and duration is observed. However, in spite of this broad distribution in the signal amplitude and duration, the aspect ratio between upward and downward signal components is always kept constant for a particular class of signal. This observation supports the hypothesis that individual cells do not generate the signals, but instead, the signal is a result of a synchronized activity of a cluster of cells. The variability in signal amplitude and duration is caused by variability in the number of cells that reach synchronization.

References

1. Beeler, B. Y. G. W. & Reutert, H. By g. w. beeler*. 177–210 (1977).

2. Shih, H. T. Anatomy of the action potential in the heart. *Texas Hear. Inst. J.* **21**, 30–41 (1994).

3. Platkiewicz, J. & Brette, R. A threshold equation for action potential initiation. *PLoS Comput. Biol.* **6**, 25 (2010).

Chapter 4

Temporal aspects of discrete signals

Individual bio-electrical signals measured in HOPE cell populations are characterized by a relatively rapid rising phase followed by slower falling phase. The falling phase obeys to a single exponential decay. For all types of signals, time constants fall between 2 and 30 seconds. The time constants are several orders of magnitude slower that the device time constant (τ<1s). It is concluded that intrinsic biological processes determine this time dependence of the signal shape.

4.1 Introduction

The objective of this chapter is to dissect the shape of the individual signal into the components that can be quantified. If we know the temporal dependence of an individual signal we may get insight into the flux of ions across the cell membrane. This information can them be used to compare with the behavior of well-know ion channels in cells. A convenient way to illustrate our goal is the description of an action potential in nervous cells. The shape of an action potential is described in Figure 4.1.

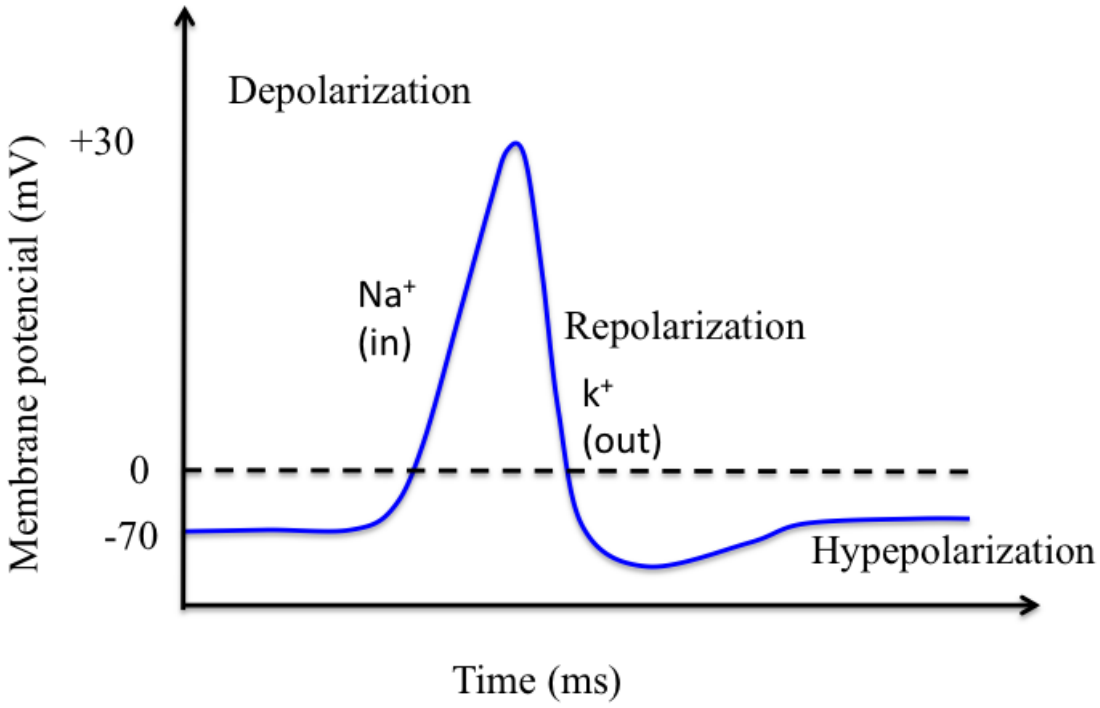

Figure 4.1: The shape of a single action potential. The components due to the inward flow of Na^+ and outward flow of K^+ are represented.

The shape of the action potential signal in Figure 4.1 is described in the following way. Initially, the cell membrane is at the resting potential of -70 mV. Then suddenly a specific ion channel opens. This channel allows Na^+ to move into the cell. The ion movement is driven by the concentration gradient (there are more Na^+ outside the cell than inside). Because sodium is a positively charged ion, it will change the relative voltage inside the cell relative to outside. The Na^+ entering the cell will cause it to become less negative. This is known as depolarization, meaning the membrane potential moves towards zero. The concentration gradient for Na^+ is so strong that it will continue to enter the cell even after the membrane potential has become zero, so that the membrane potential will reach +30 mV.

As the membrane potential reaches +30 mV, other voltage-gated channels are opening in the membrane. These channels are now specific for the potassium ion. A concentration gradient acts on K^+, as well. As K^+ starts to leave the cell, taking a positive charge with it, the membrane potential begins to move back towards its resting voltage. This is called re-polarization, meaning that the membrane voltage moves back towards the -70 mV value. Repolarization returns the membrane potential to the -70 mV value, but it overshoots that value (hyper-polarization). This is because K^+ channels are slightly delayed in closing[1, 2].

In summary, the shape of an action potential signal is very well described by the interplay of two well-know ion channels, the voltage-gated Na^+ channel and the voltage-gated K^+ channel[3, 4]. Can we provide a similar description for the signals reported in this chapter for non-excitable cells? In other words can we gain insight into the ion channels involved in shaping the signals reported here?

Before we can provide an interpretation of the signal shape in terms of ionic channels, we have to look in close detail to an action potential and how it is measured. The shape of the action potential described above, reflects the variation of the potential across the cell membrane. It can be measured using a needle like electrode that measures a single cell. The method is known as patch clamp technique[5, 6].

Here we use extracellular electrodes, so we only have access to the extracellular voltage. Furthermore, the action potential travels along the axon of a neuron or in a nerve. When we attach an electrode to a nerve cell, we measure thousands of cells and therefore, thousands of action potentials. We can begin to appreciating that the signal shape of an action potential depicted in Figure 4.1 will not be recorded using extracellular electrodes. Strangely, the signal shapes are alike in a sense that both can have a biphasic shape but for very different reasons. This will be explained later.

In order to explain the shape of a signal recorded using extracellular electrodes, we have to keep in mind two important aspects. The first aspect to retain is that we do not measure a single action potential, but a compound action potential formed by a myriad of action potentials. Figure 4.2 illustrates this concept.

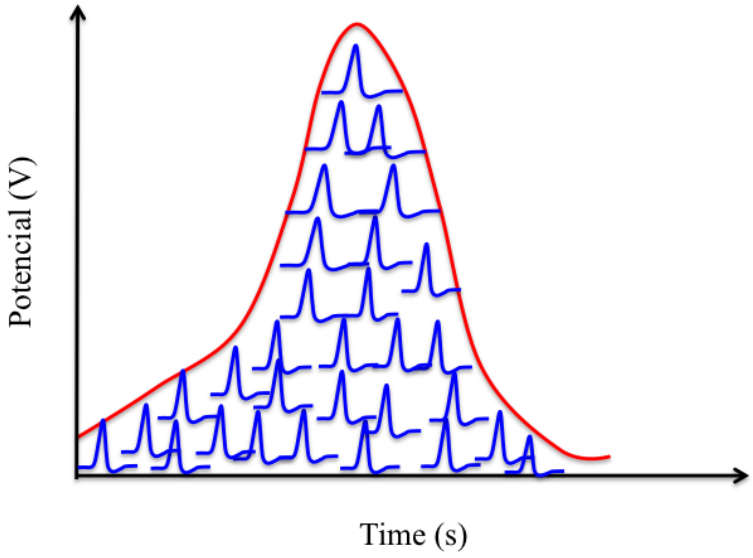

Figure 4.2: Schematic diagram showing the concept of a compound action potential formed by a myriad of action potentials. Diagram inspired in reference 10.

The second aspect is that the compound action potential travels along the nerve as a wave. There are two recording electrodes (S1 and S2) touching the nerve, each connected to the input of the differential amplifier (see Figure 4.3).

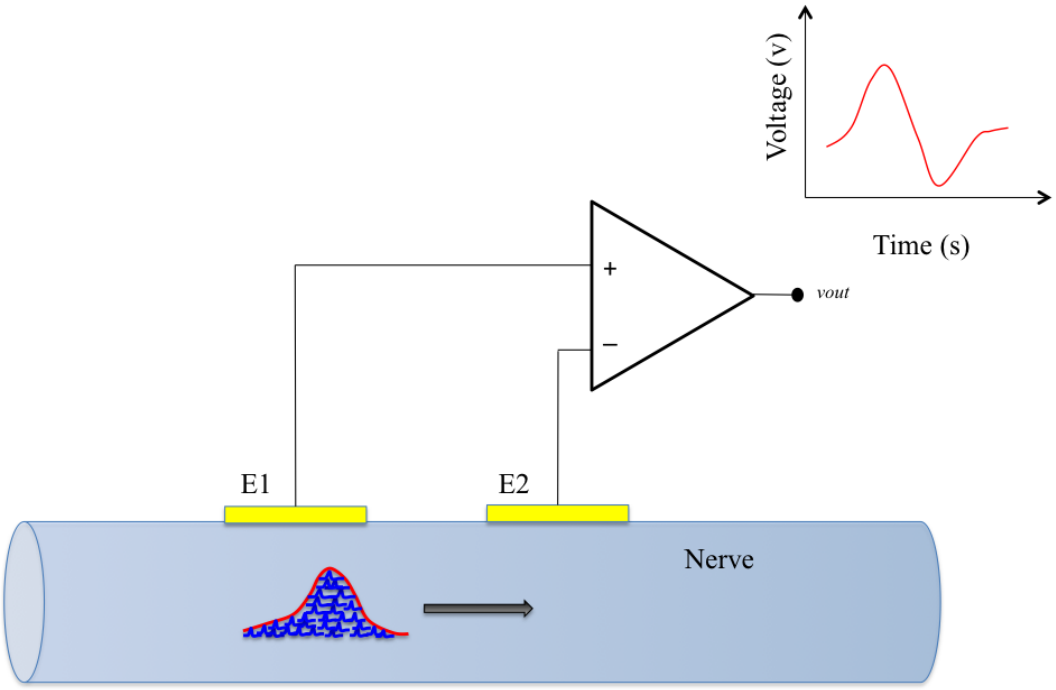

Figure 4.3: Traveling compound signal along a nerve and recorded using a differential voltage amplifier.

No signal is recorded when the two sensing electrodes are at the same potential. Now imagine that the compound signal travels along the nerve. The shape of the compound signal will depend on the inter-electrode distance and on the velocity of the signal. When the signal has reached the first recording electrode (E1), the potential difference between the two is detected and the trace is displayed as an upward voltage deflection.

As the signal progresses between both recording electrodes, the recorded potential returns to the base line (no voltage difference between the two recording electrodes). As the signal passes the second electrode (E2), a deflection of the same size but opposite sign will be recorded. The sign is negative because of the way the amplifier compares the two inputs. If the electrodes are sufficiently far apart, a time span without a deflection will be recorded before the signal reaches the second electrode. The duration of this signal segment will depend on the distance between electrodes and the speed of the signal on the nerve. A biphasic signal is measured but this is related with the way the electrodes are positioned and the traveling speed of the nerve signal.

The above example is particular relevant for our signals because as in a nerve we also measure a large ensemble of cells. The extracellular recorded signal is also a compound signal made of synchronized individual cell signals. However, unlike the measuring set-up presented above we do not use a differential amplifier. Instead, we grounded one of the voltage amplifier terminals. Therefore in our experimental set-up the biphasic signal shape cannot be explained by the way instrumentation is connected.

In order to perform the experiments we have chosen HOPE cell cultures. The Mushroom sensing device, a square golden electrode with side l=2000 μm, therefore with 4 mm^2 of active area was used.

This chapter is organized as follows: it begins by presenting the typical signal shapes and the regions of the signals that were analyzed in detail. A large number of signal return to steady state were inspected using a single exponential formalism. The time constants were extracted and analyzed. Finally, in the discussion and conclusions section, the meaning of the signal rise time is presented. This discussion also elaborates on the possible origin of the broad distribution of decay time constants reported here.

4.2 Results

The shape of an individual bio-electrical signal is often characterized by a fast rise time followed by a slow decay to a steady state value. This behavior can be observed both in monophasic as well as in biphasic signals. Figure 4.4 illustrates the four most common signal shapes recorded.

Some signal shapes are mirrored images. For instance, a Monophasic Fast Upward (MUp) signal looks like the mirror image of the Monophasic Fast Downward (MDown) signal. Biphasic signals also have mirror images. Both upward and downward signals (monophasic or biphasic) are recorded in the same time trace, often separated in time by just a few seconds apart. Therefore, it is clear that mirrored signals are an intrinsic property of the cell signaling mechanism and not a consequence of changing the polarity of the recording system.

To gain insight into the biological or physical nature of the signal shape, we decide to inspect the time dependence of the voltage decay. For each signal shape we analyze the decay. Figure 4.4 illustrates the region of the signal under analysis. This region is marked by a yellow shaded color.

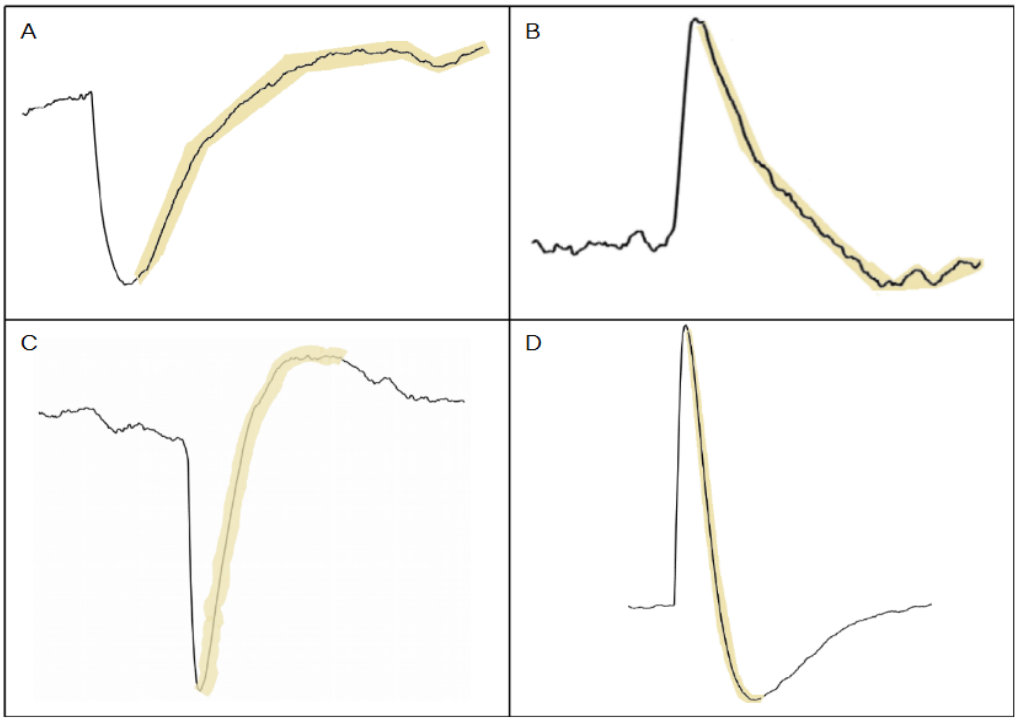

Figure 4.4: Typical signal shapes recorded in Hope cell populations using the mushroom type of device. The yellow shaded curve denotes the decay under analysis.

For each type of signal shape outlined in Figure 4.4, we quantify the decay of the voltage to steady state value. A number of approximately 10 to 12 signals (of each type) were selected to carry out this analysis. The decay was quantified by plotting the data in a semi-logarithmic time scale. This procedure allows us to verify if the decay follows an exponential law and to estimate the corresponding time constant. In order to perform this analysis, decays were first isolated from the rest of the curve, then the offset voltage value was removed and values were converted to positive voltage values. Figure 4.5 shows a semi-logarithmic plot of 12 decays recorded for the MDown type of signal.

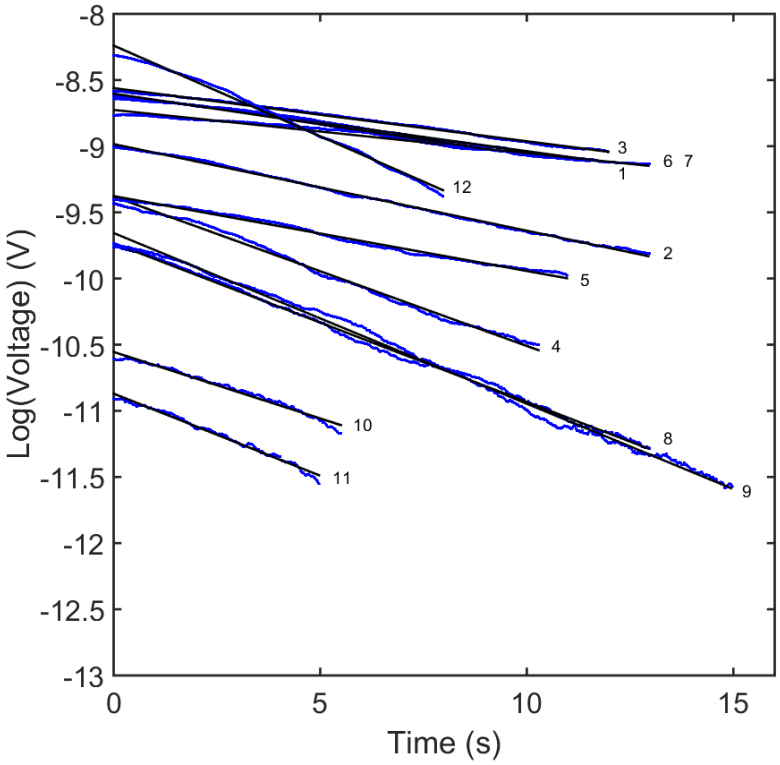

Figure 4.5: Semi-logarithmic of the decays measured on Monophasic Fast Downward (Figure 4.4 A). Experimental data is represented by the blue curve and the solid black curve shows the fitting to a straight line.

By fitting the straight lines on the semi-logarithmic plot on Figure 4.5 we estimate the corresponding time constants. The estimated time constant for each signal are represented on the Figure 4.6. A board distribution of values ranging from 7 up to 30 seconds is observed. A similar procedure was followed for all the signals represented in Figure 4.4. The corresponding analysis is shown in the Figure 4.7 to Figure 4.12.

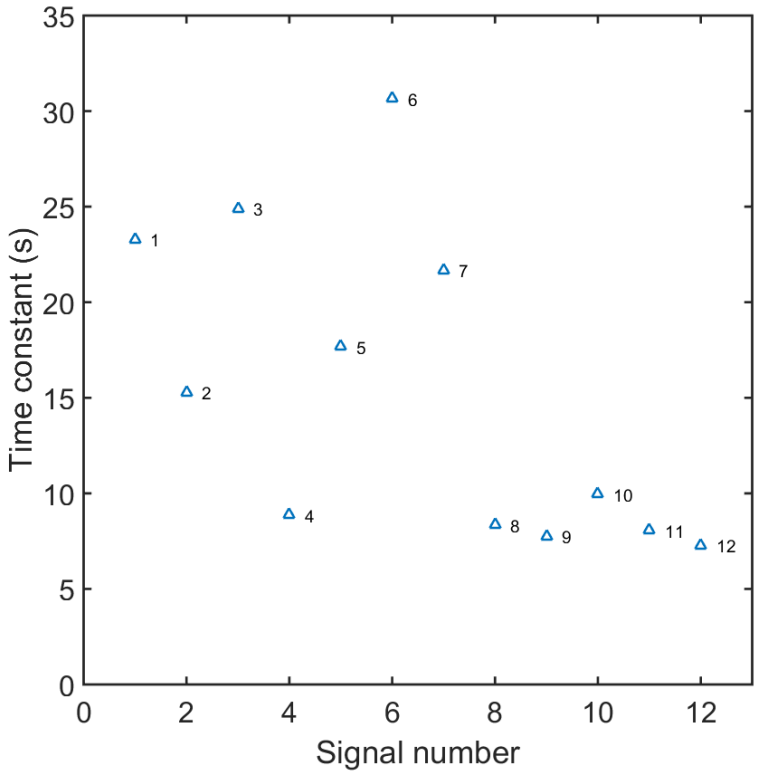

Figure 4.6: Plot of all time constant estimated for the MDown type of signals. The time constants were estimated from the slopes of the straight lines shown in Figure 4.5.

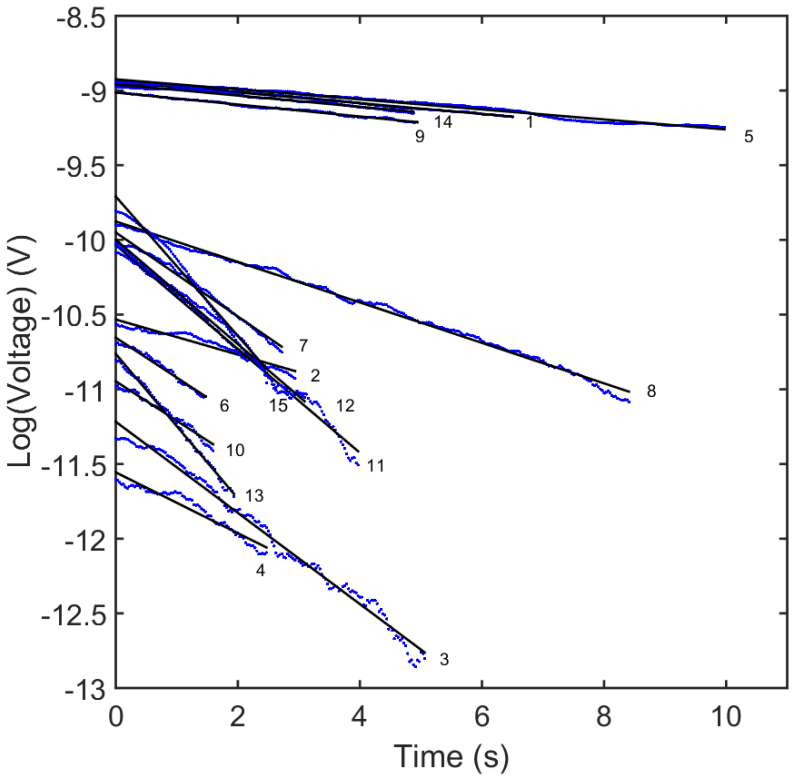

Figure 4.7: Semi-logarithmic plot of a set of decays measured on MUp type of signals. Blue dotted lines are the experimental data and the back solid curve is the experimental fit using a straight line.

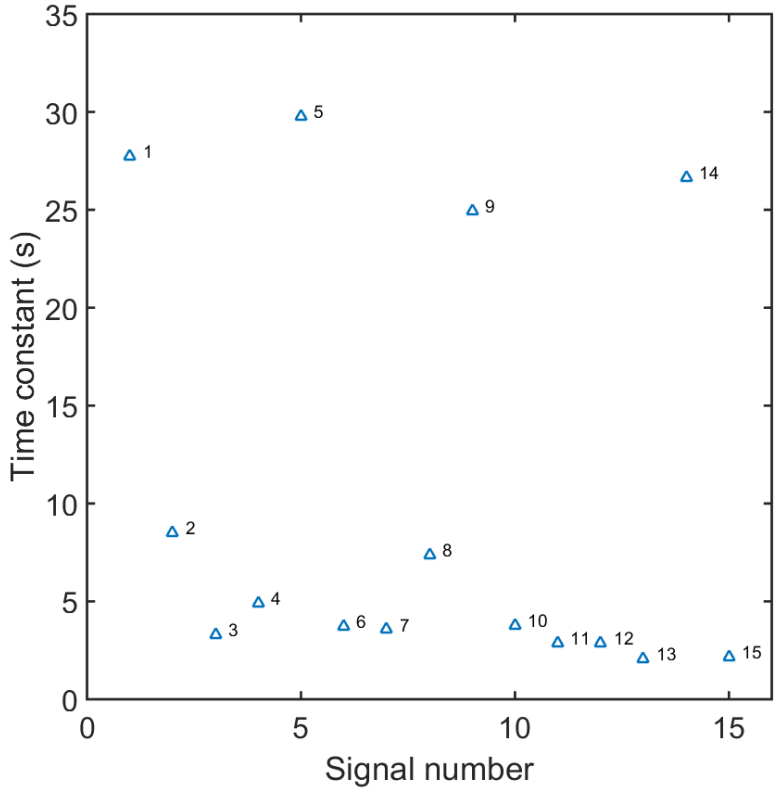

Figure 4.8: Plot of all time constant estimated for the MUp type of signals. The time constants were estimated from the slopes of the straight lines shown in Figure 4.7.

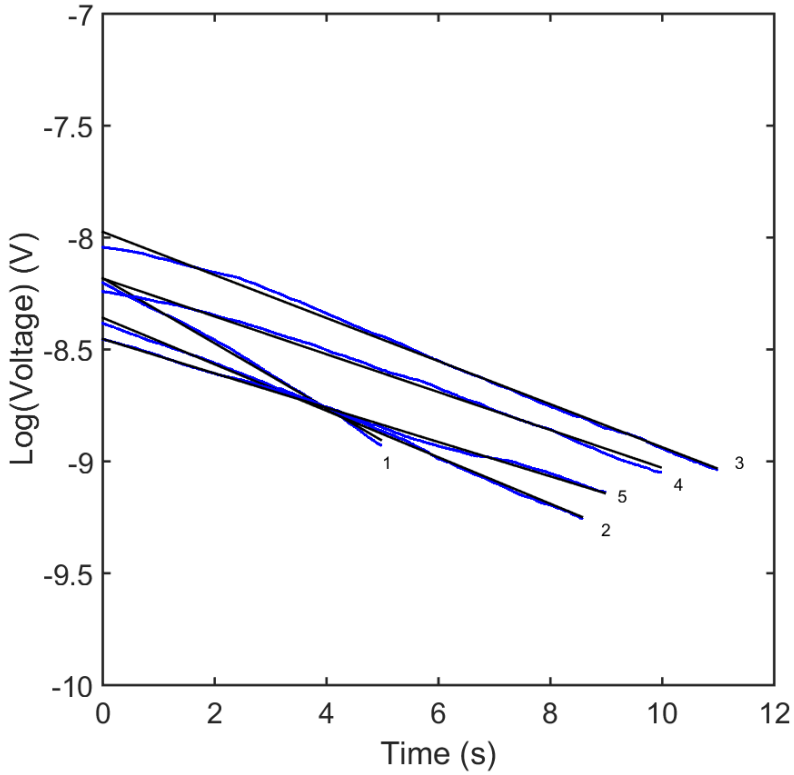

Figure 4.9: Semi-logarithmic plot of a set of decays measured on Biphasic Fast Downward (BFDown) type of signals (Figure 4.4 C). Blue lines are the experimental data and the back solid curve is the experimental fit using a straight line.

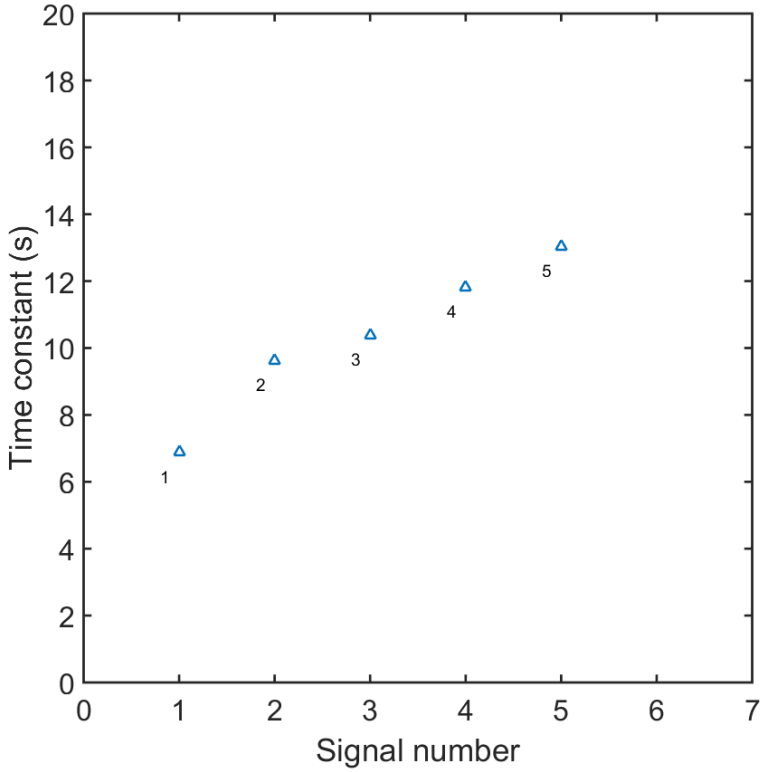

Figure 4.10: Plot of all time constant estimated for BFDown type of signals. The time constants were estimated from the slopes of the straight lines shown in Fig. 4.9.

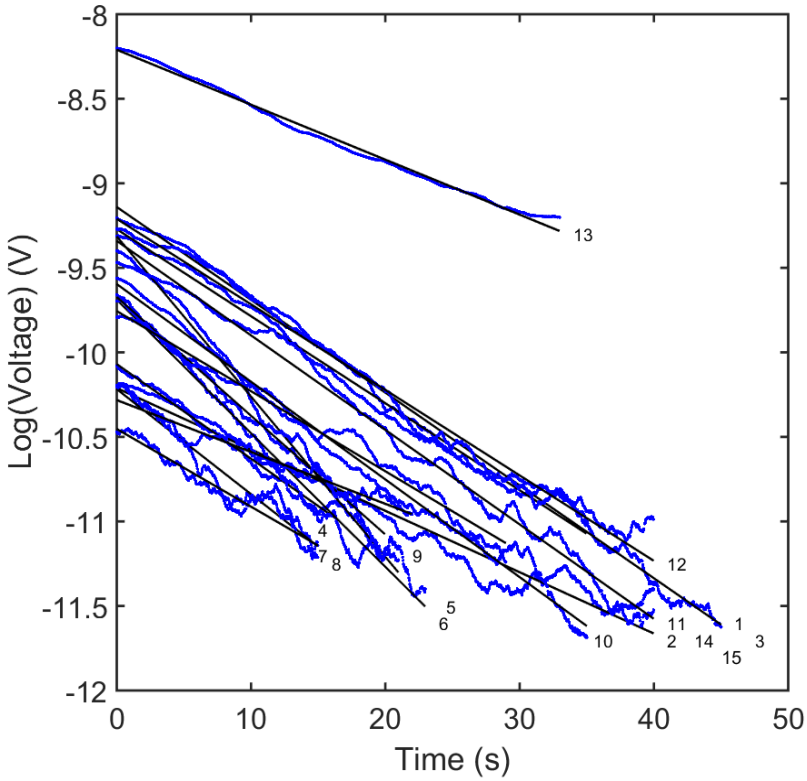

Figure 4.11: Semi-logarithmic plot of a set of decays measured on Biphasic Fast Upward (BFUp) type of signals (Figure 4.4 D). Blue lines are the experimental data and the back solid curve is the experimental fit using a straight line.

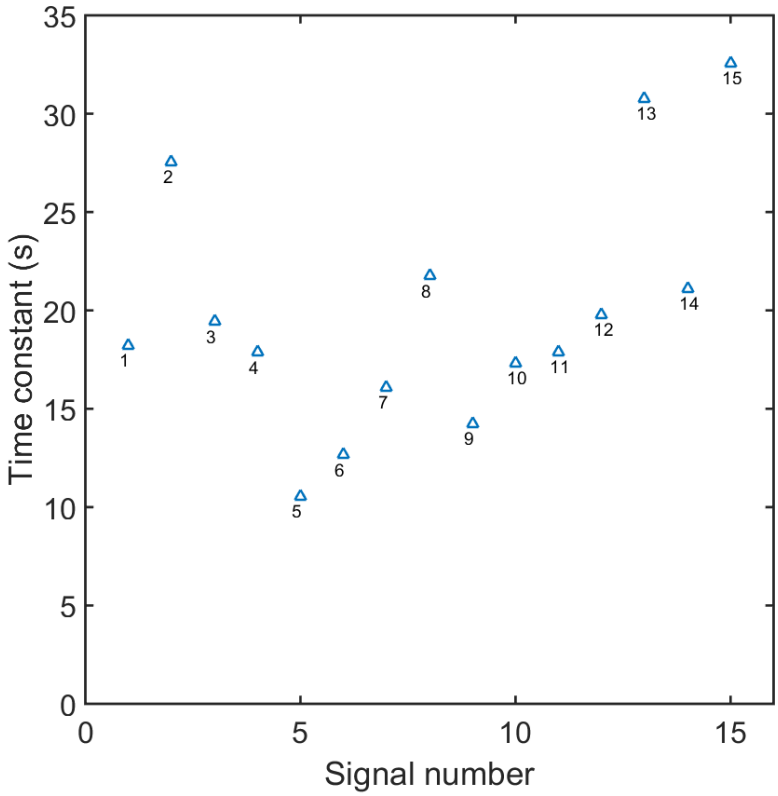

Figure 4.12: Plot of all time constant estimated for the BFUp type of signals. The time constants were estimated from the slopes of the straight lines shown in Figure 4.11.

To briefly summarize the data collected and displayed in the previous plots from Figure 4.5 to Figure 4.12, we have decided to classify data, the time constants, in two groups: the first group takes in account the all data presented in plots for each signals in Figure 4.4, and the second group takes in account the data plotted in the points densest area of the dispersion graphs for each signal in Figure 4.4, group of values which it has less dispersion between them.

For all points in each of the four dispersion graphs is established an interval limited by of minimum and maximum values of points found in each graph. We have also calculated the difference between the maximum and minimum values among all points in each graph, which is taken as a measure of maximum dispersion of values plotted for each graphs.

In the analysis of the data presented above it is taken into attention to the densest area of points in the graphs. In the crowdest area it is established an interval with a minimum and maximum value. Also in this area it is estimated the average time constants and their dispersion. Table I shows the results of this analysis.

Table I: Summary of all the time constants estimated for the signals analyzed in Figure 4.5-4.12.

Signal type	**MDown**	**MUp**	**BFDown**	**BFUp**
Interval of time constants (s)	[7; 30]	[2; 30]	[6; 14]	[10; 33]
Dispersion of interval time constants (s)	23	28	8	23
Average time constant (s)	15.3	10.3	10.4	19.9
Densest area interval (s)	[7; 10]	[2; 8]	[6; 14]	[15; 20]
Densest area interval dispersion (s)	5	6	8	5
Densest area average time constant (s)	8.4	6.5	10.4	17.99

4.3 Discussion and conclusions

This study shows that the bio-electrical signal shapes are comprised of a fast rise time followed by a slow decay in time. The signal decay obeys to a pure exponential law. A single exponential behavior is observed in all signal shapes analyzed. The time constants are distributed between 2 and 30 seconds.

Based on the premises that the signal is a result of a synchronized cell activity, we can conclude the following aspects related with the signal shape. The cell synchronization is a fast process. An instruction must flow trough the cell population to instruct the cells to change very rapidly their polarization. This occurs in a time span typically below 1 second. This aspect is quite impressive and requires a communication mechanism between cells. Assuming that we can synchronize 100 cells and that each cell has a diameter of 10 μm occupying an area of 78 μm^2. 100 cells will occupy 7800 μm^2. The distance that an instruction must travel is equivalent to the diameter (d) of a circular region with a radius r and an area of 7800 μm^2, $r = \sqrt{(7800 \mu m^2/\pi)} = 50$ μm and d = 100 μm. If the signal rise time is 1s, then the instruction responsible for the synchronization must travel at the speed of 100 μm/s. This speed value is very much in line with typical values for speed of traveling calcium waves for instance[7, 8].

One important conclusion is that the time require to reach the peak voltage is a measure of the synchronization speed for a particular cell population. Once synchronization is reached we have a population of cells with their membranes polarized. What is happening next? Are the cells still keeping their concerted behavior and the decay is an algebraic sum of a myriad of ions flowing across individual membranes? Or the population looses synchronization? At this moment we do not have enough data to extract a definitive conclusion on the nature of the exponential decay of the signal.

It is important to rule out the contribution of the device time constant as a factor affecting the signal shape. The signal has to travel trough the electrical double-layer at the interface between the cell membrane and the electrode. As described in previous chapters, a parallel RC circuit describes electrical double-layer. Low frequency impedance measurements provide values for R and C. In the past and already published this data[9]. We have shown that the interface capacitance reaches 1.1 μF and the parallel resistance is approximate 320 kΩ. The equivalent RC time constant is below 1s. Therefore, the device time constant cannot explain the decays with time constants reaching 30s presented here.

References

1. Beeler, B. Y. G. W. & Reutert, H. By g. w. beeler*. 177–210 (1977).

2. Luo, C. H. & Rudy, Y. Original Contributions A Model of the Ventricular Cardiac Action Potential. *Circ. Res.* **68**, 1501–1526 (1991).

3. Shih, H. T. Anatomy of the action potential in the heart. *Texas Hear. Inst. J.* **21**, 30–41 (1994).

4. Platkiewicz, J. & Brette, R. A threshold equation for action potential initiation. *PLoS Comput. Biol.* **6**, 25 (2010).

5. Jaskova, K., Pavlovicova, M. & Jurkovicova, D. Electrophysiological variability in the SH-SY5Y cellular line. *Gen. Physiol. Biophys.* **31**, 375–382 (2014).

6. Mason, M. J., Simpson, A. K., Mahaut-Smith, M. P. & Robinson, H. P. C. The interpretation of current-clamp recordings in the cell-attached patch-clamp configuration. *Biophys. J.* **88**, 739–750 (2005).

7. Kuga, N., Sasaki, T., Takahara, Y., Matsuki, N. & Ikegaya, Y. Large-scale calcium waves traveling through astrocytic networks in vivo. *J. Neurosci.* **31**, 2607–2614 (2011).

8. Benninger, R. K. P., Zhang, M., Steven Head, W., Satin, L. S. & Piston, D. W. Gap junction coupling and calcium waves in the pancreatic islet. *Biophys. J.* **95**, 5048–5061 (2008).

9. Mestre, A. L. G. *et al.* Ultrasensitive gold micro-structured electrodes enabling the detection of extra-cellular long-lasting potentials in astrocytes populations. *Sci. Rep.* **7**, 1–11 (2017).

10. http://www.medicine.mcgill.ca/physio/vlab/other_exps/CAP/recording.htm

Chapter 5

The influence of the electrode geometry on the bio-electrical signal shape

By using electrodes with different active sensing areas and geometries a relation between the electrode design and the signal shape, namely, signal duration and power is established. It is verified that signal power increases with electrode sensing area. Furthermore, the signal duration also increases with electrode width, but it does not scales linearly. These findings support the view that the bio-electrical signal is a traveling ionic wave.

5.1 Introduction

This chapter presents a study that analysis how the sensing electrode geometry and electrode dimensions affect the signal shape recorded by an extracellular electrode. This study relies on two hypotheses, which are the following ones:

1- A discrete signal is result of a synchronized activity of an ensemble of cells;

2- The synchronized activity generates an oscillation travels across the cell population like a wave.

In the following paragraphs, we will outline the predictions of these two hypotheses and we compare the experimental observations.

We begin by discussing the first hypothesis. The measured signal is a result of a synchronized oscillation involving a well-defined number of cells. Each cell contributes with a small voltage to the measured signal. Assuming that the electrode is smaller than the area occupied by the synchronized cell population, it is then expected that the total voltage measured by the extracellular electrode is the sum of all the small voltages generated by each individual cells on top of the sensing electrode. Therefore, our first prediction is the following one:

- Prediction 1: A linear relation between the electrode area and the signal amplitude is expected.

The second hypothesis assumes that the synchronized oscillation travels trough the cell population. It is a traveling wave. The extracellular voltage signal begins when the wave hit the electrode and ends when the wave leaves the electrode. The signal duration is equal to the time that takes for the wave to cross the sensing electrode. This time is defined by the wave speed and by the width of the electrode. For a particular wave speed, the larger the electrode width, the longer the signal. This prediction can be stated in the following way:

- Prediction 2: The signal duration is proportional to the electrode width.

Knowing the electrode width and the signal duration, we can calculate the wave traveling speed. The relation is expected to be linear. In a similar way as prediction 1, this observation also requires that the electrode width is shorter or equal than half the wavelength. Very large electrodes can measure simultaneously several waves. If this occurs measurements will be distorted.

One part of the work carried out in this thesis use interdigitated electrodes. A traveling wave can cross several fingers, and in each crossing will generate a signal. If this occurs the recorded signals are expect to be periodic. The distance between fingers should define the signal periodicity. Therefore, we may state the third prediction as follows:

- **Prediction 3**: When interdigitated electrodes are used, signals should be periodic with a period defined by the distance between adjacent electrode fingers. To observe periodicity caused by interdigitated electrodes, the wave must cross several electrode fingers. This may require that the wave travels at distances longer than the distance between two adjacent fingers. For instance in a IBID interdigitated device the fingers are separated apart by 750 micrometers, therefore a single wave has to travel this distance plus two sensing electrode widths. In total the wave must travel 950 micrometers to produce two signals in the recording electrode.

In this chapter, we will verify if the experimental data is in agreement with the three above predictions. We begin this chapter by describing the electrode geometries as well as the cell cultures used. Then we describe the relation between electrode area and signal power or amplitude. The relation between signal duration and electrode width is also inspected using interdigitated electrodes. Finally, the influence of the electrode geometry on signal periodicity is also verified using interdigitated electrodes.

5.2 Experimental

Figure 5.1 shows the geometries of the sensing electrodes used in this study. Devices with a square shape, a circular shape and an interdigitated geometry were fabricated and used to measure bio-electrical signals. Two types of interdigitated electrodes were fabricated; one device has finger width (w) of 5 µm and the other a finger width of 100 µm. The device active areas are also represented on Table I.

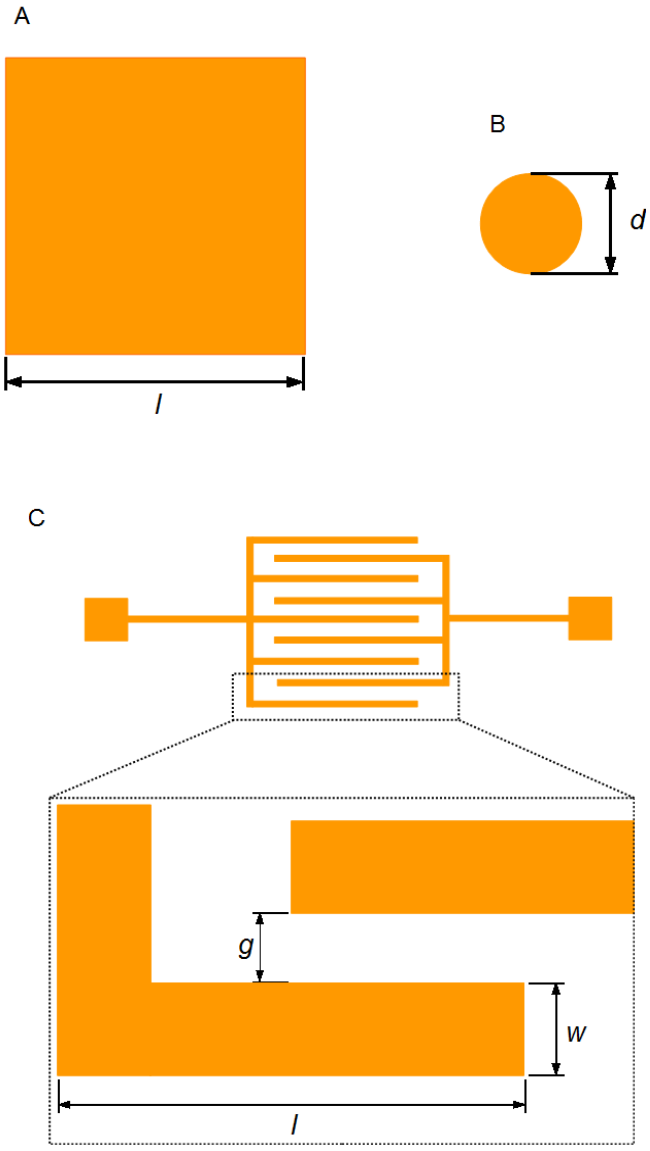

Figure 5.1: Sensing devices and geometries used. Geometry A relates to Mushroom (square) sensing device, a gold square surface with side length l; geometry B relates to IBIDI circular sensing device, a gold circle with diameter d; geometry C relates to IBIDI Interdigitated and PHILIPS sensing devices, a gold cross-finger tracks electrode, which has length l, width w and gap space between tracks named g.

Table I: Device geometries features and dimensions of every sensing electrodes on Figure 5.1.

Device name	**Geometry**	**No. of fingers**	**Length** (*l*) (μm)	**Width** (*w*) (μm)	**Gap** (*g*) (μm)	**Diameter** (*d*) (μm)	**Area** (μm^2)
Mushroom	Square	--------	2000	2000	--------	----------	4×10^6
IBIDI Inter.	Interdigitated	5	3254	100	325	----------	1.6×10^6
IBIDI Circ.	Round	--------	----------	----------	--------	250	49.1×10^3
PHILIPS	Interdigitated	5	1000	5	10	----------	25×10^3

HOPE cells populations were used in all the devices. In order to minimize variability only one type of signal was studied, the Biphasic Fast Upward (BFUp) type of signal. The shape of the BFUp signal is outline on Figure 5.2 together with the important signal parameters. The area of each signal was obtained by calculating the integral of the curve using a triangular approximation.

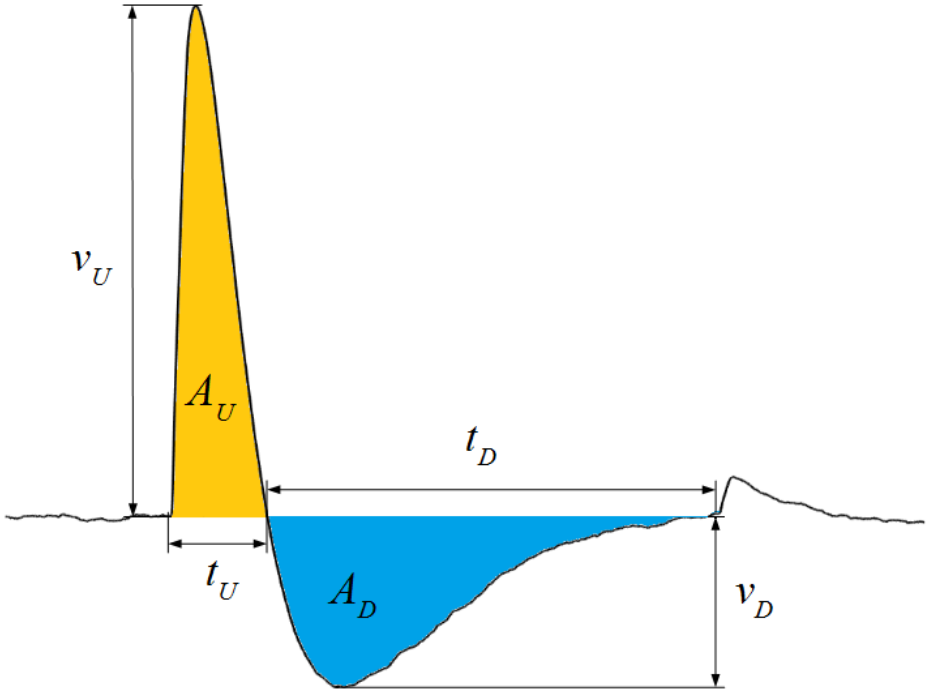

Figure 5.2: Shape of a Biphasic Fast Upward signals shape (BFUp) recorded in HOPE cells. The figure also shows the relevant parameters that characterize the signal.

Since there is large variability on signal duration and signal amplitude. Signals were distributed in bins and their distribution statistically analyzed using histograms.

5.3 Results

In order to verify the hypothesis outlined in the introduction section of the present chapter, a 40 signals cell signals were analyzed. To minimize variability, data analysis was limited to only one type of cell (HOPE cells) and also to only one type of signal, the BFUp signal. The BFUp signal was selected because it was the most frequent observed signal in HOPE cells.

The first hypothesis is to verify how the electrode area correlates with the signal amplitude. In order to perform this analysis, we measure the signal duration recorded in each type of electrode. Since there is a distribution of signal duration, the data was distributed in bins with a well-defined temporal width and a histogram was built.

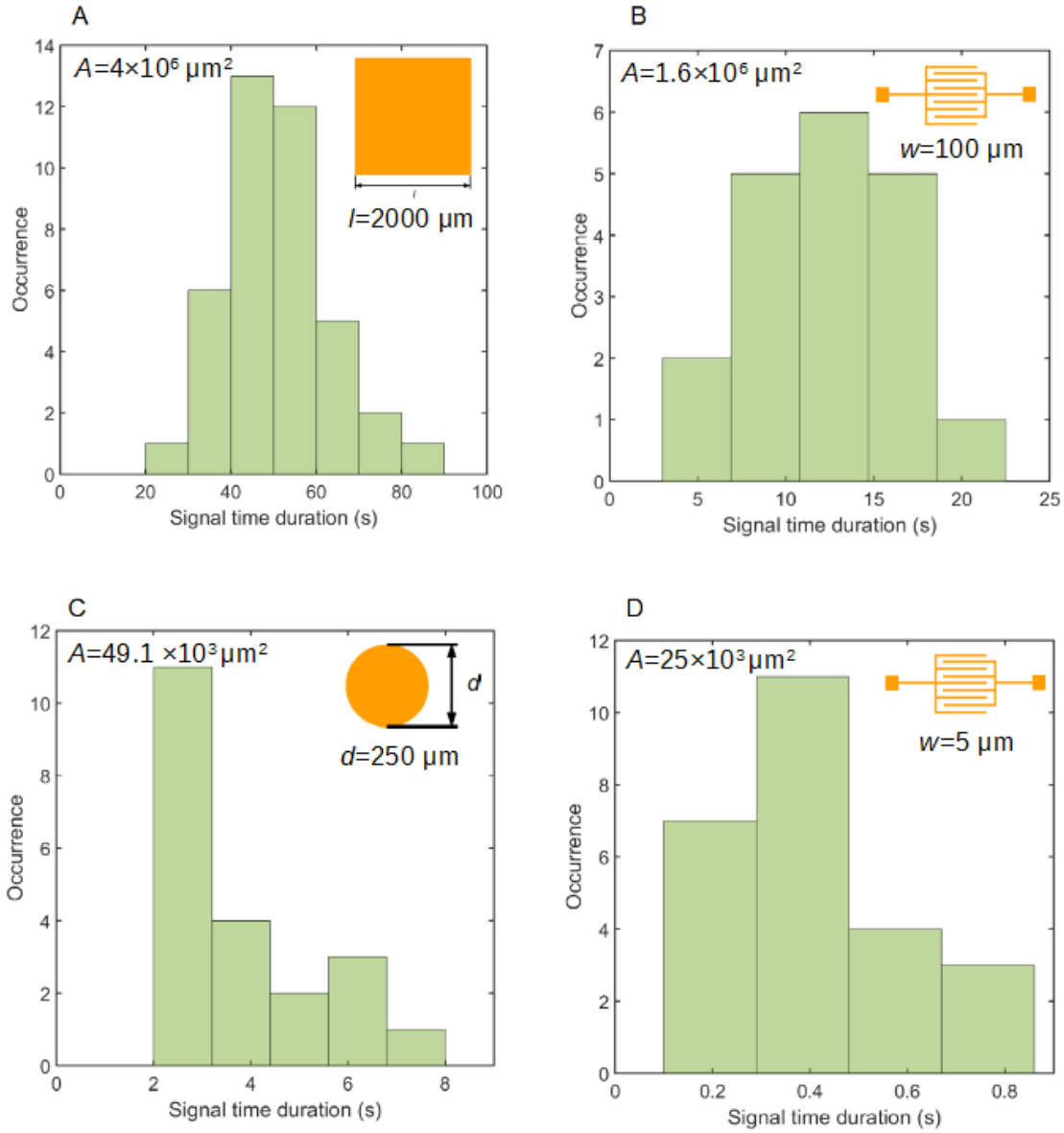

Figure 5.3: Signal duration of Hope cells BFUp signal when measured on four different sensing devices. Each histogram is tagged with a letter from A to D, which represents a different sensing device: A- Mushroom electrode; B- IBIDI Interdigitated electrode; C- IBIDI circular electrode; D- PHILIPS electrode.

Figure 5.3 shows the histograms of the signal duration observed for the four electrodes listed in Table I. The width of each bin varies according to the sensing device used. Large area devices require bins of 10s. Bins of 1s width are more adequate for small area devices and ultra-small area devices as the PHILIPS device requires bins of 0.1s.

Figure 5.4 shows the relation between the electrode active area and signal duration. To simplify the analysis, only the most common value for signal duration was considered. The most common value was extracted from the histograms on Figure 5.3. As expected, (from the prediction 1) the signal duration increases linearly with the electrode area.

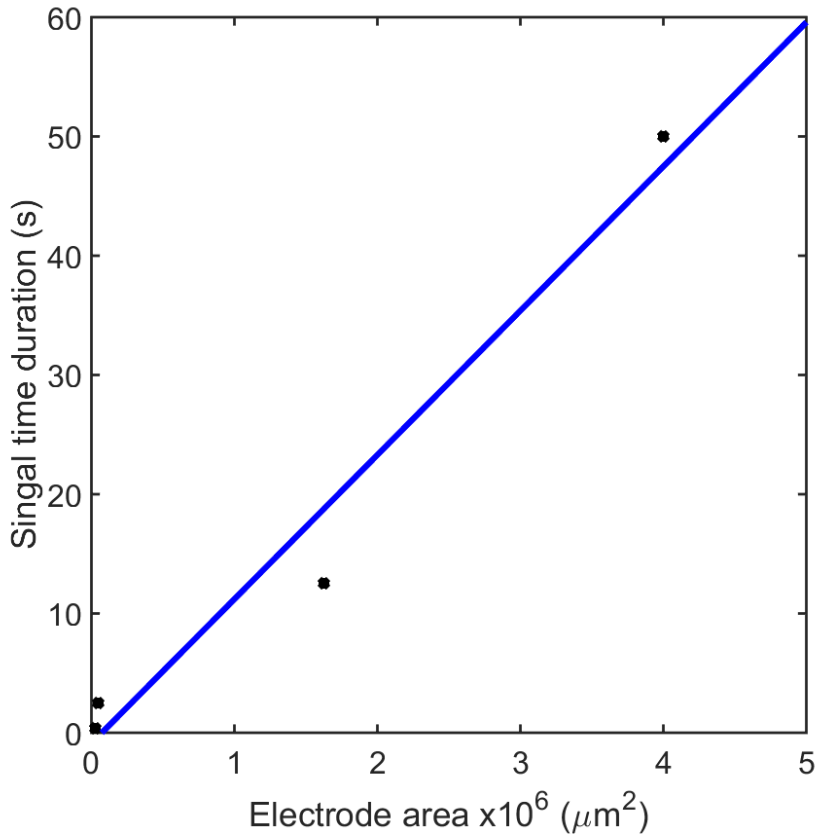

Figure 5.4: Relation between sensing area and signal duration. It can be observed the larger is the active area of an electrode, the longer it is the signal duration.

As addressed in the previous chapter 3, the area under the voltage signal curve should reflect the amount of charge involved in the signal. However, we do not know the value of the current therefore, we cannot calculate the total charge involved in the signal. The histograms on Fig. 5.5 are plotted as function of the area under the voltage signal. Voltage as function of time is not really a physical parameter. We express this signal area in volts times seconds (μV×s).

Figure 5.5 shows the distribution of the signal area for the different devices under study. The larger the electrode area the larger the signal area. This relationship is expected because larger electrodes probe more cells.

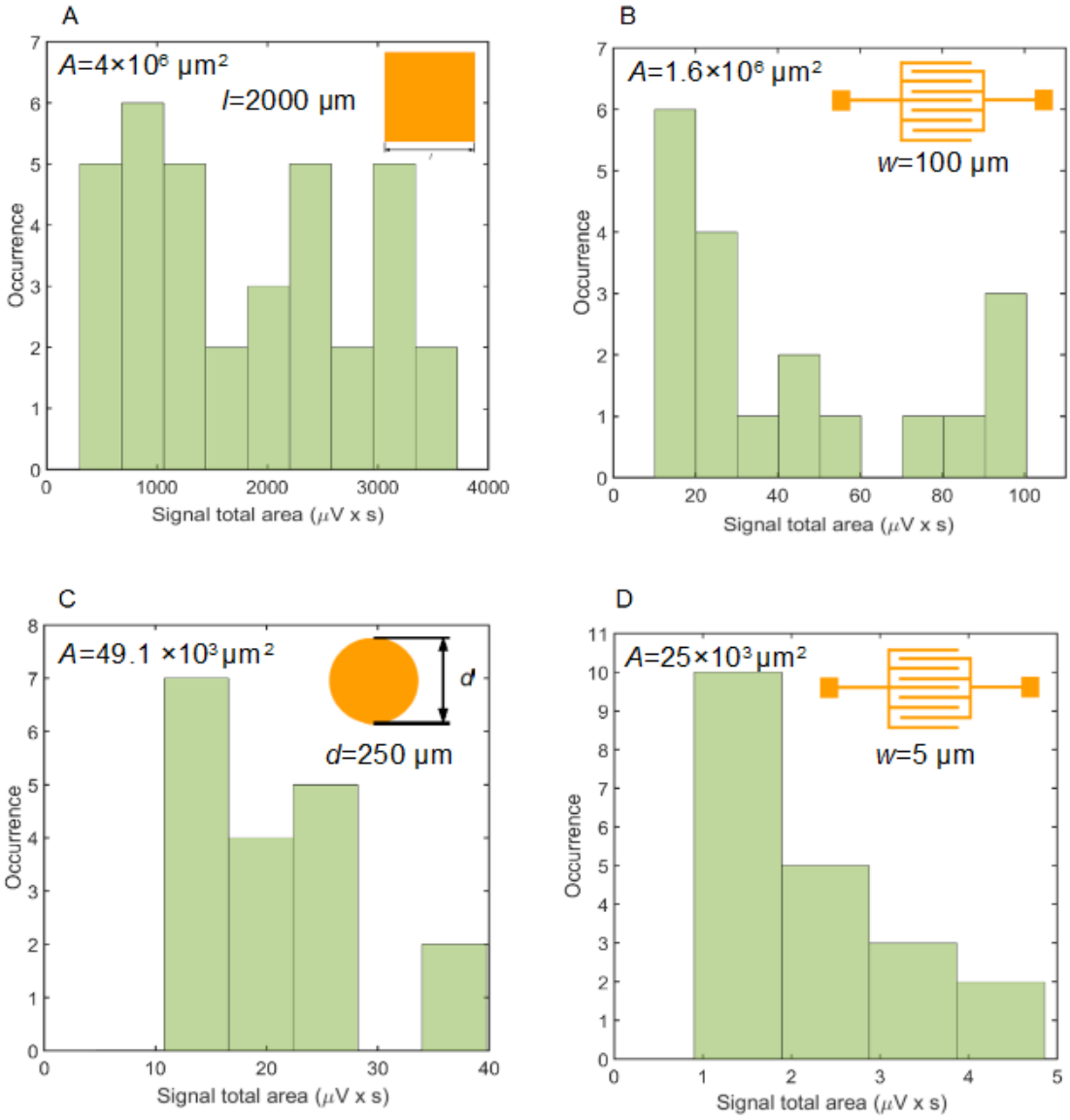

Figure 5.5: Distribution of voltage signal areas for the different devices. Each histogram is tagged with a letter from A to D, which represents a different sensing device: A- Mushroom electrode; B- IBIDI Interdigitated electrode; C- IBIDI circular electrode; D- PHILIPS electrode.

Table II summarizes all the results related with the device active area. It is clear that both signal duration and signal area correlate with the electrode active area for all the device geometries under study.

Table II: Signal duration and signal area obtained using different device geometries. The cells used are populations of HOPE cells.

Device name	**Structure/shape**	**Width** (*w*) (μm)	**Area** (μm^2)	**Average signal duration** (s)	**Signal area** (μV×s)
Mushroom	Square	2000	4×10^6	50.0	700
IBIDI Inter.	Interdigitated	100	1.6×10^6	12.5	17.5
IBIDI Circ.	Round	250	49.1×10^3	2.5	12.5
PHILIPS	Interdigitated	5	25×10^3	0.4	1.5

In the following section we analyze if prediction nº2 is supported by our experimental data. Prediction nº2 says that the duration of a signal is proportional to the electrode width.
In order to verify this hypothesis, we used the physical widths of the interdigitated type of devices.

This is because the geometry is identical in both devices. According to Table II, PHILIPS device has a finger width (*g*) of 5μm and the IBIDI device a finger width of 100μm. The ratio between electrode widths is 100/5=20. Therefore, one expects that the signal recorded on IBIDI should be in average 20 times slower than an average signal measuring in the PHILIPS device. According to the data presented on Table II, the ratio between signal duration is 12.5/0.4=30. This value is 50% higher than the expected value of 20.

The above calculations assume that the wave speed is constant in all experiments. This may not be necessary true. The experiments were carried out in different days and the biological signaling process may be change according to the cell life cycle. The cells may change the wave speed in function of the biological function and the information that is transmitted. We can estimate the wave speed for each electrode. For the PHILIPS device the wave speed is 5/0.4= 12.5 μm/s and for the interdigitated IBIDI device the estimated wave speed is 100/12.5= 8 μm/s.

Similar relations can in principle be also established between the round and the square electrode. The two electrodes have different geometries but one expects that the signal duration also scales in accordance with their physical dimensions (see Table III). In this case the dimensions are the diameter and the lateral width. The ratio between the longest distances in the two types of electrodes is 2000/250=8 while the ratio between signal duration is 50/2.5= 20. The temporal ratio between signals is 2.5 times higher than the ratio between physical dimensions. The signal duration is following the expected trend, but does not scale up with the device dimensions. We can also estimate the wave speed in both electrodes. For the square electrode the average wave speed is 2000/50=40 μm/s. For the round electrode we can estimate an average speed of 250/2.5=100 μm/s.

Table III: Comparison between the signals measured in the IBIDI round electrode with the signals measure in the square type of electrode (Mushroom).

Parameter	**Mushroom sensing device (square shape)**	**IBIDI sensing device (circular shape)**	**Parameter ratio (Mushroom/ IBIDI)**
Electrode width (*w*)	2000 µm	250 µm	8
Electrode area	4×10^6 µm^2	4987 µm^2	802
Signal duration	50s	2.5s	20
Signal area	700 µV×s	12.5 µV×s	56

Using the concept of a traveling wave, and provided that we use an interdigitated electrode geometry, we can predict that the same wave can cross several times the same sensing electrode producing periodic signals in the external circuit. Knowing the distance between adjacent electrodes and the traveling wave speed on, we can predict the period of the signal. Let's begin our analysis for the PHILIPS device. The electrode width is 5 µm and the space between fingers is 10 µm. Therefore, the sensing electrodes are separated apart by 25 µm. If the wave travels at 12.5 µm/s, we expect an average time between signals of approximately 2 seconds. This is only true if there is only a single wave traveling. Figure 5.6 shows and example recorded in PHILIPS devices where the signals are indeed separated by approximately 2 seconds.

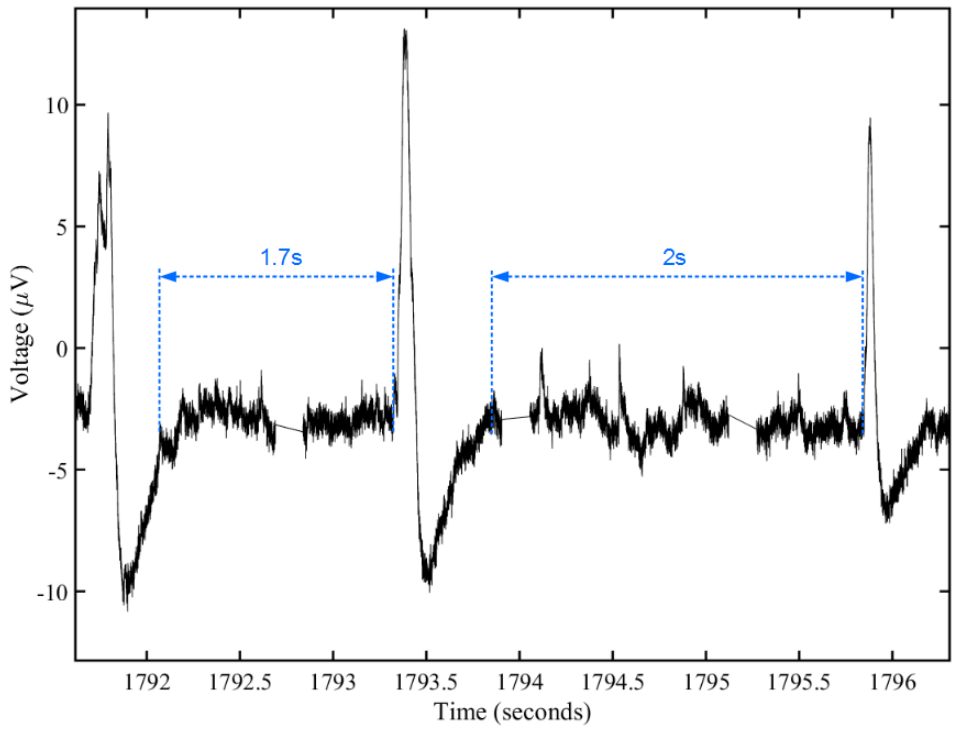

Figure 5.6: A short time trace of discrete signals separated by approximately 2s. This period is predicted if the same wave crosses two fingers of the same sensing electrode. The data was recorded using a PHILIPS sensing device.

Let's now analyze the case of an interdigitated IBIDI device. The distance between the sensing electrodes is now 2×325+100=750 µm. The wave speed in this device is estimated to be 8 µm/s. Therefore, two signals should be apart approximately by 750/8=94 seconds. Figure 5.7 shows a time trace with two signals that fit on this expected behavior caused by a wave that travels a distance longer than two electrode fingers. The prediction number 3 is experimentally verified.

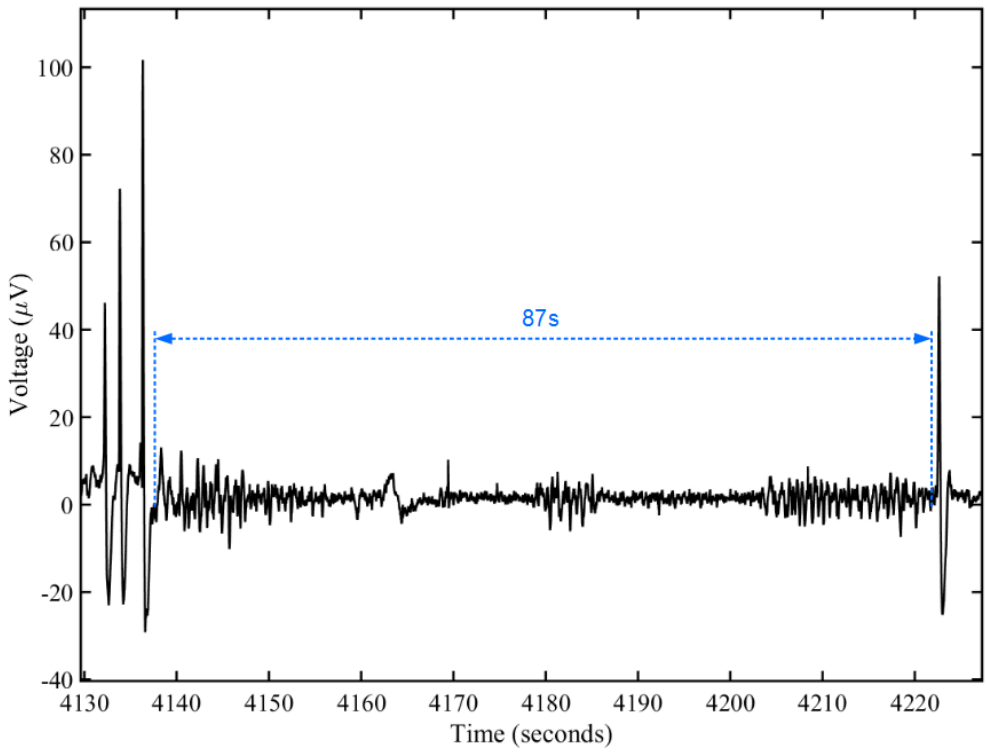

Figure 5.7: A short time trace of discrete signals separated by approximately 87s. This period is predicted if the same wave crosses two fingers of the same sensing electrode. The data was recorded using a IBIDI Inter. sensing device.

Table III compares the average signal duration measured in four types of devices, the square shaped electrode (Figure 5.3 A), the finger-shaped electrode with a track width of w=100 µm (Figure 5.3 B), the round electrode (Figure 5.3 C), and another finger-shaped electrode with a track width of w = 5µm (Figure 5.3 D).

Comparing Figure 5.3 A (square electrode) with Figure 5.3 C (round electrode), the average signal duration is significant higher (50s) on the large area device when compared with the smaller area device (only 2.5s). The ratio between the signal duration is 20. This ratio does not scale with

the ratio of the areas that reaches 802. Also, it is very different from the ratio between the widths of the electrodes, which is only 8.

It is clear the signal duration increases with the electrode area. However, this increase does not goes proportionally with the electrode dimensions. It is important to note, that comparison is not straightforward because the electrodes do not have the same shape, one electrode has a square shape and the other is round.

A total number of 40 signals were analyzed. The majority of the signals (25 out of 40 signals) have duration between 40 and 60 seconds. For a particular sensing electrode the average signal duration was considered the signal duration corresponding to the highest number of occurrences. For the case of Figure 5.3 the average signal duration was 50 seconds.

5.4 Discussion and conclusion

In this chapter, we analyze the experimental data using the concept that the signal is caused by a traveling wave across the cell population. Assuming that the wave travels with a constant speed in different experiments, we made a series of predictions.

According to this prediction, the electrode design should control the basic features of the signal. Among the predictions made are the following ones; (i) the signal duration should be determined by the electrode width, (ii) the signal power should be proportional to the active area and (iii) the electrode design will introduce periodicity in the signals.

The experimental data confirms that the signal power scales with the electrode area. Signals duration increase with electrode width but does no scale up in a linear fashion as should be. Also based on the data recorded we can estimate a broad distribution of wave speeds ranging from 8 μm/s up to 100 μm/s. These wave speed values are in agreement with traveling wave speed for calcium waves reported in the literature[1, 2, 3]. The reason why the wave speed changes from device to device or from experiment to experiment is not clear yet. We do not know if this is related with an intrinsic biological effect to encode biological information.

References

1. Kuga, N., Sasaki, T., Takahara, Y., Matsuki, N. & Ikegaya, Y. Large-scale calcium waves traveling through astrocytic networks in vivo. *J. Neurosci.* **31**, 2607–2614 (2011).

2. Innocenti, B., Parpura, V. & Haydon, P. G. Imaging extracellular waves of glutamate during calcium signaling in cultured astrocytes. *J. Neurosci.* **20**, 1800–1808 (2000).

3. Koenigsberger, M., Seppey, D., Bény, J. L. & Meister, J. J. Mechanisms of propagation of intercellular calcium waves in arterial smooth muscle cells. *Biophys. J.* **99**, 333–343 (2010).

Chapter 6

Frequency modulation in bio-electrical signals: blueshifted and redshifted signals

Bio-electrical signal patterns modulated in frequency are presented and discussed. Signal patterns named blueshift and redshift have been recorded in human tumors (glioblastoma) and in cancer cell cultures. The term blueshift is used to designate the phenomena when the signal frequency increases with time. The term redshift is used to designate the phenomena when the signal frequency decreases with time. Blue and redshift start from a typical equilibrium state with a frequency of approximately 0.7Hz. Blueshift increases up to 2Hz and redshift decreases down to 17mHz. Both blue and redshift follow an exponential law as function of time. A comparison with other biological systems shows that redshift has also been reported for cardiac systems.

6.1 Introduction

In this chapter several signal patterns modulated in frequency are described. These patterns appear in bursts and are characterized by a change in frequency while signal amplitude remains constant. These bursts were referred as frequency modulated signals.

To the best of our knowledge, it is the first time these signal patterns have been recorded and quantified in cancer cells. A search in the literature reveals the heart beating rate also decreases with time following an exponential law. The common feature between action potentials in a cardiac system and cancer cells is a traveling electrical oscillation trough the biological tissue. In this respect both systems have some resemblances, which will be discussed in this chapter.

This chapter is organized as follows; it begins by presenting the phenomena of blue and redshift observed in cell cultures as well as in brain tumors (*ex-vivo*). Next, the frequency modulation is quantified using a single exponential law. Then in the discussion section, the similarities between the propagation of electrical oscillation in a cardiac system and electrical oscillations in cancer cells are discussed.

6.2 Experimental

Here in the experimental data showing blue and red shift is presented. Blueshift appears at the onset of a burst and redshift appears at the end of the burst. Fig. 6.1 shows a typical signal pattern. Relatively quiet or silent regions separate bursts. Some bursts have blueshift, others redshift. A burst may exhibit even both types of behavior. The term blueshift is used to describe an increase in frequency with time (shift to higher frequencies), and the term redshift is used to characterize the decrease in frequency with time (shift to lower frequencies).

This type of frequency modulation was recorded in a variety of cells, including primary cultures of astrocytes (from rat), glioma cells derived from tumors, human tumors as well as in immortal cell line cultures including the C6, and U87 lines. Both red and blueshift has also been recorded in several device designs and with different active sensing areas and it is always a result of a spontaneous cell activity. The frequency modulation is not a systematic feature in all bursts of activity. Often signal bursts begin and end abruptly or without a particular trend.

Figure 6.1. shows an example of a typical signal burst recorded from C6 cells using a PHILIPS sensing device. Signals were recorded in current detection mode. The burst begins with a clear blueshift (blue line) and it terminates with a redshift (red colored line). In between there is a relatively quiet region highlighted in black.

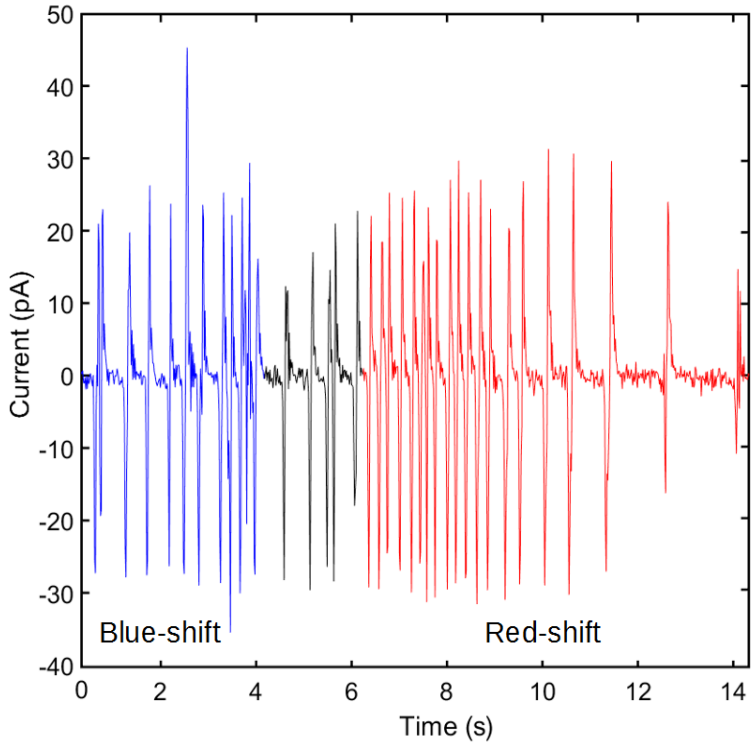

Figure 6.1: Burst of activity showing a blueshift and redshift behavior. This frequency modulation was measured in C6 cell culture using a PHILIPS device.

In order to quantity both blue and redshifted signals, the time between consecutive signals (instant frequency) is plotted as function of time. To carry out this plot one has to define the initial time, in other words when is t = 0s. For the blueshift, the initial time is assumed to be the time at which occurs the first signal in the blueshift sequence. For the redshift the time at which occurs the first signal at constant frequency was also assumed to be the initial time. This time is named "Relative time".

To characterize the frequency modulation we make graphs where the relative time is plotted on the x-axis and the corresponding time between consecutive signals is plotted on the y-axis. In the following sections we carried out this analysis for blue and redshifted signals in a separated order.

6.2.1 Blueshift

Fig. 6.2 shows a signal time trace with a well-defined blueshift measured in C6 cells and using a PHILIPS sensing device. The blue shift is quantified using the procedure outlined in above.

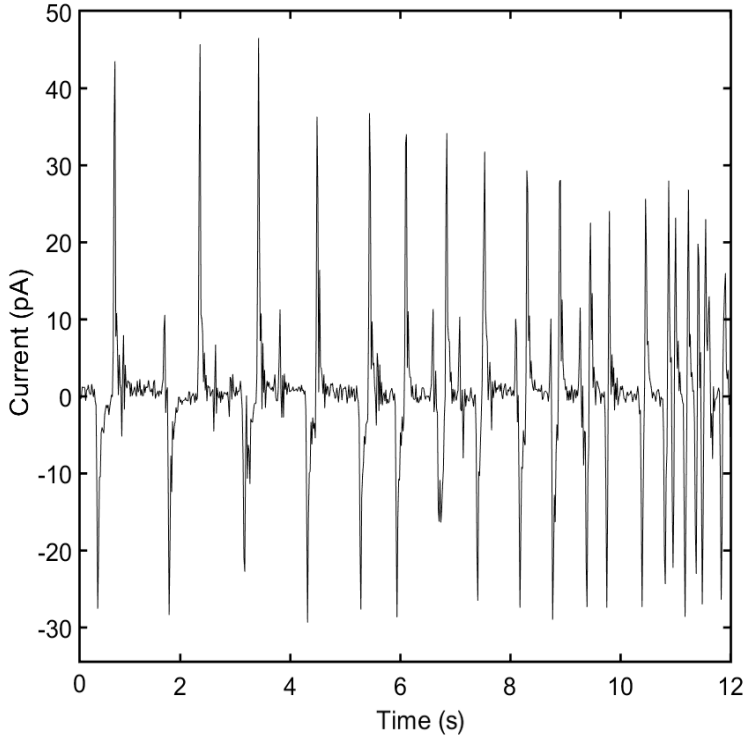

Figure 6.2: Blueshift at the onset of a burst. This burst was measured in C6 cells using a PHILIPS sensing device.

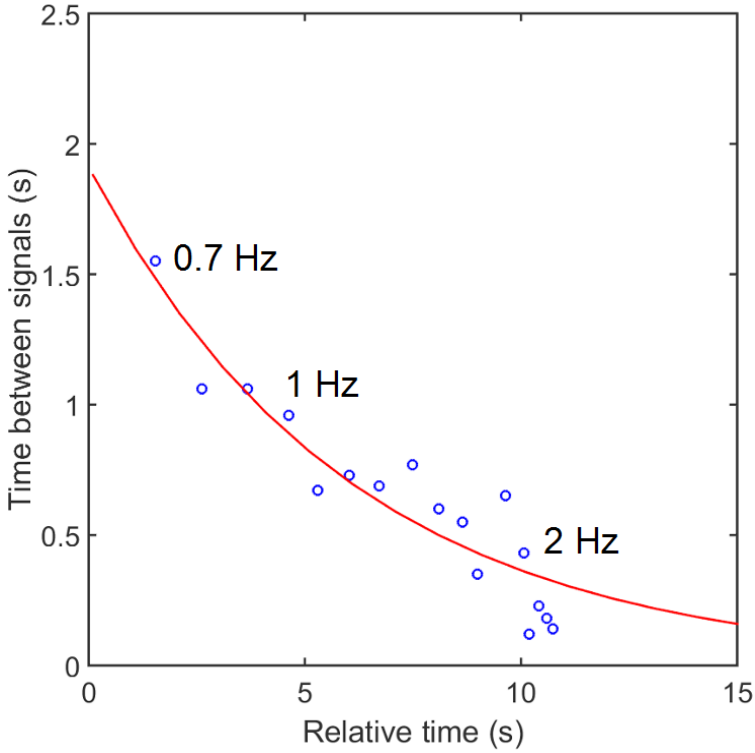

Figure 6.3: Quantification of the blueshift represented in Figure 6.1 and 6.2. The relative time begins at the time when the first signal occurs.

Figure 6.3 shows the time between consecutive signals plotted as function of the relative time following the procedure as defined above. At t = 0s the time between consecutive signals is approximately 1.5s (0.7Hz), then the signals get more frequent and they reach a period of approximately of 0.25s (4Hz) between the last few signals.

Figure 6.3 also shows the corresponding instant frequency values of the in between remaining signals. The frequency increases from 0.7Hz up to 4Hz, hence the signal frequency increases from starting to ending point approximately 3 times in a time scale of only 10 seconds.

The experimental data on Figure 6.3 can be reasonably fitted with an exponential law:

$$\Delta t = A \exp(-t/\tau) + \Delta t_{\infty} \qquad (1)$$

where $\Delta t = 5\times10^{-4}$s is the expected period of the signal when t = ∞. Δt is the time between consecutive signals, A is a constant and τ is the time constant. For the fitting in Figure 6.3 the constant A = 1.9 and the estimated time constant is τ = 6.04s (~ 0.17Hz). To show the quality of the exponential law fitting is convenient to represent the data in a semi-logarithmic plot as shown in Figure 6.4. The exponential law seems to be a reasonable description of the behavior.

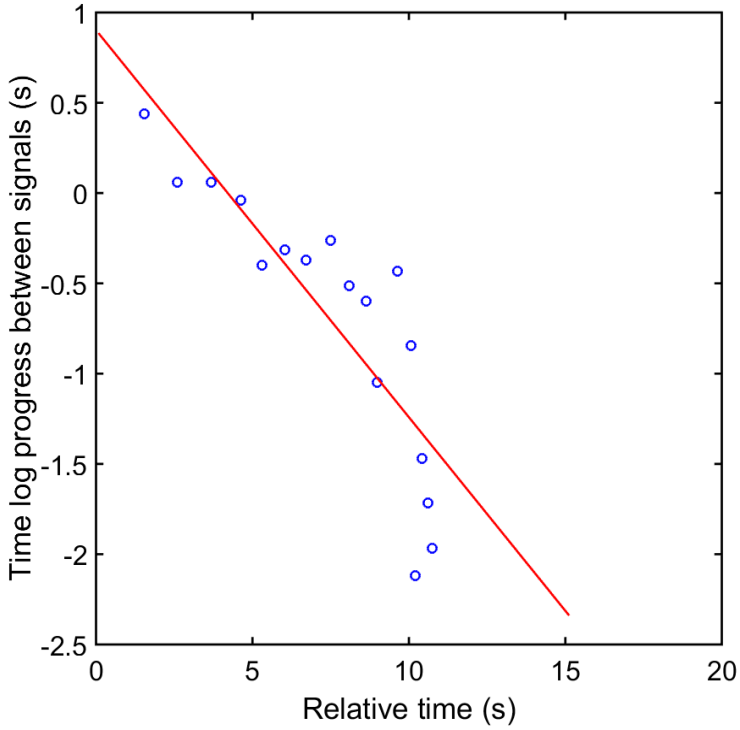

Figure 6.4: Semi-logarithmic plot of blueshift in Fig. 6.1/6.2. The continuous straight red line is the fit with the exponential law in (Eq.1), whose new parameters are A = 0.9 and τ = 4.66s (~ 0.21Hz).

6.2.2 Redshift

Figure 6.5 shows a time trace identified as redshift and measured in a U87 cell population using a small circular IBIDI sensing device. The redshift is quantified using the procedure previously described for blue and red shift.

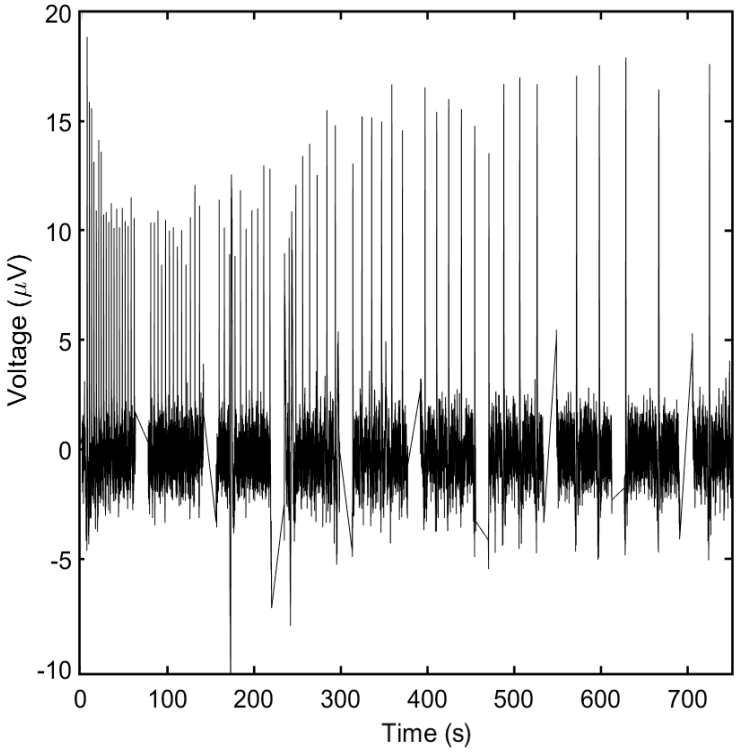

Figure 6.5: Signal burst with a redshift behavior. This burst was measured in a U87 cell population using a small circular IBIDI sensing device.

Figure 6.6 shows the time between two consecutive signals plotted as function of the relative time. The frequency modulated pattern show a frequency decrease from 0.4Hz down to 17mHz.

Figure 6.7 shows the semi-logarithmic plot of the data on Fig. 6.6. There is a clear change in slope at around 200 seconds. It is clear that the overall data is best described by a double exponential power law:

$$\Delta t = A\,exp(-t/\tau_1) + B\,exp(-t/\tau_2) + \Delta t_0 \qquad (2)$$

Here A and B are simple constants and τ_1 and τ_2 are the time constants related with frequency shift of cells signaling activity observed in bursts. Using equation (2) and the two straight lines in Fig. 6.7 it is obtained the following parameters: $A = 0.97$, $\tau_1 = 188.68$s, and, $B = 0.92$, $\tau_2 = 243.90$s.

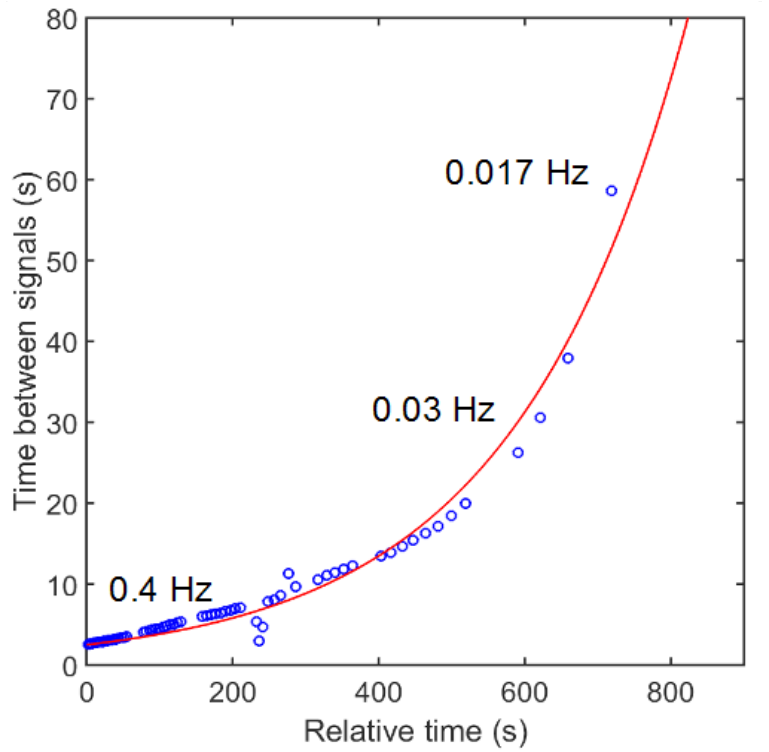

Figure 6.6: Plot of the time between consecutive signals as function of the relative time for a redshifted signal pattern. The continuous red line is the a single exponential fitting (Eq.1) with A=2.51s and τ = 237.76s.

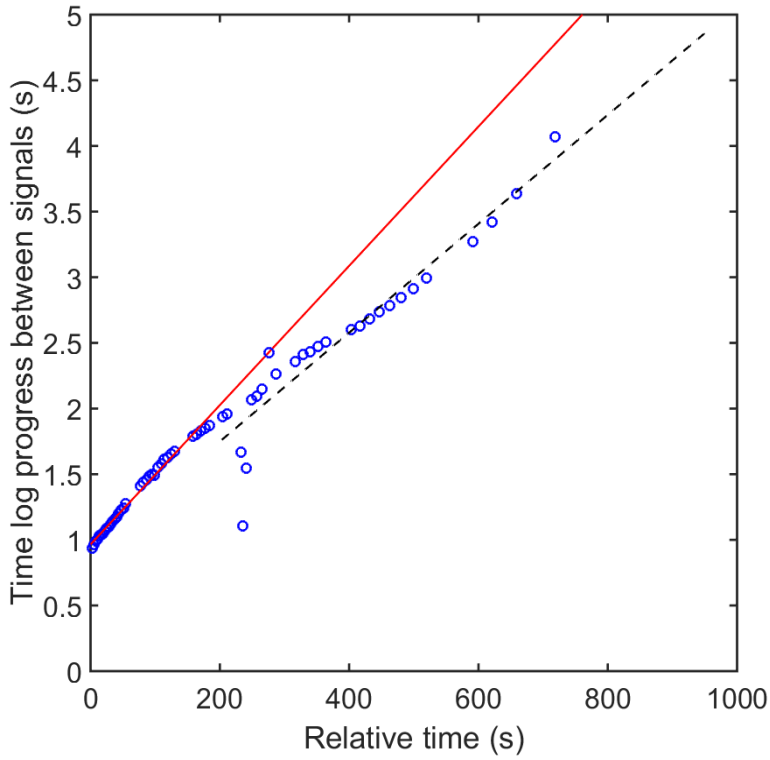

Figure 6.7: Semi-logarithmic plot of redshift in Fig. 6.5 to extract parameter for double exponential law (Eq.2). The continuous straight red line is the fit of the burst first 180s and related with A = 0.97 and τ_1 = 188.88s (~ 5.3mHz); the dashed black line is the burst fit from 200s on and it relates with B = 0.92 and τ_2 = 243.9s (~ 4.1mHz). Dashed line may be result of instrumental deviation.

When looking at Fig. 6.8 one can see two models, single and double, of exponential fitting curves about the previous U87 cells measured in IBIDI sensing device. The red-lined curve over data is the same as in Fig.6.6 which is drawn by a single exponential law already presented in (1). The black-lined one is the fitting curve it gets from the double exponential law shown in (2).

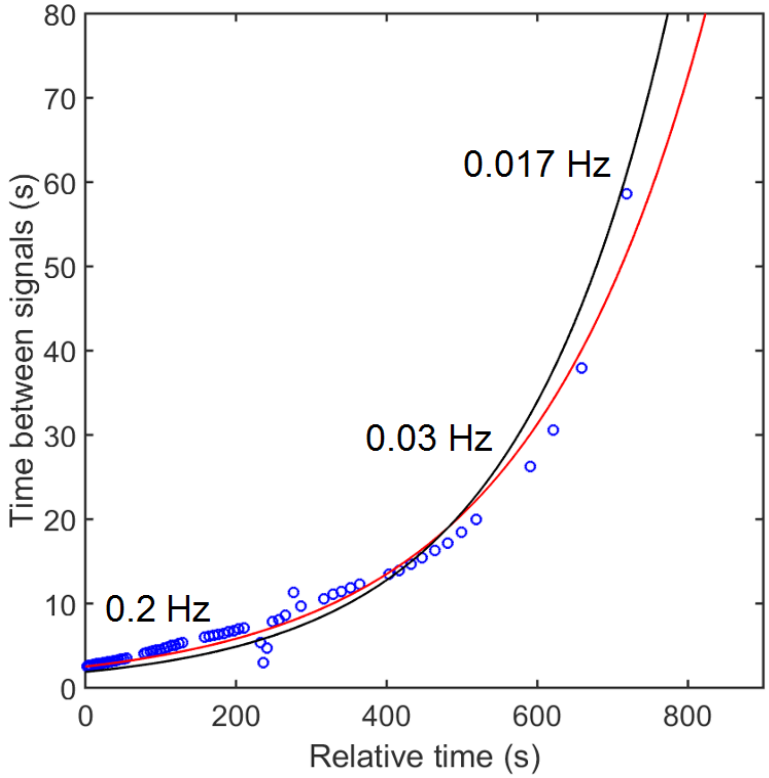

Figure 6.8: The single exponential curve to fit the data (red-lined curve) is directly compared with the double exponential fitting curve for the same data (black-lined curve). When replacing in (2) the time constants τ_1 and τ_2 by Figure 6.7 linear regression slopes inverse and exponential multiplier factors A_1 and A_2 by Figure 6.9 linear regression offset, one can actually see until $t = 400$s both curves are very close to each other, between time interval of [400s, 500s] curves overlap, and from $t = 500$s and on exponential curves tend to tell apart through the *xx* axis more and more.

Figure 6.9 shows three different redshift behavior recorded during a single experiment carried out using U87 cells and a circular IBIDI device. The initial frequency is approximately equal in all the traces (0.2Hz) but decreases and it end ups very near to 20mHz (17mHz-25mHz) in different time spans (250s-700s). The data on Fig. 6.9 shows that the time constant change from 106s up to 237s. This means that the redshift time constants are not defined by a particular device or cell population.

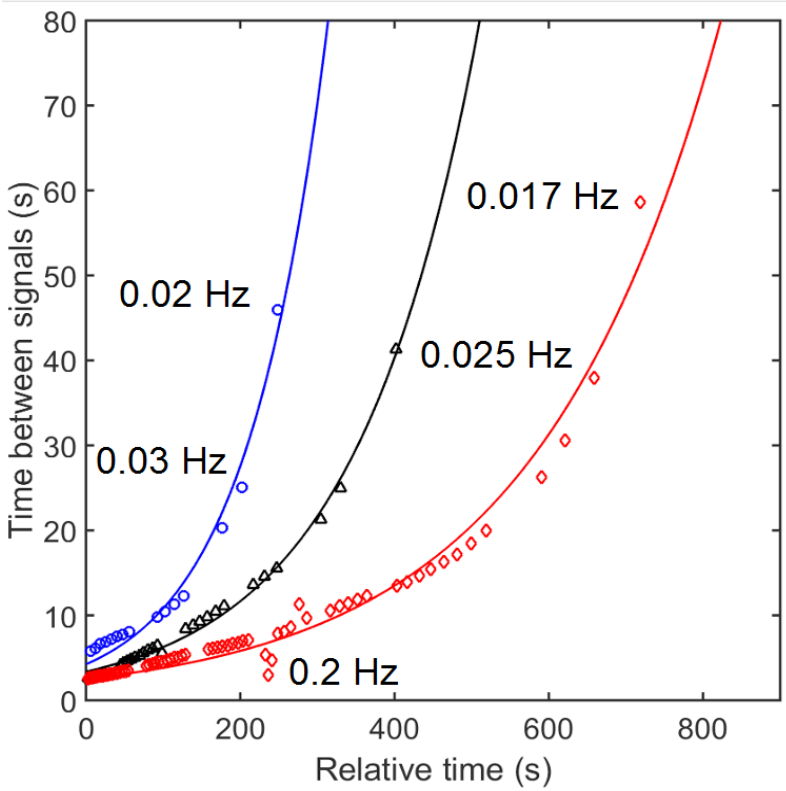

Figure 6.9: Three different redshift behaviors recorded in a U87 cell population using a small circular IBIDI sensing device. The are estimated using the single exponential law shown in (1). Therefore their respective constants A and time constants τ are: A_1=4.24 and τ_1 = 106.38s (~9.4mHz) for the blue-lined redshift fitting curve; A_2 = 3.37 and τ_2 = 161.29s (~ 6.2mHz) for the black-lined redshift fitting curve; A_3 = 2.51 and τ_3=237.76s (~ 4.2mHz) for the red-lined redshift fitting curve, the same as in Figure 6.6.

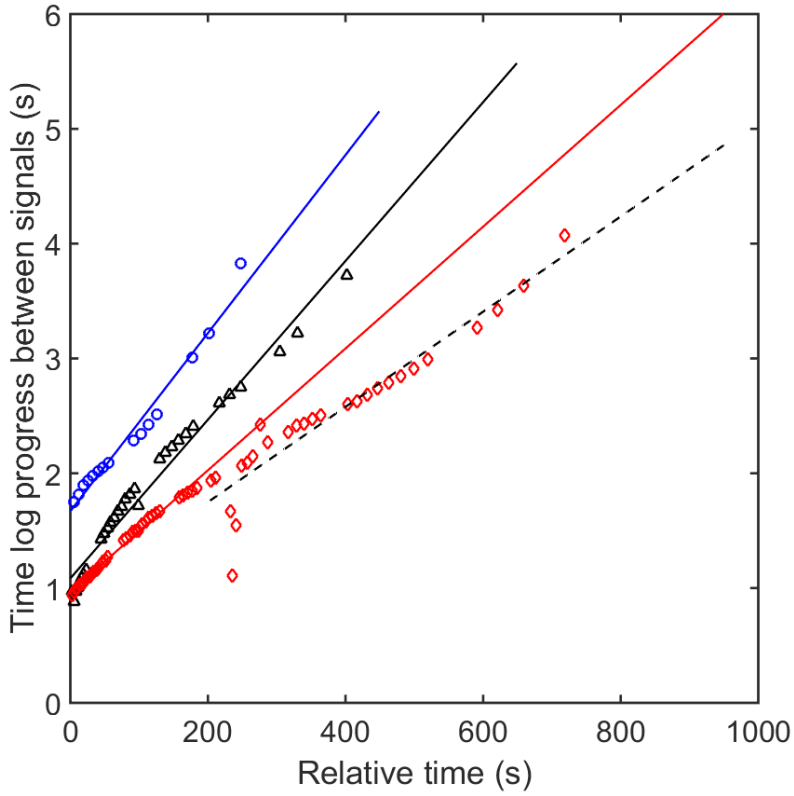

Figure 6.10: Semi-logarithmic of each single exponential fitting curve in Fig. 6.9. The color of each straight line relates to the single exponential with the same colored line in Fig. 6.9. From the blue straight line one gets parameters A_1 = 1.67 and τ_1 = 128.21s (~ 7.8mHz); the black straight line obtains parameters A_2 = 1.08 and τ_2 = 144.93s (~ 6.9mHz); the red straight line, which is the same as in Fig. 6.7, for the first 180s of its own burst gets parameters values A_3 = 0.97 and τ_3=188.68s (~ 5.3mHz), and the dashed black line is seen as distortion of measurements and it has parameter; A_3 = 0.92 and τ_3 = 243.9s (~ 4.1mHz).

6.3 Dependence on cell type and chip geometry

In this section we analyze how the frequency modulation depends on the cell type as well as on the device geometry. Table I summarizes the major results obtained.

For the case of C6 cells the time constants for blueshift (τ_B) and for redshift (τ_R) are comparable and in a time scale of 1 to 10 seconds. This seems to be also true for the signals measured on a brain tumor, but now in a time scale between 20 to 50 seconds. The slowest time scales have been measured for the U87 type of cells. Quite relevant is the shortest and the longest time measured between signals. The shortest period (Δt_0) measured is around 2 seconds and the longest period (Δt_∞) between signals is from 50 to 60 seconds recorded for the U87 cells. The blue shift is a quite rare phenomena, this explains the lack of some data on Table I related with blueshift.

The data presented on Table I does not allow to extract clear conclusions about the possible role of the cell type and device geometry on the frequency modulation phenomena. The data suggests that the frequency modulation is controlled by a biological process that coordinates the cell signaling mechanism and not necessary by the cell type or by the physical aspects of the device geometry.

Table I: time constants for blue and redshifted signals recorded on different devices and cell types.

Cell type	**Device type**	**Blue-shift (τ_B)** (s)	**Red-shift (τ_R)** (s)
C6	PHILIPS	1.04, 3.27, 3.55, 6.04, 9.16	1.65, 2.58, 2.78, 3.15, 3.76, 6.68, 6.92, 8.31
HOPE	PHILIPS	----------	269.25, 279.1
Tumor 6a	Planar bacterial cellulose	26.31, 3252.03	25.67, 31.33, 33.93, 43.94
U87	Small circular IBIDI	----------	106.84, 161.29, 237.76

6.4 Discussion and conclusions

The frequency modulation phenomena presented in this chapter is well described by an exponential law. Exponential laws are common to many physical mechanisms and biological processes. A particular relevant biological system is the one related with studies on heart beating rate variability. Some studies show that an accelerated heart (induced for instance by exercise) brings the beating rate down to the normal rate following a single exponential decay[1, 2, 3, 4, 5]. The proposed physiological explanations for this behavior are complex and some involve the actuation of a biological regulation mechanisms[1]. In spite of this complexity, there is a striking similarity between cardiac cells and cancer cells. Both systems generated periodic oscillations using a synchronization mechanism. A cardiac beat is a traveling chemical wave alike the one measured in cancer cell populations and reported here. Basically, the only difference is the time scale of the process. A cardiac signal occurs in a time scale of milliseconds while the oscillations reported here could last for several seconds.

The overall conclusion is that a burst of activity terminates following and exponential decay in frequency. The mechanism controlling this exponential decay remains unclear. For the case of cardiac systems the community has proposed a biological regulation system. In general words this means that chemical signals carried by molecules play the role for realization of synchronized signaling of the cells. This is a general and accepted view. However, for our system this chemical explanation sounds implausible. There are tow basic reasons. Firstly, because in cancer cells populations or in tumors there is not a decision organ sending chemical messages, secondly molecules diffuse slowly in liquids and a chemical diffusion mechanisms needs identical molecules reaching all cells within a short time.

We propose that the exponential decay in frequency is a property of a biological system that synchronizes to produce electrical oscillations. In principle this phenomena should be more often observed. The reason why is not often reported may be due to the fact that observation tools currently available rely essentially on optical fluorescence microscopy, and these instruments do not have enough sensitivity to observe this frequency modulation phenomena.

References

1. Beltrame, T. *et al.* Associations between heart rate recovery dynamics with estradiol levels in 20 to 60 year-old sedentary women. *Front. Physiol.* **9**, 1–10 (2018).

2. Stirling, J. R., Zakynthinaki, M., Refoyo, I. & Sampedro, J. A model of heart rate kinetics in response to exercise. *J. Nonlinear Math. Phys.* **15**, 426–436 (2008).

3. Zakynthinaki, M. S. Simulating heart rate kinetics during incremental and interval training. *Biomed. Hum. Kinet.* **8**, 144–152 (2016).

4. Sacha, J. Interaction between heart rate and heart rate variability. *Ann. Noninvasive Electrocardiol.* **19**, 207–216 (2014).

5. Zakynthinaki, M. S. Modelling heart rate kinetics. *PLoS One* **10**, 1–26 (2015).

Chapter 7

Conclusions and suggestions for further development

Bio-electrical signals were recorded in cancer cell lines. Although, cancer cells are non-electrogenic, they generate slow electrical oscillations that can be recorded by extracellular electrodes. Different types of electrodes with different geometries and active sensing areas were used in this study.

Bio-electrical signals were first classified according to their shape. Once this classification was implemented, each class of signal was analyzed. This analysis includes a quantitative study of the upward and downward signal components. A broad distribution of signal power is observed. Since signals are a result of a cell synchronization mechanism, the variability in the signal power was attributed to the variability on the number of cells synchronized. This study was carried out in Chapter 3.

Chapter 4 reports a detailed characterization of the signal shape time dependence. It was shown that signal shapes are comprised of a fast rise time followed by a slow decay. The signal decay obeys to a pure exponential law. A single exponential behavior is observed in all signal shapes analyzed. The time constants are broad distributed between 2 and 30 seconds. One crucial conclusion of this signal processing study, is that the time require to reach the peak voltage, is a measure of the synchronization speed for a particular cell population. A rapid communication signaling mechanism is required for the cells to synchronize their biological activity. We propose that the information is carried by traveling waves, similar to calcium waves reported in other biological systems.

In Chapter 5 it is demonstrated that the area and the geometry of the sensing electrode controls the shape of the signal, namely the duration and the amplitude of the signal. It was verified that signal power increases with electrode sensing area. Furthermore, the signal duration also increases with electrode width. These findings further support the view that bio-electrical signals in cancer cell populations fit in the framework of traveling oscillations.

The role of the electrode geometry in shaping the electrical recorded is a relevant finding of this study. This relation between signal properties and electrode properties is crucial for the optimization of the electrode geometry and area to achieve recordings with a high signal to noise ratio. Signal patterns modulated in frequency were presented and discussed on Chapter 6. Often bursts of cell activity, begin and terminate with a signal patterns modulated in frequency. The frequency of the signal increases with time at the onset of the burst (blue shift). The burst terminates by an exponential decrease of the frequency as function of the time (red shift). The biological processes behind frequency-modulated patterns are not clear yet.

The frequency-modulated patterns were compared with frequency patterns observed in other biological systems. The cardiac beating can also exhibit a red shift. This similarity between cardiac and cancer cells is interesting, because a cardiac tissue like a cancer cell population is also an ensemble of synchronized cells, and both systems use traveling oscillations to communicate. This thesis addresses a number of relevant and novel aspects of bio-electrical signaling in cancer cell populations. However, it also raises a number of questions. In order to address these questions close interdisciplinary work with Biology is required.

Among the suggestions to pursue the research carried out in this work, we can suggest the validation of our findings with complementary and well-accepted optical techniques, namely optical fluorescence methods. This task it may not be a trivial one. Optical methods may not have the required sensitivity to observe the weak signals electrically recorded and presented here. This lack of sensitivity may impose a severe limitation on the validation and acceptance of our findings by the biological community.

There is also a strong need of fundamental understanding related with the biological aspects of the bio-electrical signaling in cancer cells. Currently, we do not know which cell membrane ion channel is involved in the signaling mechanisms. This research is still in its infancy.

In the Electronic Engineering context, the easiest path to continue this research is to optimize the electrode design for a particular cell population. The information provided in this thesis shows clearly that the electrode area and geometry plays an important role on the shape and power of the signal. The sensing area of a recording electrode must be approximate equal to the area occupied by a synchronized cell cluster. This strategy will allow us to observe only synchronized clusters. If the electrode is smaller than the size of the synchronized cluster, signal power is lost. On the other side if the electrode is too large, several uncorrelated clusters will be recorded, and it will be difficult to disentangle signals from different cell clusters.

Annex I: Signals Library

C6 cells on Mushroom electrode: Monophasic Fast Downward (MDown)

<table>
<tr><td>Signal shape and defining parameters</td><td colspan="6"> 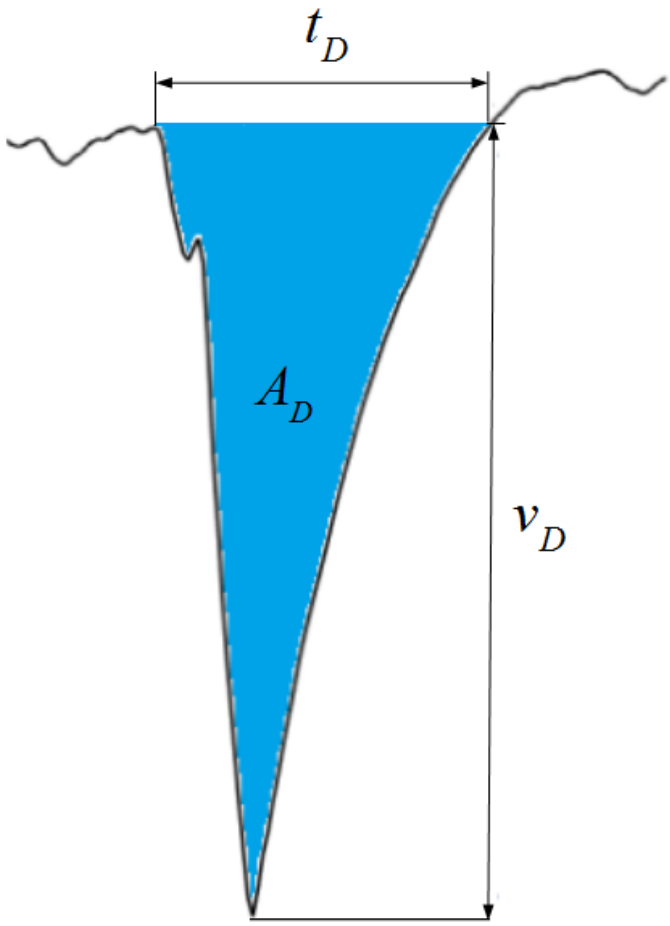
</td></tr>
<tr><td>signation</td><td colspan="3">Full name</td><td colspan="3">Acronym</td></tr>
<tr><td></td><td colspan="3">Monophasic Fast Downward</td><td colspan="3">MDown</td></tr>
<tr><td>Electrode system where it was recorded</td><td>Inter digitated</td><td>PEDOT</td><td>Mush</td><td>IBIDI large</td><td colspan="2">IBIDI small</td></tr>
<tr><td></td><td></td><td></td><td>X</td><td></td><td colspan="2"></td></tr>
<tr><td rowspan="2">Biological system where it is observed</td><td>Astrocytes</td><td colspan="2">Tumors</td><td>C6</td><td>Neurons</td><td>Other</td></tr>
<tr><td></td><td colspan="2"></td><td>X</td><td></td><td></td></tr>
<tr><td rowspan="2">Matching with ionic channels</td><td>Calcium pump</td><td colspan="2">Sodium pump</td><td></td><td></td><td></td></tr>
<tr><td>[ref1]</td><td colspan="2"></td><td></td><td></td><td></td></tr>
<tr><td>Electrical properties</td><td colspan="6">Governing equation and statistics</td></tr>
<tr><td>Amplitude-Duration ratio</td><td colspan="6">$v_D = 0.1261 t_D + 0.3456 \pm 0.0402$</td></tr>
</table>

C6 cells on Mushroom electrode: Monophasic Fast Upward (MUp)

<table>
<tr><td>Signal shape and defining parameters</td><td colspan="6"> 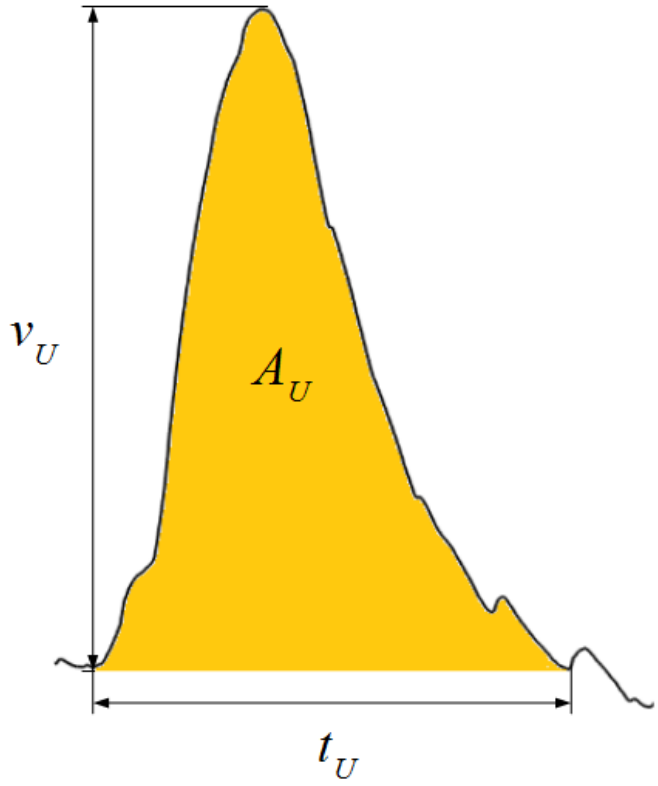
</td></tr>
<tr><td>Designation</td><td colspan="3">Full name</td><td colspan="3">Acronym</td></tr>
<tr><td></td><td colspan="3">Monophasic Fast Upward</td><td colspan="3">MUp</td></tr>
<tr><td>Electrode system where it was recorded</td><td>Inter digitated</td><td>PEDOT</td><td>Mush</td><td>IBIDI large</td><td colspan="2">IBIDI small</td></tr>
<tr><td></td><td></td><td></td><td>X</td><td></td><td colspan="2"></td></tr>
<tr><td rowspan="2">Biological system where it is observed</td><td>Astrocytes</td><td colspan="2">Tumors</td><td>C6</td><td>Neurons</td><td>Other</td></tr>
<tr><td></td><td colspan="2"></td><td>X</td><td></td><td></td></tr>
<tr><td rowspan="2">Matching with ionic channels</td><td>Calcium pump</td><td colspan="2">Sodium pump</td><td></td><td></td><td></td></tr>
<tr><td>[ref1]</td><td colspan="2"></td><td></td><td></td><td></td></tr>
<tr><td>Electrical properties</td><td colspan="6">Governing equation and statistics</td></tr>
<tr><td>Amplitude-Duration ratio</td><td colspan="6">$v_U = 0.0085 t_U + 1.5020 \pm 0.0618$</td></tr>
</table>

C6 cells on Mushroom electrode: Biphasic Fast Downward (BFDown)

<table>
<tr><td>Signal shape and defining parameters</td><td colspan="6"> 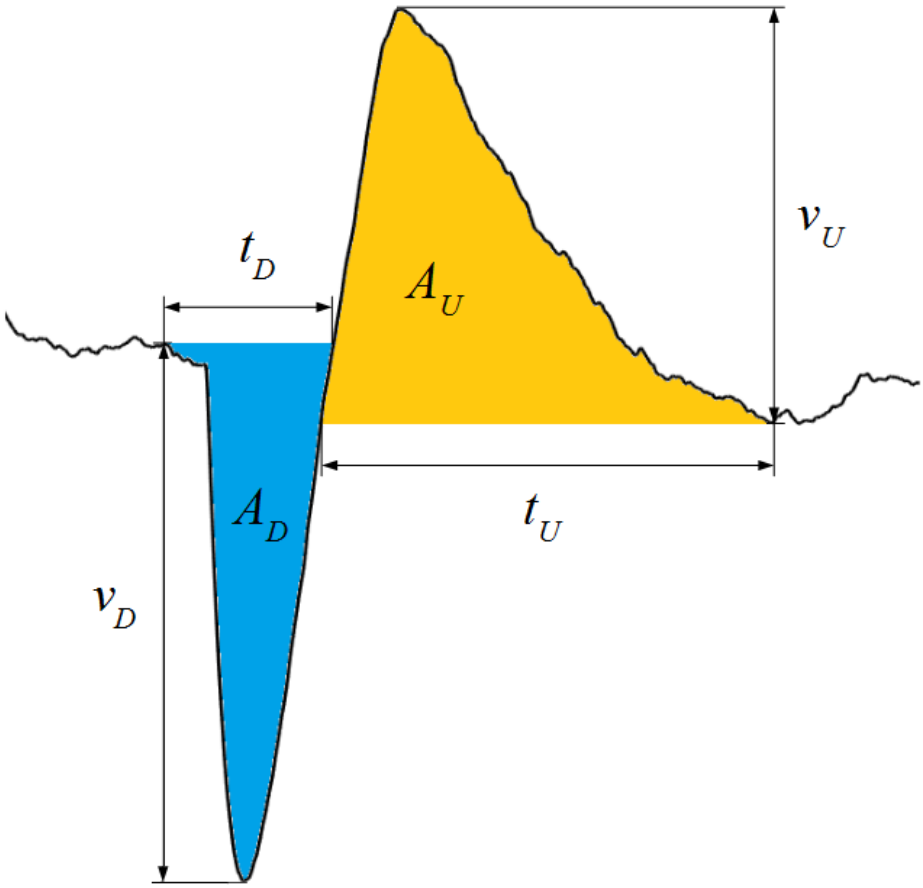
</td></tr>
<tr><td>Designation</td><td colspan="3">Full name</td><td colspan="2">Acronym</td></tr>
<tr><td></td><td colspan="3">Biphasic Fast Downward</td><td colspan="2">BFDown</td></tr>
<tr><td>Electrode system where it was recorded</td><td>Inter digitated</td><td>PEDOT</td><td>Mush</td><td>IBIDI large</td><td>IBIDI small</td></tr>
<tr><td></td><td></td><td></td><td>X</td><td></td><td></td></tr>
<tr><td rowspan="2">Biological system where it is observed</td><td>Astrocytes</td><td colspan="2">Tumors</td><td>C6</td><td>Neurons</td><td>Other</td></tr>
<tr><td></td><td colspan="2"></td><td>X</td><td></td><td></td></tr>
<tr><td rowspan="2">Matching with ionic channels</td><td>Calcium pump</td><td colspan="2">Sodium pump</td><td></td><td></td><td></td></tr>
<tr><td>[ref1]</td><td colspan="2"></td><td></td><td></td><td></td></tr>
<tr><td>Electrical properties</td><td colspan="6">Governing equation and statistics</td></tr>
<tr><td>Spikes amplitude ratio</td><td colspan="6">$v_U = 0.1886 v_D + 1.0110 \pm 0.0802$</td></tr>
<tr><td>Spikes duration ratio</td><td colspan="6">$t_U = 1.3964 t_D + 11.7428 \pm 0.6286$</td></tr>
<tr><td>Spikes area ratio</td><td colspan="6">$A_U = 0.6081 A_D + 10.9661 \pm 0.2084$</td></tr>
</table>

C6 cells on Mushroom electrode: Biphasic Fast Upward (BFUp)

Signal shape and defining parameters	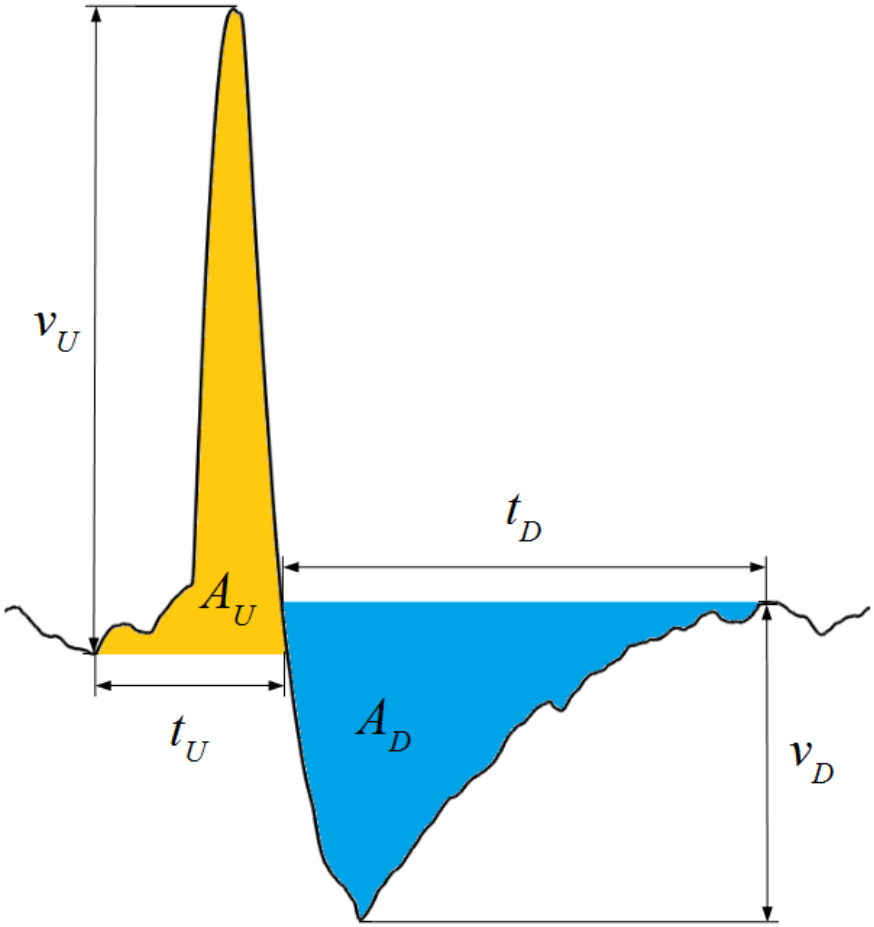

Designation	**Full name**			**Acronym**		
	Biphasic Fast Upward			*BFUp*		
Electrode system where it was recorded	Inter digitated	PEDOT	Mush	IBIDI large	IBIDI small	
			X			
Biological system where it is observed	**Astrocytes**	**Tumors**		**C6**	**Neurons**	**Other**
				X		
Matching with ionic channels	Calcium pump	Sodium pump				
	[ref1]					
Electrical properties	**Governing equation and statistics**					
Spikes amplitude ratio	$v_U = 1.8536 v_D + 0.6388 \pm 0.2296$					
Spikes duration ratio	$t_U = 0.2540 t_D + 4.7593 \pm 0.1491$					
Spikes area ratio	$A_U = 1.0889 A_D + 1.7124 \pm 0.2302$					

C6 cells on Mushroom electrode: Biphasic Symmetric (BS)

<table>
<tr><td>Signal shape and defining parameters</td><td colspan="6"> 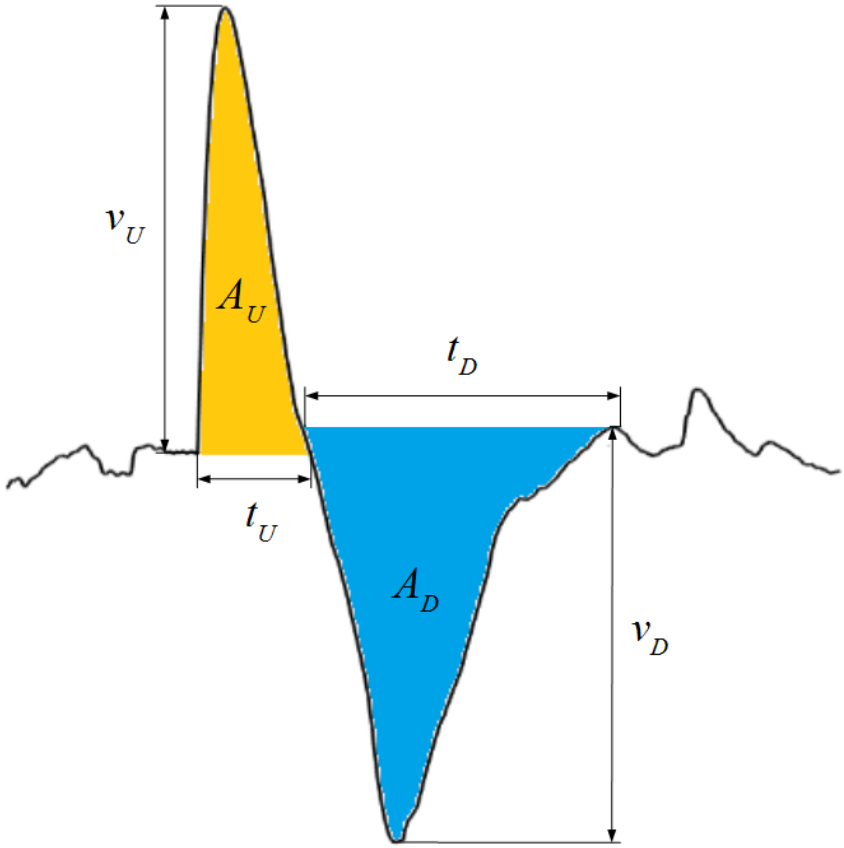
</td></tr>
<tr><td>Designation</td><td colspan="3">Full name</td><td colspan="3">Acronym</td></tr>
<tr><td></td><td colspan="3">Biphasic Symmetric</td><td colspan="3">BS</td></tr>
<tr><td>Electrode system where it was recorded</td><td>Inter digitated</td><td>PEDOT</td><td>Mush</td><td>IBIDI large</td><td colspan="2">IBIDI small</td></tr>
<tr><td></td><td></td><td></td><td>X</td><td></td><td colspan="2"></td></tr>
<tr><td rowspan="2">Biological system where it is observed</td><td>Astrocytes</td><td colspan="2">Tumors</td><td>C6</td><td>Neurons</td><td>Other</td></tr>
<tr><td></td><td colspan="2"></td><td>X</td><td></td><td></td></tr>
<tr><td rowspan="2">Matching with ionic channels</td><td>Calcium pump</td><td colspan="2">Sodium pump</td><td></td><td></td><td></td></tr>
<tr><td>[ref1]</td><td colspan="2"></td><td></td><td></td><td></td></tr>
<tr><td>Electrical properties</td><td colspan="6">Governing equation and statistics</td></tr>
<tr><td>Spikes amplitude ratio</td><td colspan="6">$v_U = 1.1634 v_D - 0.0497 \pm 0.1966$</td></tr>
<tr><td>Spikes duration ratio</td><td colspan="6">$t_U = 0.3061 t_D - 6.0754 \pm 0.2245$</td></tr>
<tr><td>Spikes area ratio</td><td colspan="6">$A_U = 0.4357 A_D + 5.4420 \pm 0.1342$</td></tr>
</table>

HOPE cells on Mushroom electrode: Monophasic Fast Downward (MDown)

<table>
<tr><td>Signal shape and defining parameter</td><td colspan="6"> 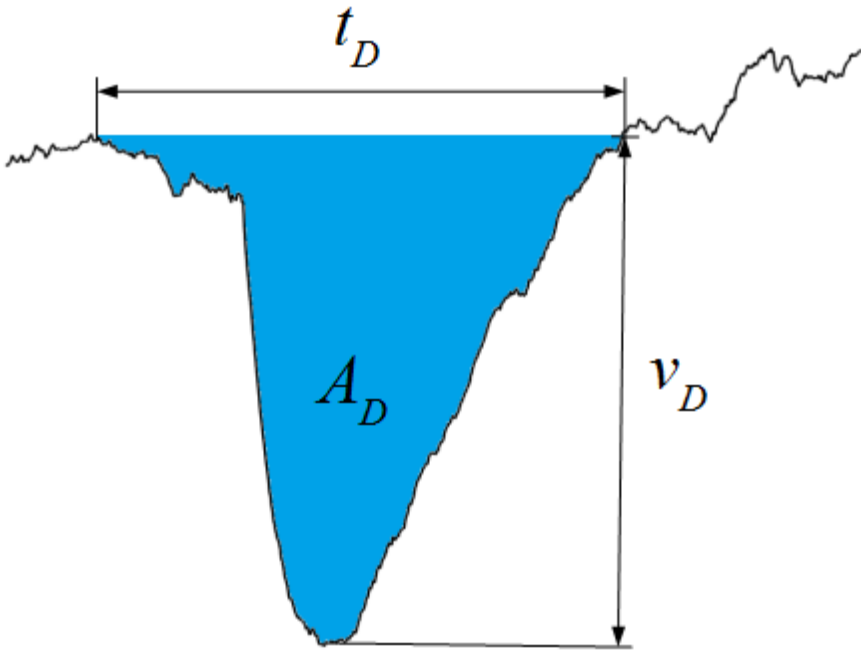
</td></tr>
<tr><td>Designation</td><td colspan="3">Full name</td><td colspan="2">Acronym</td></tr>
<tr><td></td><td colspan="3">Monophasic Fast Downward</td><td colspan="2">MDown</td></tr>
<tr><td>Electrode system where it was recorded</td><td>Inter digitated</td><td>PEDOT</td><td>Mush</td><td>IBIDI large</td><td>IBIDI small</td></tr>
<tr><td></td><td></td><td></td><td>X</td><td></td><td></td></tr>
<tr><td rowspan="2">Biological system where it is observed</td><td>Astrocytes</td><td colspan="2">Tumors</td><td>C6</td><td>Neurons</td><td>Other</td></tr>
<tr><td></td><td colspan="2"></td><td></td><td></td><td>HOPE</td></tr>
<tr><td rowspan="2">Matching with ionic channels</td><td>Calcium pump</td><td colspan="2">Sodium pump</td><td></td><td></td><td></td></tr>
<tr><td>[ref1]</td><td colspan="2"></td><td></td><td></td><td></td></tr>
<tr><td>Electrical properties</td><td colspan="6">Governing equation and statistics</td></tr>
<tr><td>Amplitude-Duration ratio</td><td colspan="6">$v_D = 2.4441 t_D - 80.2015 \pm 2.2119$</td></tr>
</table>

HOPE cells on Mushroom electrode: Monophasic Fast Upward (MUp)

<table>
<tr><td>Signal shape and defining parameter</td><td colspan="6"> 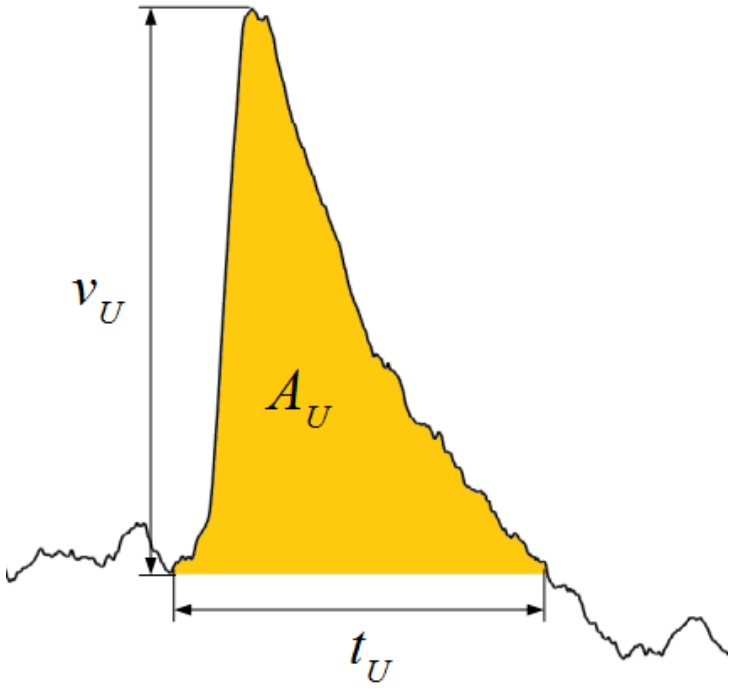
</td></tr>
<tr><td>Designation</td><td colspan="3">Full name</td><td colspan="2">Acronym</td></tr>
<tr><td></td><td colspan="3">Monophasic Fast Upward</td><td colspan="2">MUp</td></tr>
<tr><td>Electrode system where it was recorded</td><td>Inter digitated</td><td>PEDOT</td><td>Mush</td><td>IBIDI large</td><td>IBIDI small</td></tr>
<tr><td></td><td></td><td></td><td>X</td><td></td><td></td></tr>
<tr><td rowspan="2">Biological system where it is observed</td><td>Astrocytes</td><td colspan="2">Tumors</td><td>C6</td><td>Neurons</td><td>Other</td></tr>
<tr><td></td><td colspan="2"></td><td></td><td></td><td>HOPE</td></tr>
<tr><td rowspan="2">Matching with ionic channels</td><td>Calcium pump</td><td colspan="2">Sodium pump</td><td></td><td></td><td></td></tr>
<tr><td>[ref1]</td><td colspan="2"></td><td></td><td></td><td></td></tr>
<tr><td>Electrical properties</td><td colspan="6">Governing equation and statistics</td></tr>
<tr><td>Amplitude-Duration ratio</td><td colspan="6">$v_U = 0.7021 t_U + 21.9919 \pm 0.8483$</td></tr>
</table>

HOPE cells on Mushroom electrode: Biphasic Fast Downward (BFDown)

<table>
<tr><td>Signal shape and defining parameter</td><td colspan="6"> 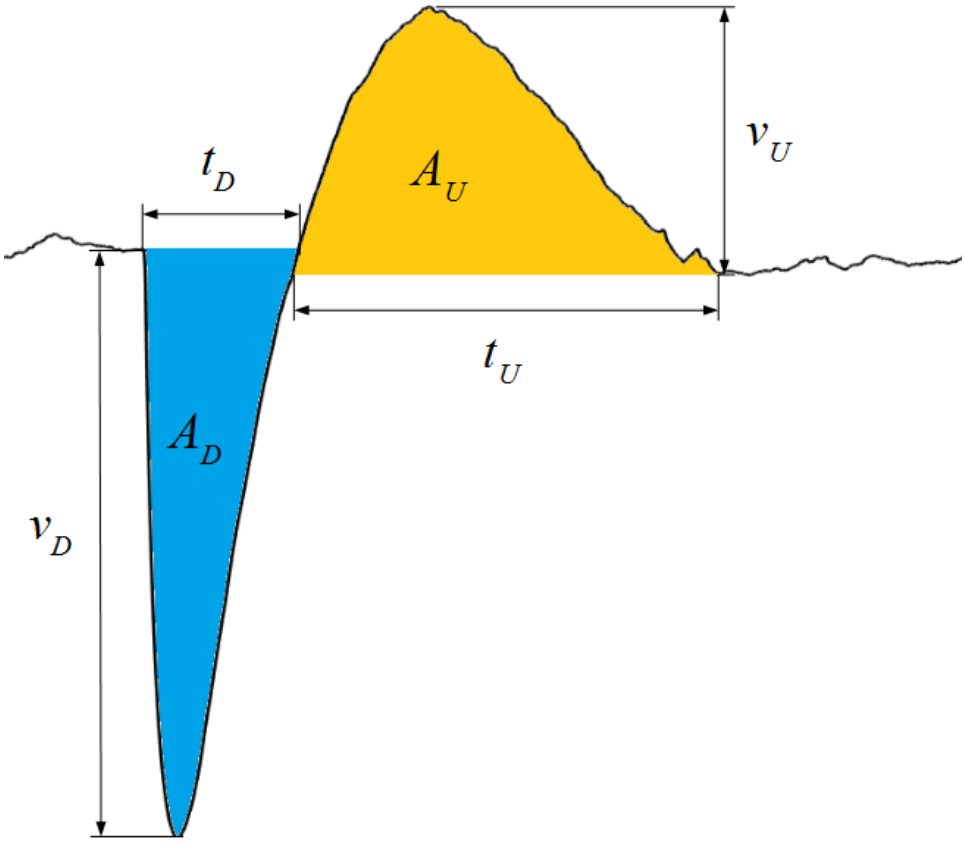
</td></tr>
<tr><td>Designation</td><td colspan="3">Full name</td><td colspan="2">Acronym</td></tr>
<tr><td></td><td colspan="3">Biphasic Fast Downward</td><td colspan="2">BFDown</td></tr>
<tr><td>Electrode system where it was recorded</td><td>Inter digitated</td><td>PEDOT</td><td>Mush</td><td>IBIDI large</td><td>IBIDI small</td></tr>
<tr><td></td><td></td><td></td><td>X</td><td></td><td></td></tr>
<tr><td rowspan="2">Biological system where it is observed</td><td>Astrocytes</td><td colspan="2">Tumors</td><td>C6</td><td>Neurons</td><td>Other</td></tr>
<tr><td></td><td colspan="2"></td><td></td><td></td><td>HOPE</td></tr>
<tr><td rowspan="2">Matching with ionic channels</td><td>Calcium pump</td><td colspan="2">Sodium pump</td><td></td><td></td><td></td></tr>
<tr><td>[ref1]</td><td colspan="2"></td><td></td><td></td><td></td></tr>
<tr><td>Electrical properties</td><td colspan="6">Governing equation and statistics</td></tr>
<tr><td>Spikes amplitude ratio</td><td colspan="6">$v_U = 0.2880 v_D + 5.1836 \pm 0.0881$</td></tr>
<tr><td>Spikes duration ratio</td><td colspan="6">$t_U = 1.0365 t_D + 13.7561 \pm 0.4989$</td></tr>
<tr><td>Spikes area ratio</td><td colspan="6">$A_U = 0.5134 A_D + 150.9487 \pm 0.2859$</td></tr>
</table>

HOPE cells on Interdigitated electrode: Biphasic Fast Downward (BFDown)

<table>
<tr><td>Signal shape and defining parameter</td><td colspan="6"> 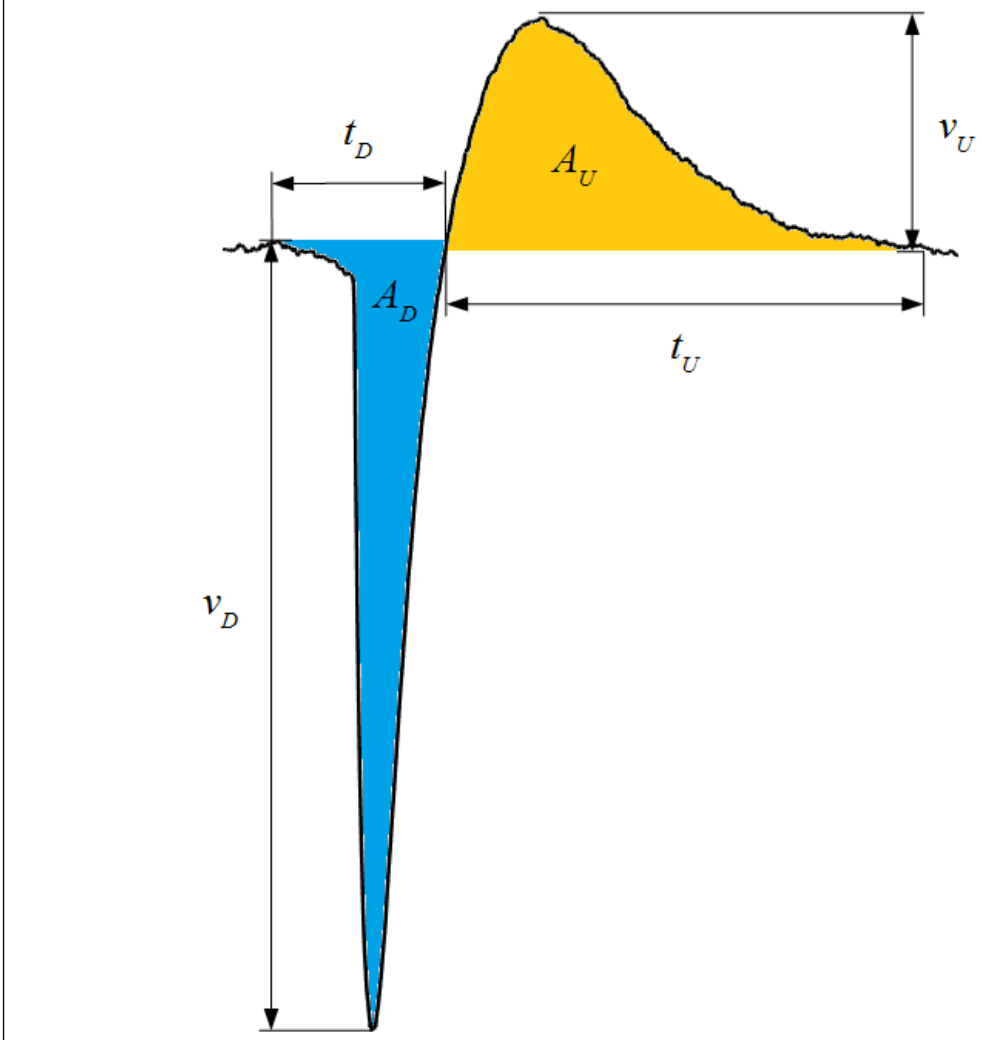
</td></tr>
<tr><td>Designation</td><td colspan="3">Full name</td><td colspan="2">Acronym</td></tr>
<tr><td></td><td colspan="3">Biphasic Fast Downward</td><td colspan="2">BFDown</td></tr>
<tr><td>Electrode system where it was recorded</td><td>Inter digitated</td><td>PEDOT</td><td>Mush</td><td>IBIDI large</td><td>IBIDI small</td></tr>
<tr><td></td><td>X</td><td></td><td></td><td></td><td></td></tr>
<tr><td rowspan="2">Biological system where it is observed</td><td>Astrocytes</td><td colspan="2">Tumors</td><td>C6</td><td>Neurons</td><td>Other</td></tr>
<tr><td></td><td colspan="2"></td><td></td><td></td><td>HOPE</td></tr>
<tr><td rowspan="2">Matching with ionic channels</td><td>Calcium pump</td><td colspan="2">Sodium pump</td><td></td><td></td><td></td></tr>
<tr><td>[ref1]</td><td colspan="2"></td><td></td><td></td><td></td></tr>
<tr><td>Electrical properties</td><td colspan="6">Governing equation and statistics</td></tr>
<tr><td>Spikes amplitude ratio</td><td colspan="6">$v_U = 0.2101 v_D + 5.2468 \pm 0.0706$</td></tr>
<tr><td>Spikes duration ratio</td><td colspan="6">$t_U = 1.4789 t_D + 31.8115 \pm 1.0841$</td></tr>
<tr><td>Spikes area ratio</td><td colspan="6">$A_U = 0.5402 A_D + 202.7970 \pm 0.3642$</td></tr>
</table>

HOPE cells on Mushroom electrode: Biphasic Fast Upward (BFUp)

<table>
<tr><td>Signal shape and defining parameter</td><td colspan="6"> 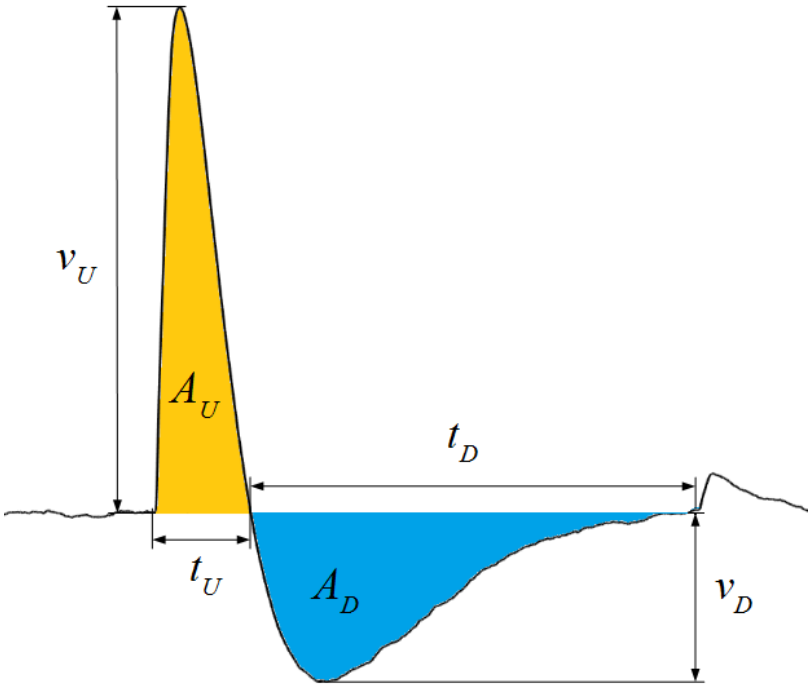
</td></tr>
<tr><td>Designation</td><td colspan="3">Full name</td><td colspan="2">Acronym</td></tr>
<tr><td></td><td colspan="3">Biphasic Fast Upward</td><td colspan="2">BFUp</td></tr>
<tr><td>Electrode system where it was recorded</td><td>Inter digitated</td><td>PEDOT</td><td>Mush</td><td>IBIDI large</td><td>IBIDI small</td></tr>
<tr><td></td><td></td><td></td><td>X</td><td></td><td></td></tr>
<tr><td rowspan="3">Biological system where it is observed</td><td>Astrocytes</td><td colspan="2">Tumors</td><td>C6</td><td>Neurons</td><td>Other</td></tr>
<tr><td></td><td colspan="2"></td><td></td><td></td><td>HOPE</td></tr>
<tr><td></td><td colspan="2"></td><td></td><td></td><td></td></tr>
<tr><td rowspan="2">Matching with ionic channels</td><td>Calcium pump</td><td colspan="2">Sodium pump</td><td></td><td></td><td></td></tr>
<tr><td>[ref1]</td><td colspan="2"></td><td></td><td></td><td></td></tr>
<tr><td>Electrical properties</td><td colspan="6">Governing equation and statistics</td></tr>
<tr><td>Spikes amplitude ratio</td><td colspan="6">$v_U = 1.6713 v_D + 87.5115 \pm 0.6683$</td></tr>
<tr><td>Spikes duration ratio</td><td colspan="6">$t_U = 0.1366 t_D + 8.5950 \pm 0.1239$</td></tr>
<tr><td>Spikes area ratio</td><td colspan="6">$A_U = 0.7194 A_D + 430.9381 \pm 0.1593$</td></tr>
</table>

HOPE cells on IBIDI Circular electrode: Biphasic Fast Upward (BFUp)

Signal shape and defining parameter	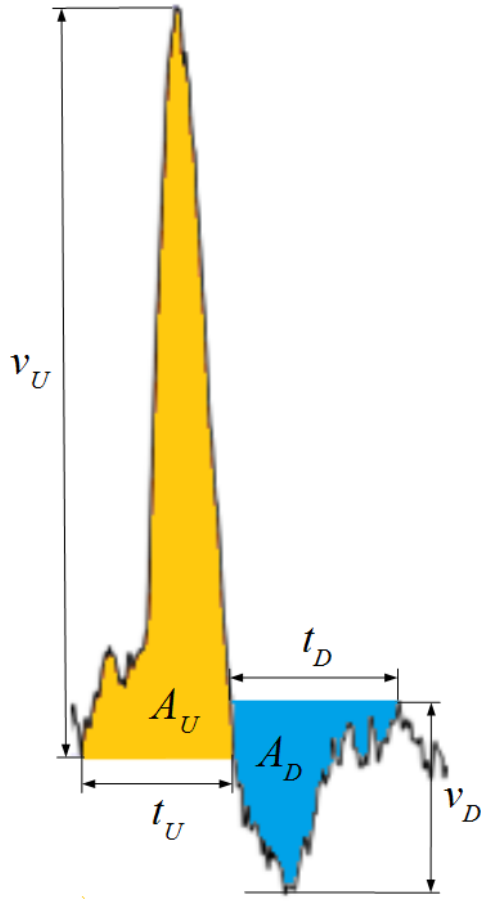						
Designation	**Full name**			**Acronym**			
	Biphasic Fast Upward			*BFUp*			
Electrode system where it was recorded	Inter digitated	PEDOT	Mush	IBIDI large	IBIDI small		
					X		
Biological system where it is observed	**Astrocytes**	**Tumors**		**C6**	**Neurons**	**Other**	
						HOPE	
Matching with ionic channels	Calcium pump	Sodium pump					
	[ref1]						
Electrical properties	**Governing equation and statistics**						
Spikes amplitude ratio	$v_U = 2.3635 v_D + 2.7809 \pm 1.2305$						
Spikes duration ratio	$t_U = 0.4180 t_D + 0.3934 \pm 0.1749$						
Spikes area ratio	$A_U = 1.5896 A_D + 0.1119 \pm 0.4906$						

HOPE cells on Interdigitated electrode: Biphasic Fast Upward (BFUp)

<table>
<tr><td>Signal shape and defining parameter</td><td colspan="6"> 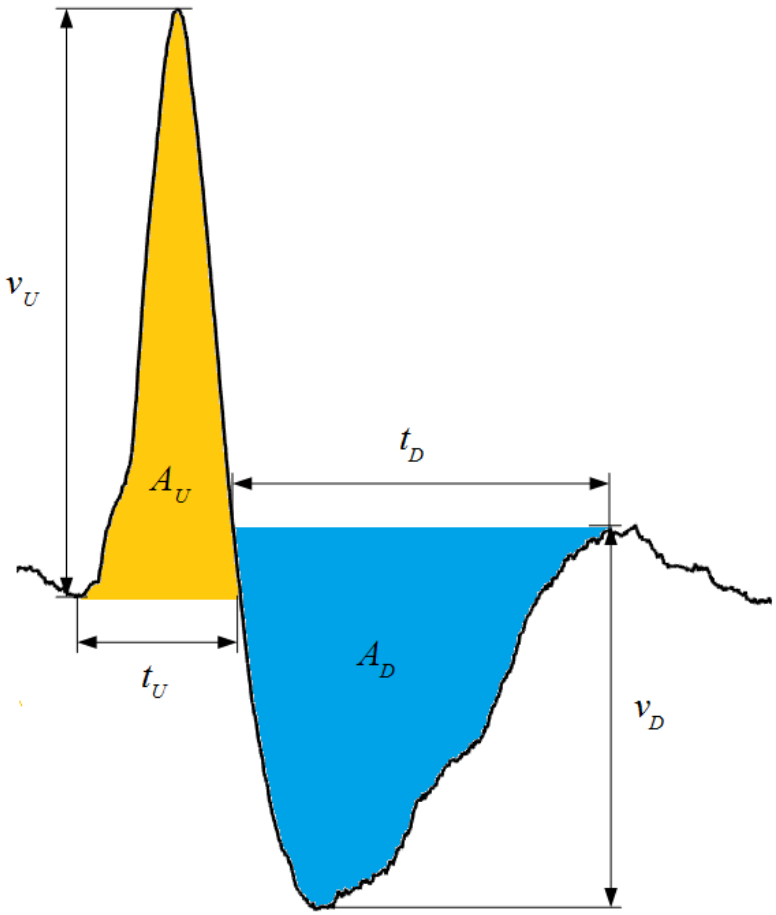
</td></tr>
<tr><td>Designation</td><td colspan="3">Full name</td><td colspan="2">Acronym</td></tr>
<tr><td></td><td colspan="3">Biphasic Fast Upward</td><td colspan="2">BFUp</td></tr>
<tr><td>Electrode system where it was recorded</td><td>Inter digitated</td><td>PEDOT</td><td>Mush</td><td>IBIDI large</td><td>IBIDI small</td></tr>
<tr><td></td><td>X</td><td></td><td></td><td></td><td></td></tr>
<tr><td rowspan="2">Biological system where it is observed</td><td>Astrocytes</td><td colspan="2">Tumors</td><td>C6</td><td>Neurons</td><td>Other</td></tr>
<tr><td></td><td colspan="2"></td><td></td><td></td><td>HOPE</td></tr>
<tr><td rowspan="2">Matching with ionic channels</td><td>Calcium pump</td><td colspan="2">Sodium pump</td><td></td><td></td><td></td></tr>
<tr><td>[ref1]</td><td colspan="2"></td><td></td><td></td><td></td></tr>
<tr><td>Electrical properties</td><td colspan="6">Governing equation and statistics</td></tr>
<tr><td>Spikes amplitude ratio</td><td colspan="6">$v_U = 1.6718 v_D + 1.7209 \pm 0.183$</td></tr>
<tr><td>Spikes duration ratio</td><td colspan="6">$t_U = 0.3025 t_D - 0.67 \pm 0.05$</td></tr>
<tr><td>Spikes area ratio</td><td colspan="6">$A_U = 0.5259 A_D - 2.8223 \pm 0.0237$</td></tr>
</table>

HOPE cells on PHILLIPS electrode: Biphasic Fast Upward (BFUp)

<table>
<tr><td>Signal shape and defining parameter</td><td colspan="6"> 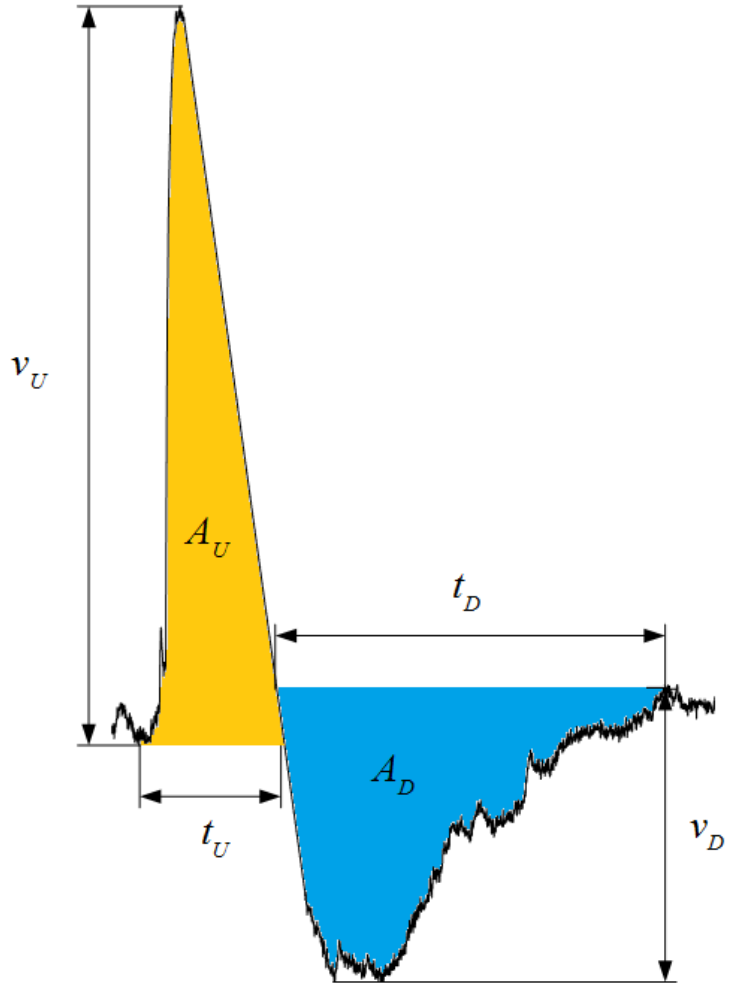
</td></tr>
<tr><td>Designation</td><td colspan="3">Full name</td><td colspan="3">Acronym</td></tr>
<tr><td></td><td colspan="3">Biphasic Fast Upward</td><td colspan="3">BFUp</td></tr>
<tr><td>Electrode system where it was recorded</td><td>Inter digitated</td><td>PEDOT</td><td>Mush</td><td>PHILLIPS</td><td colspan="2">IBIDI small</td></tr>
<tr><td></td><td></td><td></td><td></td><td>X</td><td colspan="2"></td></tr>
<tr><td rowspan="2">Biological system where it is observed</td><td>Astrocytes</td><td colspan="2">Tumors</td><td>C6</td><td>Neurons</td><td>Other</td></tr>
<tr><td></td><td colspan="2"></td><td></td><td></td><td>HOPE</td></tr>
<tr><td rowspan="2">Matching with ionic channels</td><td>Calcium pump</td><td colspan="2">Sodium pump</td><td></td><td></td><td></td></tr>
<tr><td>[ref1]</td><td colspan="2"></td><td></td><td></td><td></td></tr>
<tr><td>Electrical properties</td><td colspan="6">Governing equation and statistics</td></tr>
<tr><td>Spikes amplitude ratio</td><td colspan="6">$v_U = 1.75 v_D + 11.91 \pm 1.074$</td></tr>
<tr><td>Spikes duration ratio</td><td colspan="6">$t_U = 0.25 t_D + 0.03 \pm 0.1183$</td></tr>
<tr><td>Spikes area ratio</td><td colspan="6">$A_U = 0.7 A_D + 0.44 \pm 0.323$</td></tr>
</table>

HOPE cells on IBIDI Circular electrode: Square-Like (SL)

<table>
<tr><td>Signal shape and defining parameter</td><td colspan="6"> 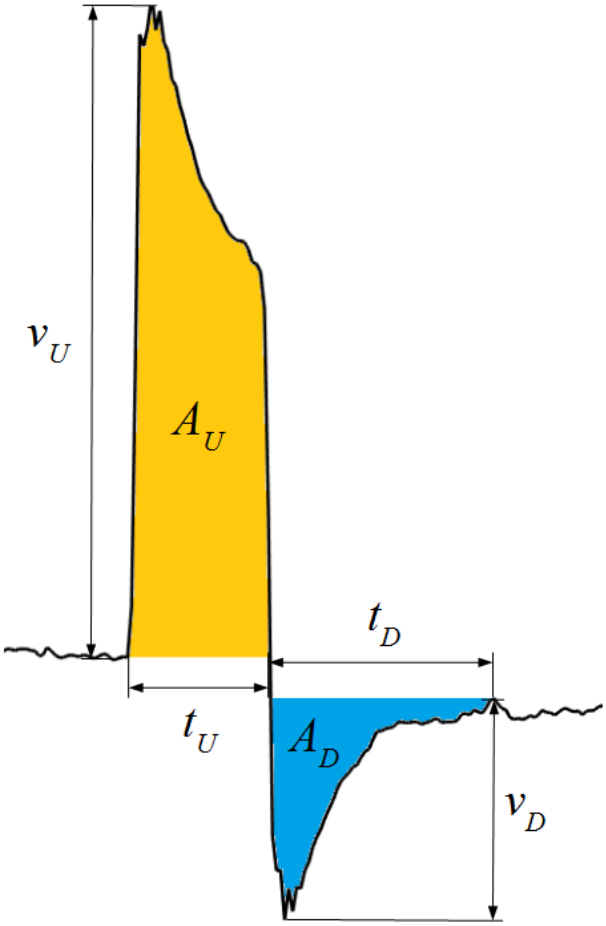
</td></tr>
<tr><td>Designation</td><td colspan="3">Full name</td><td colspan="2">Acronym</td></tr>
<tr><td></td><td colspan="3">Square-Like</td><td colspan="2">SL</td></tr>
<tr><td>Electrode system where it was recorded</td><td>Inter digitated</td><td>PEDOT</td><td>Mush</td><td>IBIDI large</td><td>IBIDI small</td></tr>
<tr><td></td><td></td><td></td><td></td><td></td><td>X</td></tr>
<tr><td rowspan="2">Biological system where it is observed</td><td>Astrocytes</td><td colspan="2">Tumors</td><td>C6</td><td>Neurons</td><td>Other</td></tr>
<tr><td></td><td colspan="2"></td><td></td><td></td><td>HOPE</td></tr>
<tr><td rowspan="2">Matching with ionic channels</td><td>Calcium pump</td><td colspan="2">Sodium pump</td><td></td><td></td><td></td></tr>
<tr><td>[ref1]</td><td colspan="2"></td><td></td><td></td><td></td></tr>
<tr><td>Electrical properties</td><td colspan="6">Governing equation and statistics</td></tr>
<tr><td>Spikes amplitude ratio</td><td colspan="6">$v_U = 0.0738 v_D + 28.7894 \pm 0.2743$</td></tr>
<tr><td>Spikes duration ratio</td><td colspan="6">$t_U = 0.3636 t_D + 1.6974 \pm 0.3374$</td></tr>
<tr><td>Spikes area ratio</td><td colspan="6">$A_U = 1.2840 A_D + 44.8098 \pm 1.2630$</td></tr>
</table>

U87 cells on Mushroom electrode: Biphasic Fast Downward (BFDown)

Signal shape and defining parameters	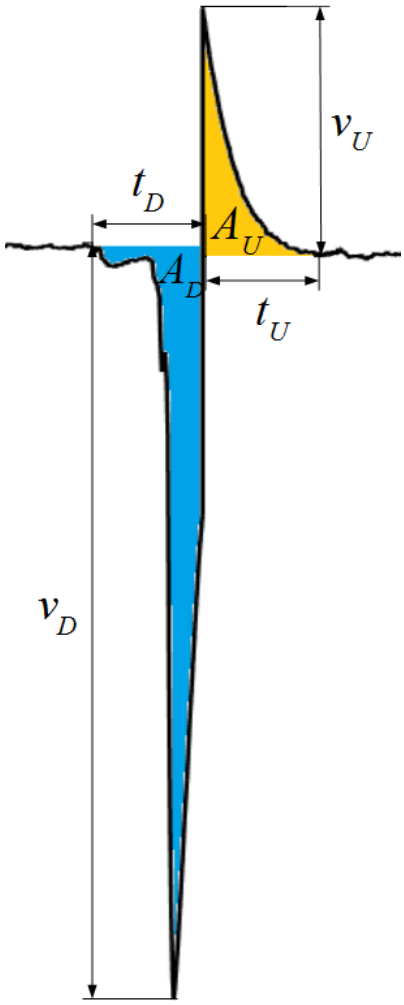					
Designation	**Full name**			**Acronym**		
	Biphasic Fast Downward			*BFDown*		
Electrode system where it was recorded	Inter digitated	PEDOT	Mush	IBIDI large	IBIDI small	
			X			
Biological system where it is observed	**Astrocytes**	**Tumors**		**C6**	**Neurons**	**Other**
						U87
Matching with ionic channels	Calcium pump	Sodium pump				
	[ref1]					
Electrical properties	**Governing equation and statistics**					
Spikes amplitude ratio	$v_U = 0.4427 v_D - 34.6460 \pm 0.1138$					
Spikes duration ratio	$t_U = 0.0605 t_D + 26.7646 \pm 0.5994$					
Spikes area ratio	$A_U = 1.3430 A_D - 843.1387 \pm 0.4164$					

U87 cells on Mushroom electrode: Biphasic Fast Upward (BFUp)

<table>
<tr><td>Signal shape and defining parameters</td><td colspan="6"> 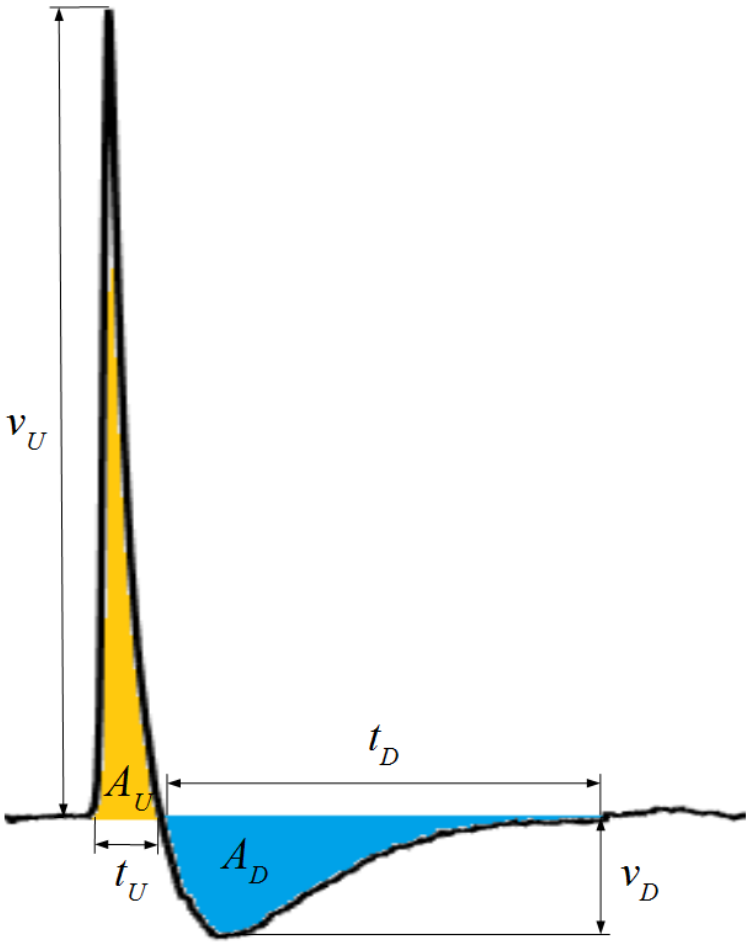
</td></tr>
<tr><td>Designation</td><td colspan="3">Full name</td><td colspan="3">Acronym</td></tr>
<tr><td></td><td colspan="3">Biphasic Fast Upward</td><td colspan="3">BFUp</td></tr>
<tr><td>Electrode system where it was recorded</td><td>Inter digitated</td><td>PEDOT</td><td>Mush</td><td>IBIDI large</td><td colspan="2">IBIDI small</td></tr>
<tr><td></td><td></td><td></td><td>X</td><td></td><td colspan="2"></td></tr>
<tr><td rowspan="2">Biological system where it is observed</td><td>Astrocytes</td><td colspan="2">Tumors</td><td>C6</td><td>Neurons</td><td>Other</td></tr>
<tr><td></td><td colspan="2"></td><td></td><td></td><td>U87</td></tr>
<tr><td rowspan="2">Matching with ionic channels</td><td>Calcium pump</td><td colspan="2">Sodium pump</td><td></td><td></td><td></td></tr>
<tr><td>[ref1]</td><td colspan="2"></td><td></td><td></td><td></td></tr>
<tr><td>Electrical properties</td><td colspan="6">Governing equation and statistics</td></tr>
<tr><td>Spikes amplitude ratio</td><td colspan="6">$v_U = 1.4585 v_D + 167.0974 \pm 0.3515$</td></tr>
<tr><td>Spikes duration ratio</td><td colspan="6">$t_U = -0.1706 t_D + 15.1623 \pm 0.4767$</td></tr>
<tr><td>Spikes area ratio</td><td colspan="6">$A_U = 0.2817 A_D + 1.2468 \times 10^3 \pm 0.1569$</td></tr>
</table>

Neurons cells (N2A) on Mushroom electrode: Biphasic Fast Upward (BFUp)

<table>
<tr><td>Signal shape and defining parameter</td><td colspan="6"> 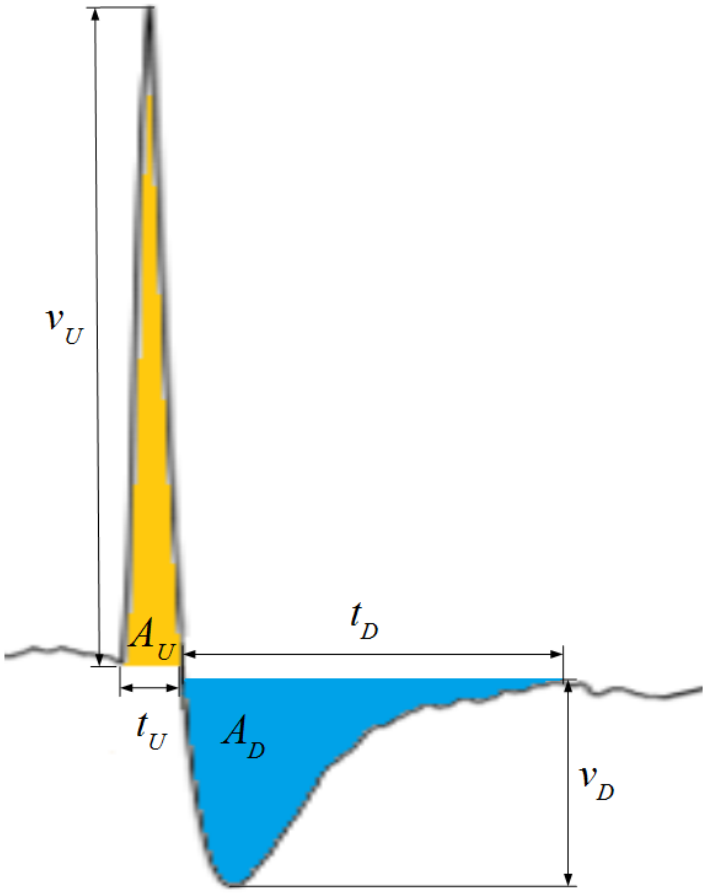
</td></tr>
<tr><td>Designation</td><td colspan="3">Full name</td><td colspan="2">Acronym</td></tr>
<tr><td></td><td colspan="3">Biphasic Fast Upward</td><td colspan="2">BFUp</td></tr>
<tr><td>Electrode system where it was recorded</td><td>Inter digitated</td><td>PEDOT</td><td>Mush</td><td>IBIDI large</td><td>IBIDI small</td></tr>
<tr><td></td><td></td><td></td><td>X</td><td></td><td></td></tr>
<tr><td rowspan="2">Biological system where it is observed</td><td>Astrocytes</td><td colspan="2">Tumors</td><td>C6</td><td>Neurons</td><td>Other</td></tr>
<tr><td></td><td colspan="2"></td><td></td><td>X</td><td></td></tr>
<tr><td rowspan="2">Matching with ionic channels</td><td>Calcium pump</td><td colspan="2">Sodium pump</td><td></td><td></td><td></td></tr>
<tr><td>[ref1]</td><td colspan="2"></td><td></td><td></td><td></td></tr>
<tr><td>Electrical properties</td><td colspan="6">Governing equation and statistics</td></tr>
<tr><td>Spikes amplitude ratio</td><td colspan="6">$v_U = 1.6022 v_D + 115.7405 \pm 0.2592$</td></tr>
<tr><td>Spikes duration ratio</td><td colspan="6">$T_U = 0.1387 t_D + 12.1744 \pm 0.1730$</td></tr>
<tr><td>Spikes area ratio</td><td colspan="6">$A_U = 0.4985 A_D + 1.1396 \times 10^3 \pm 0.0769$</td></tr>
</table>